Mohammad Ashrafi

Experimental Investigation of Temperature Dependency of Relative Permeability Data in Heavy Oil Systems with Applications to Thermal Recovery

Thesis for the degree of Philosophiae Doctor

Trondheim, May 2013

Norwegian University of Science and Technology
Faculty of Engineering Science and Technology
Department of Petroleum Engineering and
Applied Geophysics

NTNU – Trondheim
Norwegian University of
Science and Technology

NTNU
Norwegian University of Science and Technology

Thesis for the degree of Philosophiae Doctor

Faculty of Engineering Science and Technology
Department of Petroleum Engineering and Applied Geophysics

ISBN 978-82-471-4243-1 (printed ver.)
ISBN 978-82-471-4244-8 (electronic ver.)
ISSN 1503-8181

Doctoral theses at NTNU, 2013:73

Printed by NTNU-trykk

This thesis is dedicated to my dear parents for all they have done for me and to my brothers and sister

Abstract

Heavy oil and tar sands are important hydrocarbon resources that are destined to play an increasingly important role in the oil supply of the world. A huge proportion of total world oil resources are in the form of these highly viscous fluids. The main recovery mechanism for these kinds of reservoirs is to somehow reduce their viscosity by the application of heat. In these extra heavy oil reservoirs, the reservoir has almost no injectivity, and therefore conventional steam flooding is hard to conduct. Steam Assisted Gravity Drainage (SAGD), however, reduces the viscosity of bitumen in place and the heated bitumen drains due to gravity forces towards the production well, where it is produced. Modeling and evaluating the production mechanisms in this process requires a thorough understanding of multi-phase flow parameters like relative permeability.

Relative permeability data depend on a number of different parameters among others temperature and fluid viscosity. Viscosities of the flowing fluids drop with temperature, which can affect the relative permeability data. There has been a long debate on the actual impact of temperature on the relative permeabilities. Although some authors have reported saturation range shifts and relative permeability curve variations by temperature, others have attributed these variations to artifacts inherent in the methods used and the systems tested. Viscous instabilities and fingering issues have been blamed for temperature dependencies reported, and some researchers have reported that relative permeability data changes due to oil/water viscosity ratio changes at different temperatures.

The variations in the experimental conditions have resulted in different and even contradictory results. There is specifically few experimental works conducted on Athabasca oil systems, and previously reported trends mainly apply to less viscous oils. This implies that the actual effect of temperature on flow behavior of fluids in the rock is case specific. Due to the contradictory reports and conclusions, which are due to variation in the systems being tested, it seemed necessary to conduct our own core flooding experiments, and investigate the curves of relative permeability. The objective was to obtain the imbibition relative permeability curves in an Athabasca oil type reservoir at different temperatures and oil viscosities, and figure out any possible trends of variations with temperature.

Before conducting the core flooding experiments, some fluid behavior experiments were done to figure out the properties of bitumen used in this study. These include fluid compositions, density, viscosity, molecular weight and oil/steam interfacial tension. These properties were further used in numerical simulation studies.

Core floodings were conducted on glass bead packs and sand packs saturated with heavy oils with varying viscosities. Displacement experiments with water were performed at different temperatures, and unsteady-state method of relative permeability measurement was conducted. The relative permeability data were determined by history matching the oil production data and pressure differential data in each experiment.

Results indicated a change in the water saturation range in the oil-water relative permeability curves. The shift was towards higher water saturations, meaning an increase in irreducible water saturation and a decrease in residual oil saturation. Regarding the shape of relative permeability data, no unique trend of either rising or falling with temperature was found for oil and water relative permeability curves. The viscous instabilities are believed to be present in the experiments.

As the same saturation range shift occurs by comparing the results at the same temperature level and by only changing the oil viscosity, this suggests that the temperature dependency of relative permeabilities can be attributed to the drop in oil to water viscosity ratio by temperature.

The variations of relative permeability data with temperature was therefore found to be more related to artifacts in the experimental procedures like viscous fingering, and fluid viscosity changes than fundamental flow properties.

Numerical simulations were accomplished on field scale SAGD and ES-SAGD (Expanding Solvent SAGD) operations testing the effect of relative permeability curves. Temperature dependent relative permeability data were tested and Oil production was found to be strongly dependant on the end point data. It is therefore suggested to use this option as a matching criterion when trying to history match SAGD field data.

Since the main experimental part of this study deals with temperature dependency of relative permeability data, the introduction of this thesis is totally devoted to introducing this concept and its measurement methods and a literature review on the works performed so far. The main thesis is composed of three main parts, the fluid behavior experiments on bitumen, one-dimensional flow studies and multi-dimensional flow part. The results of fluid behavior experiments are given in chapter 2. Chapters 3 and 4 are devoted to one-dimensional flow works and chapters 5 and 6 present the part of this thesis dealing with two and three-dimensional flow. It should, however, be mentioned that chapters 4 to 6 can be read independently, as the contents of these chapters are taken from previously published papers with some minor revisions.

Acknowledgement

I would like to thank my supervisor, professor Ole Torsæter, who has always been helpful and has provided me the inspiration for work during my PhD studies. I am indebted to my dear friend and colleague, Yaser Souraki, for all the effort and kind support he has provided me during the experiments and technical discussions. We had a nice and unique opportunity to experience and practice team work during our PhD studies. I would also like to thank Dr.Hassan Karimaie for introducing me to the adventurous environment of laboratory. He taught me that it takes courage to "do it yourself" in the laboratory. My sincere gratitude goes to SINTEF petroleum research staff specially Dr.Bård J.A. Bjørkvik, Dr.Torleif Holt, Dr.Erik Lindeberg and Øyvind Haave for the helpful comments and technical support during the experiments.

This research was supported by Statoil ASA. This financial support is greatly acknowledged, and the technical meetings and exchanges of ideas with heavy oil team from Statoil research center in Trondheim are highly appreciated. I would like to express my gratitude to all the team members especially Dr.Jostein Alvestad, Dr.Eimund Gilje, Dr.Dagrun Kjønsvik, Dr.Fridtjov Munkvold and Dr.Siddhartha Seth Bengra.

My sincere appreciation extends to Dr.Curtis Hays Whitson, Dr.Lars Høier and Dr.Jon Kleppe from the department of petroleum engineering and applied geophysics for the great experience I have had during the course work under their supervision.

During the experimental work in the laboratory a lot of technical problems showed up. The discussions and great experience provided by Dr.Nanji Hadia, to cope with these issues, are greatly acknowledged. I would also like to thank the laboratory engineer, Roger Overå, the workshop technician, Håkon Myhren, and the electrician, Åge Sivertsen for all the technical support they have provided during my experiments.

A lot of nice people in the department of petroleum engineering and applied geophysics have helped to provide a nice and friendly atmosphere. I would like to appreciate all the help and support from these people including the administrative personnel, the data engineers and all the other technical personnel, whose kindness have inspired me and made my work at this department a memorable experience.

I have experienced a great social life and have made a lot of good friends, whom I am thankful to, during my stay in Trondheim. I would like to express my sincere gratitude to all my dear friends at the department, who have made our work environment such a lovely place. I am indebted to all of them for the great moments we shared. It was a unique opportunity to live in Trondheim and get to know the new culture and language.

I should express my appreciation to all who have helped me in getting involved in Norwegian culture.

Last but not least, I would like to express my appreciation to my lovely family, my mum, dad, sister and my two brothers. I am indebted to my dear mum and dad for being supportive and caring during my whole life. I would like to thank them for all they have done for me.

26 February 2013

Trondheim

63˚ N, 10˚ E

Nomenclature

A	Cross sectional area of flow, cm^2
c	Empirical constant in viscosity eq. (2.3)
C^*	Wettability number, *dimensionless*
D	Core diameter, *m*
f	Fractional flow, *fraction*
F	Force, *N*
g	Acceleration of gravity, $9.81\ m/s^2$
I_r	Relative injectivity, *dimensionless*
I_{sc}	Dimensionless instability number
k	Absolute permeability, *D*
k_e	Effective permeability, *D*
k_r	Relative permeability, *fraction*
k_{wor}	Permeability to water at residual oil saturation, *D*
K	K-value, *dimensionless*
K_f	Cryoscopic constant for the solvent, *K.kg/mol*
L	Total length of flooded system, *cm*
M	Molecular weight in eq. (2.4), *kg/mol*
M	Mobility ratio in eq. (3.1), *dimensionless*
N	Corey parameter for oil or water
N_p	Cumulative pore volumes of oil produced, *dimensionless*
p	Pressure, *atm*
P_c	Capillary pressure
q	Flow rate, cm^3/s

s Distance in direction of flow, x, y, z

S Fluid saturation, *fraction*

S_{or} Residual oil saturation, *fraction*

S_{wi} Initial water saturation, *fraction*

$\bar{S}_w$ Average water saturation, *fraction*

T Absolute temperature, K

ΔT Freezing point depression in eq. (2.4), K

u Average velocity = q/A , *cm/s*

v Constant superficial velocity, *m/s*

v_c Characteristic velocity, *m/s*

$VISC$ Fluid viscosity, *cP*

w Mass fraction of solute in solution in eq. (2.4), *dimensionless*

W_i Cumulative pore volumes of water injected, *dimensionless*

x Horizontal coordinate

z Vertical coordinate

Greek Letters

$\dot{\gamma}$ Shear rate = dv/dx, *1/sec*

Δ Difference

θ The angle between direction of flow and horizontal, °

λ Pore size distribution index in Burdine correlation

μ Dynamic viscosity, *cP*

ρ Density, g/cm^3

σ Interfacial tension, *mN/m*

τ Shear stress = F/A, N/m^2

ϕ Porosity, *fraction*

Subscripts

l	Liquid phase, *w*, *o*, *g*
o	Oil
ref	Reference condition
w	Water
2	*core outlet*

Superscript

s	start of injection
0	End Point Value
*	Normalized Value

Abbreviation

BPR	Back Pressure Regulator
CWE	Cold Water Equivalents
ES-SAGD	Expanding Solvent Steam Assisted Gravity Drainage
GB	Glass Beads
GC	Gas Chromatography
HSor	High residual oil saturation relative permeability data set
IFT	Interfacial tension
JBN	Johnson, Bossler and Naumann technique
LSor	Low residual oil saturation relative permeability data set
OIL10	An oil mixture containing 90% Athabasca bitumen and 10% n-C_{12} on a mass basis
OIL20	An oil mixture containing 80% Athabasca bitumen and 20% n-C_{12} on a mass basis
PV	Pore volume
PVT	Pressure, volume, temperature

RF	Recovery factor
SAGD	Steam Assisted Gravity Drainage
SCAL	Special Core Analysis
SCI	Solvent Co-Injection
SOR	Steam to oil ratio
SP	Sand Pack
TD	Temperature dependant relative permeability data set

Table of Contents

List of Figures

List of Tables

List of Papers

Below is a list of technical papers presented or published in different conference proceedings or journals during the course of this thesis. Paper No.1 is reviewed and discussed in chapter 2 and presented in details as Appendix A.1. Papers No. 2 and 3 comprise the main part of chapter 3 of this thesis; these two papers are also attached as Appendices A.2 and A.3. Paper No.4 is included as chapter 4 of this thesis. Papers No.5 and 6 are attached as Appendices B.1 and B.2. Papers No.7 and 8 comprise the chapters 6 and 4 of this thesis respectively.

1- "Experimental PVT Property Analyses for Athabasca Bitumen", Mohammad Ashrafi, Yaser Souraki, Hassan Karimaie, Ole Torsaeter, SPE, Norwegian University of Science and Technology (NTNU), and Bard J.A. Bjorkvik, SPE, SINTEF Petroleum Research, paper CSUG/SPE 147064 presented at the Canadian Unconventional Resources Conference, 15–17 November 2011, Calgary, Alberta, Canada.

2- "Effect of Temperature on Athabasca Type Heavy Oil – Water Relative Permeability Curves in Glass Bead Packs" Mohammad Ashrafi, Yaser Souraki, and Ole Torsaeter, Norwegian University of Science and Technology (NTNU), Energy and Environment Research, Vol. 2, No. 2, 2012.

3- "Investigating the Temperature Dependency of Oil and Water Relative Permeabilities for Heavy Oil Systems", Mohammad Ashrafi, Yaser Souraki, Ole Torsaeter, Submitted to Transport in Porous Media.

4- "Numerical Simulation Study of Field Scale SAGD and ES-SAGD Processes Investigating the Effect of Relative Permeabilities", Mohammad Ashrafi, Yaser Souraki, Ole Torsaeter, Accepted for publication in Energy and Environment Research.

5- "Experimental and Numerical Study of Steam Flooding in Fractured Porous Media", Mohammad Ashrafi, Yaser Souraki, Hassan Karimaie, and Ole Torsaeter, SPE, Norwegian University of Science and Technology (NTNU), paper SPE 144462 presented at the SPE Western North American Regional Meeting, 7-11 May 2011, Anchorage, Alaska, USA.

6- "Simulation Study of 2-D SAGD Experiment and Sensitivity Analysis of Laboratory Parameters", Mohammad Ashrafi, Yaser Souraki, Hassan Karimaie, Ole Torsaeter, and Jon Kleppe, SPE, Norwegian University of Science and Technology (NTNU), paper SPE 144582 presented at the SPE Western North American Regional Meeting, 7-11 May 2011, Anchorage, Alaska, USA.

7- “Numerical Simulation Study of SAGD Experiment and Investigating Possibility of Solvent Co-Injection”, Mohammad Ashrafi, Yaser Souraki, Hassan Karimaie, Ole Torsaeter, and Jon Kleppe, SPE, Norwegian University of Science and Technology (NTNU), paper SPE 145013 presented at the SPE Enhanced Oil Recovery Conference, 19-21 July 2011, Kuala Lumpur, Malaysia.

8- “Experimental and Numerical Investigation of Steam Flooding in Heterogeneous Porous Media Containing Heavy Oil”, Mohammad Ashrafi, Yaser Souraki, Tor Joergen Veraas, Hassan Karimaie, and Ole Torsaeter, SPE, Norwegian University of Science and Technology (NTNU), paper SPE 144168 presented at the SPE Asia Pacific Oil and Gas Conference and Exhibition, 20-22 September 2011, Jakarta, Indonesia.

Chapter 1

Introduction

This chapter gives some general definitions of the absolute and relative permeability. Most frequently used laboratory methods to measure the relative permeabilities are introduced. An extensive literature review of the laboratory and theoretical work done on the effect of temperature on relative permeabilities is presented. The chapter concludes with an outline of the material presented in this thesis.

1.1 Absolute permeability

One dimensional, linear and horizontal flow of a single phase fluid in porous media is represented by Darcy's Law in the following form:

$$q = -\frac{kA}{\mu}\frac{\partial p}{\partial s} \tag{1.1}$$

Where, k is the absolute permeability of the porous media, q is the fluid flow rate, A is the cross sectional area of flow, μ is the fluid viscosity, p is the fluid pressure and s is the distance in the direction of flow. This law states that the rate of flow of a fluid in the porous media is proportional to the absolute permeability of the porous media and inversely proportional to the viscosity of the fluid. The absolute permeability is therefore the measure of the capacity of porous medium to transmit the fluid (Amyx et al., 1960). The unit of absolute permeability in oil industry is Darcy, which is defined as the permeability of a porous medium when a single phase fluid of one centipoises viscosity that completely fills the voids of the porous medium will flow through it under conditions of viscous flow at a rate of one cubic centimeter per second per square centimeter cross-sectional area under a pressure gradient of one atmosphere per centimeter (Amyx et al., 1960). One Darcy is, however, a large permeability for the rock and the permeability of the reservoir rock is usually expressed as milliDarcies or 0.001 Darcy. The SI unit of permeability is m^2. The conversion between these two units is 1 Darcy $\approx$ 1 μm^2.

1.2 Relative permeability

The equation of Darcy's Law can be generalized for the case of a porous medium that contains more than one fluid phase by introducing the concept of effective permeability. If a rock contains several phases, namely oil, water and gas, the permeability of the rock to each of these immiscible phases in the presence of the other phases is called effective permeability to that phase. The effective permeability of rock to a fluid is a function of

its saturation in the porous media, and the effective permeability to a phase at its 100% saturation is simply equal to the absolute permeability (Honarpour et al., 1986). The Darcy's Law can therefore be considered for each fluid separately by considering the effective permeability to that fluid phase, which is independent of the other phases present in the rock. The ratio of effective permeability, k_e, of a porous medium to a fluid phase to absolute permeability, k, is defined as the relative permeability for that fluid phase:

$$k_r = \frac{k_e}{k} \tag{1.2}$$

The general form of Darcy's law for a system containing several fluid phases will therefore be as follows, including the effect of gravity:

$$v_l = \frac{kk_{rl}}{\mu_l}\left(\rho_l g \frac{dz}{ds} - \frac{dp_l}{ds}\right) \tag{1.3}$$

Where, l ($l = w, o, g$) represents any of the fluid phases that are present in the porous media, v represents the flow velocity, μ is the fluid viscosity, ρ is the fluid density, g represents the acceleration of gravity and z is the distance in vertical coordinate direction.

The relative permeability to a fluid phase is usually a function of saturation of that fluid phase only, assuming the phases are immiscible. The whole calculations of fluid flow in reservoirs are based on Darcy's law, and it is the basis of all reservoir simulation studies. It is therefore crucial to have the accurate relative permeability values to all the phases in a hydrocarbon reservoir in order to perform a successful reservoir simulation study. These relative permeability calculations are needed in the whole saturation range that is encountered in a reservoir (Honarpour et al., 1986).

1.3 Relative permeability measurement methods

There are generally two methods for measuring relative permeability by core flooding in laboratory. These methods are called "steady-state method" and "unsteady-state method". Steady-state method is based on the injection of both fluid phases simultaneously until a state of equilibrium is reached, and the saturation in the core as well as the pressure drop across the core is at steady state condition. The main concern in this method is to reduce the capillary end effects, which causes some saturation gradients at the inlet and outlet of the core. The unsteady-state method is also known as displacement technique, and is based on the injection of one fluid phase, displacing the other phase in the core. The advantage of this method is faster experimental results than the steady-state method (Honarpour et al., 1986).

1.3.1 Steady-state method of relative permeability measurement

There are numerous steady-state methods of measuring relative permeability in the laboratory. Their main difference is how they treat the problem of capillary end effects. Either the injection is done at high enough rates to minimize the saturation gradient at the boundary caused by capillary forces, or the core is placed between porous plates or test sections to minimize the end effect. In either case, the fluids to be injected are introduced into the core sample simultaneously through different piping systems. The two fluids are injected at a pre-determined fluid ratio, and the injection continues until the production ratio is equal to the injection ratio. At this condition, the saturation in the core is considered to be stable and the flow to be at steady-state condition (Amyx et al., 1960). The saturation in the core is measured by either fluid resistivity, weighing the core, volumetric balance, or in-situ methods like X-ray absorption or gamma-ray absorption (Honarpour et al., 1986). Once the saturation profile is known, the relative permeabilities corresponding to that saturation point can be calculated by applying the Darcy's law. The injection ratio is then varied to a new value, and the same procedure is applied until reaching the steady-state condition. This method can be applied either as a desaturation test or resaturation. In the desaturation test, the sample is initially at the 100% saturation of wetting phase, and the ratio of injection is started at a high value of wetting phase and gradually drops to 100% non-wetting phase. The resaturation test is vice versa, starting with a core that is 100% saturated with a non-wetting phase (Amyx et al., 1960).

1.3.2 Unsteady-state method of relative permeability measurement

Unsteady-state method of relative permeability measurement is based on the displacement of one fluid phase in the core by the injection of another immiscible fluid phase. The relative permeability ratio is then calculated from produced fluid ratio (Skjæveland and Kleppe, 1992). The unsteady-state method is advantageous in the sense that it is faster than the steady-state method. The mathematical calculation is based on the frontal advance theory developed by Buckley and Leverett (1942) that was further extended by Welge (1952). Combining the Darcy's law with the definition of capillary pressure results in the following:

$$f_{w2} = \frac{1 + \frac{k_o}{\mu_o u}\left(\frac{dP_c}{dx} - g\Delta\rho\sin\theta\right)}{1 + \frac{k_o}{k_w}\frac{\mu_w}{\mu_o}} \tag{1.4}$$

Where, f_{w2} is fraction of water in the in the outlet stream, u is the superficial velocity of total fluid leaving the core, θ is the angle between direction of flow, x, and horizontal direction, $\Delta\rho$ is the density difference between the displacing and displaced fluids.

Welge (1952) further showed that for a horizontal displacement and neglecting the effect of capillary pressure we can write:

$$\bar{S}_w - S_{w2} = W_i f_{o2} \tag{1.5}$$

Where, the subscript 2 denotes the outlet end of the core, $\bar{S}_w$ is the average water saturation in the core and W_i is the cumulative volume of water injected measured as the number of pore volumes. The values of W_i and $\bar{S}_w$ can be measured experimentally and the fraction of oil at the inlet can be determined:

$$\bar{S}_w = S_{wi} + N_p \tag{1.6}$$

$$f_{o2} = \frac{d\left(\bar{S}_w\right)}{d\left(W_i\right)} = \frac{d\left(N_p\right)}{d\left(W_i\right)} \tag{1.7}$$

Where, N_p is the volume of oil produced expressed in number of pore volumes. The value of oil fraction at the outlet face is, however, expressed through the following equation using Darcy's law:

$$f_{o2} = q_o / \left(q_o + q_w\right) = \frac{1}{1 + \frac{\mu_o / k_{ro}}{\mu_w / k_{rw}}} \tag{1.8}$$

Knowing the values of oil and water viscosity, the ratio of oil to water relative permeability can be determined using the equations presented above. Later on Johnson et al. (1959) extended the method of Welge to obtain the individual values of oil and water relative permeability. This method is known as JBN method (Johnson, Bossler and Naumann technique) and is based on the following equations:

$$\frac{f_{o2}}{k_{ro}} = \frac{d\left(1/W_i I_r\right)}{d\left(1/W_i\right)} \tag{1.9}$$

$$k_{rw} = \frac{\left(1 - f_{o2}\right)}{f_{o2}} \frac{\mu_w}{\mu_o} k_{ro} \tag{1.10}$$

Where, I_r is called the relative injectivity and represents the ratio of intake capacity at any given flood stage to the intake capacity of the system at the very beginning of the injection, when only one phase is flowing (Johnson et al., 1959):

$$I_r = \frac{\left(u / \Delta p\right)}{\left(u_s / \Delta p_s\right)} \tag{1.11}$$

Jones and Roszelle (1978) further extended the JBN method to be able to differentiate the experimental data graphically. Their method was based on finding f_o by drawing tangents to the experimental values of N_p versus W_i curve and figure out the value of S_{w2}-S_{wi} as the corresponding intercept at $W_i = 0$. They also used a modified form of equation (1.9) to determine the ratio f_o/k_{ro} as the intercept on a plot of $1/I_r$ versus W_i resulted from an experimental displacement test.

1.4 Relative permeability curves by history matching the experimental data

It is possible to obtain the relative permeability curves from the displacement experiments by either explicit or implicit methods. The most commonly used explicit methods are JBN and Jones and Roszelle methods as described earlier. The implicit method is, on the other hand, based on the numerical history matching of the experimental data. In the history matching approach, the relative permeability curves are adjusted until the calculated response of the mathematical model describing the two phase flow in the displacement experiment matches the experimental data (Maini and Okazawa, 1987). An advantage of using implicit methods is the possibility of inclusion of the capillary pressure in the calculations. This is usually neglected in explicit methods of relative permeability measurement. However, implicit techniques can be employed to include the capillary pressures as well (Wang et al., 2006). The mathematical model of the two-phase flow that occurs during a displacement experiment involves non-linear partial differential equations. These equations are presented below for a linear, horizontal, displacement of oil by water:

$$\frac{\partial}{\partial x}\left(\frac{kk_{ro}}{\mu_o}\frac{\partial P_o}{\partial x}\right)=\frac{\partial}{\partial t}\left(\phi S_o\right) \tag{1.12}$$

$$\frac{\partial}{\partial x}\left(\frac{kk_{rw}}{\mu_w}\frac{\partial P_w}{\partial x}\right)=\frac{\partial}{\partial t}\left(\phi S_w\right) \tag{1.13}$$

$$P_c = P_o - P_w \tag{1.14}$$

$$S_o + S_w = 1 \tag{1.15}$$

Where, k is the absolute permeability, ϕ is the porosity and P_c is the capillary pressure. These equations can be solved numerically by applying the finite difference method using a numerical reservoir simulator. The relative permeability curves can be estimated by a typical relative permeability correlation such as Corey (1954). The parameters in the relative permeability correlation can then be adjusted to get the best relative permeability curve that can match the experimental data.

1.5 Effect of temperature on the relative permeability curves

The effect of temperature on the relative permeability curves have long been a topic of discussions in the literature since early 60s. The reported results, however, are quite contradictory due to the different laboratory systems that have been used. The most commonly observed trends are the followings as reported by Nakornthap and Evans (1986) (Polikar, 1987):

1- An increase in the value of irreducible water saturation and a decrease in residual oil saturation are mostly reported as the temperature increases in a system. As a result of this shift in the water saturation range, the relative permeability curves are also shifted.
2- At a specific value of water saturation, the oil relative permeability increases considerably, and the water relative permeability value drops with temperature.
3- The ratio of water to oil relative permeability rises with temperature in an unconsolidated sand media, while the reverse happens in a consolidated core. This difference is due to the lower residual oil saturation in unconsolidated porous media.

Here is a brief review of the literature dealing with the temperature effects on the relative permeability data. Wilson (1956) conducted experiments using refined oil on extracted cores in a temperature range of 29°C to 71°C. His method of measurement was steady-state, and he reported no dependency of either end point saturations or relative permeabilities on the temperature. He had maintained a fixed oil to water viscosity ratio in his work. Edmondson (1965) performed some laboratory core flooding experiments mostly with refined oil and some using crude oil on Berea sandstone core plugs. The temperature range studied was 24°C to 260°C, and the unsteady-state method of relative permeability measurement was conducted. He confirmed a decrease in residual oil saturation (S_{or}) and some changes in the relative permeabilities. He concluded that the ratio of water to oil relative permeability increases at lower water saturations and vice versa happens at higher S_w values. This ratio is, however, independent of temperature when the oil to water viscosity ratio is the same. Shilolwd (1965) used the data from Edmondson (1965) and stated that relative permeabilities are not temperature dependant when plotted versus normalized saturation.

Combarnous and Pavan (1968) used a refined oil and unconsolidated core material for laboratory steady –state type of relative permeability measurement. They worked in a temperature range of 20°C up to 80°C, and reported dependency of end point saturations on the temperature. They obtained a convex shape for the oil relative permeability for high values of oil viscosity. Davidson (1969) investigated relative permeability tests for a white mineral oil system inside the sand packs. He chose the displacement method and studied the water/oil relative permeability ratio in the range of 24°C to 282°C. He concluded the dependency of the permeability ratio on temperature

in the low and high S_w range, and no dependency in the middle values of water saturation. He also reported a drop in S_{or} versus temperature. Poston et al. (1970) reported the results of water flood test using refined oils with varying viscosities. Their porous media was unconsolidated sands, and the range of temperature variations was 70°C to 300°C.Their results indicated an increase in irreducible water saturation and decrease in residual oil saturation. Their conclusion was the tendency of rock to more water wetness as the temperature rises.

Ehrlich (1970) developed a model using the adsorption theory, considering the fact that temperature changes will affect the adsorption equilibrium on a Silica or limestone porous material. He concluded based on his model that S_{or} will decreases with temperature, the ratio of water to oil relative permeability shows increasing trend with temperature in unconsolidated and decreasing trend in consolidated sand. Sinnokrot (1969, 1971) calculated relative permeabilities from measured capillary pressure data. He reported an increase in oil relative permeability and a decrease in water curve with temperature in a range of 21°C to 163°C. He further mentioned the change in wettability of rock to more water wet, a rise in S_{wi} and drop in S_{or} as the result of higher temperatures. Lo and Mungan (1973) employed the steady-state method to measure the relative permeabilities in both water wet and oil wet media from room temperature up to 149°C. According to them in both type of media the higher values of irreducible water saturation and k_{ro} as well as lower S_{or} was achieved at higher temperatures. They attributed these observations to the changes in viscosity with temperature as there was no effect of temperature for the same values of oil/water viscosity ratio.

Weinbrandt et al. (1975) examined the temperature effect on both absolute and relative permeabilities experimentally. The tested temperature range was between 22°C and 79°C, and the displacement method was conducted on consolidated sandstone cores. The absolute permeability dropped with temperature, where as both oil and water relative permeabilities were increased with increasing temperature. Similar to other studies, a rise of irreducible water saturation and drop of Sor is reported by them. They attributed, however, the changes in both absolute and relative permeabilities to the thermally induced mechanical stress caused by thermal expansion of rock. Abasov et al. (1976) used crude oil and preserved cores in their study, which was based on the dynamic displacement technique. They reported the changes in both end point saturations and relative permeabilities in a wide temperature range of 20°C to 200°C. Sufi et al. (1982) observed no significant changes in the relative permeabilities of white mineral oil and water versus temperature in the range of 21°C to 200°C. This result was obtained during displacement tests conducted in unconsolidated sand material. The end point saturations were also reported to be independent of temperature in this work. They mentioned, however, that they found a decrease in “practical” residual oil saturation with temperature due to a change in the shape of fractional flow curve as a result of viscosity ratio reduction.

Torabzadeh and Handy (1984) included the effects of both the temperature and interfacial tension (IFT) in their studies on Berea sandstone core plugs using mineral oil. The experimental range of temperature studied was 22°C to 175°C. They reported that for a high IFT system the irreducible water saturation and oil relative permeability at any saturation value increased, while the residual oil saturation and water relative permeability dropped. In a low IFT system, the irreducible water saturation did not show temperature dependency. S_{or} decreased with temperature, the value of k_{ro} increased and the water relative permeability increased up to 100°C and then became independent of temperature at higher temperatures. This happened due to conflicting effect of increasing temperature on wettability and IFT according to them. Maini and Batycky (1985) used both horizontally and vertically drilled sandstone core samples from a heavy oil reservoir to conduct temperature dependency tests using heavy crude oil. The range of temperature investigated was from room temperature up to 272°C, and the method of measurement was history matching of laboratory data. Similar trend of increasing irreducible water saturation and decreasing residual oil saturation was reported. The drop in S_{or}, however, happened up to an optimum temperature, beyond which the trend reversed. The effective oil permeability at irreducible water saturation decreased with temperature, while the effective water permeability at S_{or} was not dependent on temperature.

Miller and Ramey (1985) performed experimental core flooding investigations on both consolidated and unconsolidated porous media from room temperature up to 149°C. They used water and a refined white mineral oil, and justified no temperature dependency of either end point saturations or relative permeabilities. They stated that previously reported temperature dependent data might have been affected by viscous instabilities, capillary end effects, and difficulties in maintaining material balances. Kumar et al. (1985) performed a theoretical modeling study and came up with empirical correlations based on experimental data that relate water and oil residual saturations and relative permeabilities to temperature, interfacial tension and capillary number.

Nakornthap and Evans (1986) proposed mathematical model for the effect of temperature on the relative permeability curves. They developed analytical equations for temperature dependent relative permeability in terms of S_w, irreducible water saturation and differential changes in its value with temperature. They claimed the model is in good agreements with the experimental results reported by other researchers. Maini and Okazawa (1987) conducted unsteady-state experiments on unconsolidated silica sand using crude oil. They used the history matching technique to obtain the relative permeability curves for flooding experiments done in a wide temperature range of 21°C to 200°C. They concluded that both oil and water relative permeabilities were changing. The water relative permeability increased significantly with temperature, while the curve for oil showed variations that were inconclusive. However, they have mentioned that due to several artifacts involved in the experiments

and measurements no effect of temperature on the shape of relative permeability curves could be justified.

Closmann et al. (1988) conducted steady-state tar and water core flooding experiments on Peace River cores using thermally unaltered, thermally altered and deasphalted tar. They reported the shift of relative permeability curves towards the region of low water saturation at high temperatures for thermally unaltered tar. While the curves were closer to the Leverett oil permeability curves for thermally altered tar, and in between those of thermally unaltered and altered for deasphalted tar. Watson and Ertekin (1988) studied the effect of steep temperature gradient on relative permeabilities experimentally. They used Berea sandstone and conducted experiments from ambient to 149°C using a mineral oil and brine as fluids. They observed increase of irreducible water saturation and decrease of residual oil saturation with temperature. They also reported the drop in both oil and water relative permeability values by temperature. They attributed the variations in end point saturations to wettability changes that occurred with temperature.

Polikar et al. (1990) reported the results of steady-state and unsteady-state core flooding experiments performed using Athabasca bitumen and water on both silica and reservoir sand. The experiments covered a wide temperature range of 100 to 250°C, and good agreement was achieved between both methods of measurement. No significant temperature dependency was reported for both oil and water curves by them. They concluded that it is not possible to predict theoretically what the effect of temperature on relative permeabilities could be, and the results are system specific. The results obtained in heavy oil systems do not apply in other systems due to viscous fingering dominations. Frizzell (1990) analyzed some results of laboratory high temperature relative permeability and end point saturation data, and proposed equations for estimating the end point saturations as well as relative permeabilities with temperature and oil gravity. They specified the applicability of the equation to the temperature range of 24°C to 204°C, and unconsolidated sand type of porous media.

Kumar and Inouye (1994) conducted dynamic displacement experiments and obtained low temperature analog of the high temperature relative permeability data. They suggested this method in the case the water to oil viscosity ratio at both temperatures and the wettabilities are the same. They reported that the measured end point saturations are temperature independent and only a function of viscosity ratio. The apparent temperature dependencies reported was shown numerically and analytically to be artifacts caused by viscosity ratio variations.

Akin et al. (1999) generated hypothetical core flooding data at differing temperatures using a numerical simulator by assuming the relative permeabilities, and then tried to calculate the relative permeabilities by JBN method from the production data generated by simulation. They figured out that JBN and like techniques can lead to erroneous temperature dependent relative permeabilities due to the instabilities and viscous

fingering in heavy oil systems. They proposed a three step laboratory method to conduct flooding experiments at three different temperatures, including an ambient temperature test. The pressure, production data and saturation history during the ambient temperature test was history matched by a simulator to obtain relative permeability data. These data were then used to match the results of the higher temperature experiments, which indicated no dependency of relative permeability data on temperature. They believed that reported dependencies on temperature in the literature are due to the drop in viscosity ratio.

Esfahani and Haghighi (2004) performed wettability and relative permeability tests at both ambient and reservoir temperature on Iranian carbonate rocks. They used graphical technical by Jones and Roszelle (1978) and obtained variations in relative permeability curves. Their wettability tests showed the samples became more oil-wet at higher temperatures. Schembre et al. (2006) used a novel method to estimate the relative permeability and capillary pressure from computerized tomography (CT) scanning of imbibitions experiments at high temperatures for diatomite rocks. They used both heavy crude oil and mineral oil in their studies, and observed a drop in remaining oil saturation and the water relative permeability end point with increasing temperature. They attributed this observation to the increase in more water wettability due to the fines mobilization at a certain temperature from the rock surface. Sedaee Sola et al. (2007) conducted unsteady-state relative permeability experiments to investigate the relative permeabilities in unpreserved limestone and dolomite cores. They used heavy oils from Iranian fields, and performed the experiments at reservoir conditions between 38 and 260°C. They reported the increase of irreducible water saturation and decrease in residual oil saturation with temperature. They reported some changes in the shape of relative permeability curves, and the shift to more water wettability for dolomite and reverse for limestone cores. Hamouda et al. (2008) conducted experiments on oil-wet chalk samples to investigate the interrelation of relative permeabilities with temperature and the effect of initial fluid and flooding fluid compositions on wettability changes. They addressed some effects of temperature on relative permeability curves. They reported a shift of relative permeability curves to right as in indication of more water wetness up to 80°C, and a tendency to more oil-wet behavior at higher temperature of 130°C.

Although there are some disagreements among authors in the literature, the most frequently observed relative permeability variations caused by temperature are the shift of water saturation range to higher values, increase in oil relative permeability at each water saturation point and vice versa for water relative permeability values. This is considered by many authors as an indication of more water wetness behavior of the rock at higher temperatures. Another possible explanation has been a dramatic drop in the oil to water viscosity ratio by increasing temperature. However, it is hard to judge about the

actual phenomenon that happens in heavy oil systems due to adverse mobility ratio conditions and the likelihood of viscous instabilities in those systems.

1.6 Thesis outline

Due to the wide variations between the experimental set-ups, and different systems being tested, there is no agreement among the authors on the effect of temperature on relative permeability curves. Researchers have used both mineral and crude oil in their studies. Some studies have been done on consolidated core samples while others have used unconsolidated material like sand packs or glass beads. Neither of the reported researches on this issue applies universally, as the temperature dependency issue is dependent on a complex mixture of several contributing parameters like the porous material used, wettability, IFT, viscosity of the fluids being tested, etc.

As the issue is case specific, it seemed necessary to conduct our own core flooding experiments and investigate the dependency of relative permeability curves on temperature in the specific porous material and oil combination that is of interest to us. The objective was to mimic the actual flow behavior in an Athabasca type reservoir. However, the reservoir sand from the field was not available for the studies. It was therefore decided to use artificial core plugs made of glass beads and sand. The objective was accomplished by performing core flooding experiments, displacing Athabasca heavy oil by hot water at different temperatures and using oils with varying viscosities. The production curves and pressure differential data in each experiment were history matched to get the oil and water relative permeabilities. Although not using the representative reservoir sand, the results presented can be of interest to one studying the temperature dependency issue of relative permeability data.

Because the main experimental focus of this work was on the effect of temperature on relative permeability data, the introduction of this thesis was totally devoted to the concept of relative permeability and its measurement methods.

Prior to the core flooding experiments, it was necessary to obtain some fluid properties (PVT) of the oil. The type of oil was Athabasca heavy crude (bitumen). Properties needed for reservoir simulation studies were obtained experimentally partly in the reservoir engineering laboratory at the department of petroleum engineering and applied geophysics (IPT) and partly in collaboration with SINTEF Petroleum Research. Chapter 2 of this thesis presents the basics of the methods used and the general results. The properties measured include the viscosity versus temperature, the molar mass, density at both standard condition and high temperatures and the interfacial tension between oil and steam at high temperature conditions. A gas chromatographic analysis of the bitumen sample is also presented. These experiments are presented in a paper in detail which can be found in the Appendix A.1.

Chapter 3 deals with the core flooding experiments. The laboratory set up is described and the procedures used are discussed. The packing procedures are given, and the flooding sequences conducted are presented. The method for history matching and the relative permeability correlations tested by the simulation software also comprise parts of this chapter. The general results obtained are given and discussed in this chapter. The detailed results, however, have been reported as two papers, which are attached as Appendices A.2 and A.3 in this thesis.

Chapter 4 of this thesis presents a paper dealing with numerical simulation studies of 1-dimensional steam flooding in a heterogeneous core. Chapters 3 and 4 comprise the one-dimensional flow part of this study. The remaining chapters will talk about two and three-dimensional flow in heavy oil systems.

Some numerical reservoir simulations were conducted using CMG© reservoir simulator to investigate field scale SAGD (Steam Assisted Gravity Drainage) and ES-SAGD (Expanding Solvent SAGD) processes. This work was performed as an extension to the temperature dependency of relative permeabilities issue. As such, temperature dependent relative permeability data were tested and compared to some fixed relative permeability data in this numerical model. The resulted paper is presented as chapter 5 of this thesis.

A paper including sensitivity analysis performed on different operating and reservoir parameters in a laboratory scale SAGD and SCI (Solvent Co-Injection) model using a numerical reservoir simulator is presented in chapter 6.

Chapter 7 summarizes the work performed and presents an overall conclusion of the experiments done during this study.

Chapter 2

Fluid Properties Measurement for Athabasca Bitumen

This chapter presents the results of fluid properties analysis of Athabasca bitumen. In order to study and model the fluid flow behavior in a reservoir, it is very important to obtain exact and complete data about the rock system, fluid properties and rock-fluid interactions inside the reservoir. The PVT data, among others, are crucial for reservoir modeling purposes. Some of these properties like fluid compositions, density, viscosity, molecular weight and oil/steam interfacial tension were obtained and presented for Athabasca bitumen. Athabasca heavy crude sample was separated to its components using Gas Chromatography (GC) to determine the percentage of each component. Two types of lighter heavy oil samples were prepared by diluting the Athabasca bitumen with a solvent. The dilution procedure and viscosity measurement for these two samples are also presented. These two oil samples were used for core flooding purposes, which will be presented in chapter 3. The detailed paper containing the experimental results can be found in the Appendix A.1.

2.1 Viscosity measurement

Viscosity is the major challenge while dealing with Athabasca bitumen and in order to produce such a viscous crude oil, it is necessary to reduce the viscosity using steam, solvent or both. Viscosity is the measure of the internal friction of a fluid. It is the resistance of a fluid to flow. This friction becomes apparent when a layer of fluid is made to move in relation to another layer. The greater the friction, the greater the amount of force required to cause this movement, which is called shear. Shearing occurs whenever the fluid is physically moved or distributed, as in pouring, spreading, spraying, mixing, etc. High viscous fluids therefore require more force to move than less viscous materials.

Isaac Newton defined viscosity by considering the model represented in Figure 2.1. Two parallel flat areas of fluid of the same size "A" are separated by a distance "dx" and are moving in the same direction at different velocities "V_1" and "V_2". Newton assumed that the force required to maintain this difference in speed was proportional to the difference in speed through the liquid, or the velocity gradient. To express this, Newton wrote:

$$\frac{F}{A} = \mu \frac{dv}{dx} \tag{2.1}$$

Where μ is a constant for a given material and is called its "viscosity".

The velocity gradient, *dv/dx*, is a measure of the change in speed at which the intermediate layers move with respond to each other. It describes the shearing the liquid experiences and is thus called "shear rate". This is symbolized as "$\dot{\gamma}$". Its unit of measurement is called the "reciprocal second" (sec^{-1}).

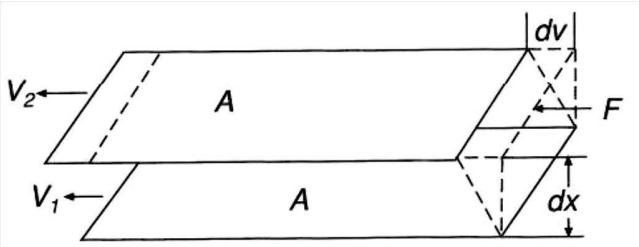

Figure 2.1 Newton's model for viscosity definition

The term *F/A* indicates the force per unit area required to produce the shearing action. It is referred to as "shear stress" and will be symbolized by "τ". Its unit of measurement is "dynes per square centimeter" ($dynes/cm^2$) or "Newtons per square meter" (N/m^2). Using these simplified terms, viscosity may be defined mathematically by this formula:

$$\mu = \text{viscosity} = \frac{\tau}{\dot{\gamma}} = \frac{\text{shear stress}}{\text{shear rate}} \tag{2.2}$$

The fundamental unit of viscosity measurement is "poise". A material requiring a shear stress of one dyne per square centimeter to produce the shear rate of one reciprocal second has a viscosity of one poise, or 100 centipoises. The International System units of viscosity are "Pascal-seconds" (Pa.s) or "milli-Pascal-seconds" (mPa.s). One milli-Pascal-second is equal to one centipoise.

The viscosity measurement for Athabasca bitumen was done using a Brookfield LVDV-II+Pro viscometer. This viscometer comes with a thermo container (Thermosel accessory) and a programmable temperature controller which allows the measurement of viscosity from ambient temperature up to 300 °C at specified and controlled temperatures. The viscometer is shown on Figure 2.2 together with Thermosel accessory and temperature controller unit. The principal of operation of the DV-II+Pro is to drive a spindle (which is immersed in the test fluid) through a calibrated spring. The viscous drag of the fluid against the spindle is measured by the spring deflection. Spring deflection is measured with a rotary transducer. The measurement range of a DV-II+Pro (in centipoises or milliPascal seconds) is determined by the rotational speed of the spindle, the size and shape of the spindle, the container the spindle is rotating in, and the full scale torque of the calibrated spring.

2.1.1 Athabasca bitumen viscosity

The bitumen sample used is obtained from an oil sand reservoir in Athabasca region, produced using SAGD method. The sample has not been exposed to any solvent and the condensed water produced together with the bitumen has been removed at high temperature. The viscosity measurements were started at the ambient temperature of 21°C, and the temperature was raised in 10°C intervals up to 300°C. At each temperature sufficient time was allowed to have a uniform sample at the desired temperature and a steady viscosity reading. A whole range of viscosity for bitumen sample versus temperature from ambient up to 300°C was obtained in two days. Two sets of measurements were done to make sure about the reproducibility of the data. Figure 2.3 compares our measured viscosity data versus bitumen viscosity given by Mehrotra and Svrcek (1986). Tabulated viscosity data versus temperature can be found in our paper given in Appendix A.1.

Khan et al. (1984) presented empirical correlations for the effect of temperature on the viscosity of gas free Athabasca bitumen. One of their correlations is given as below:

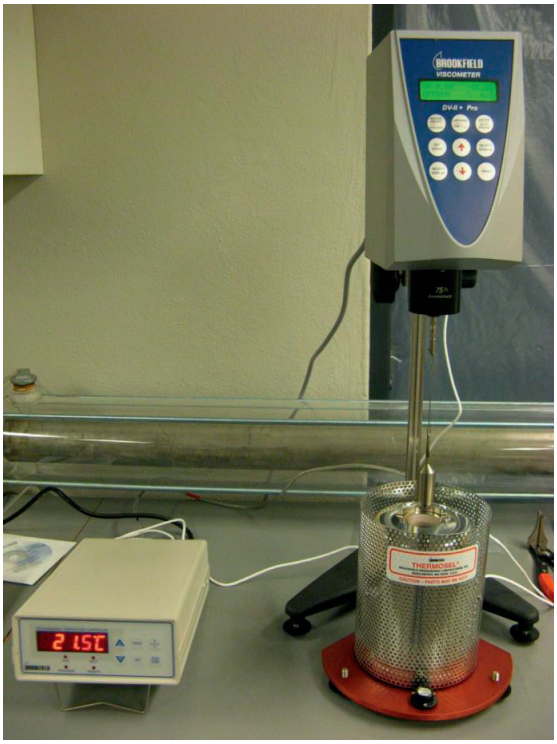

Figure 2.2 Brookfield LVDV-II+Pro Viscometer with Thermosel accessory and temperature controller unit

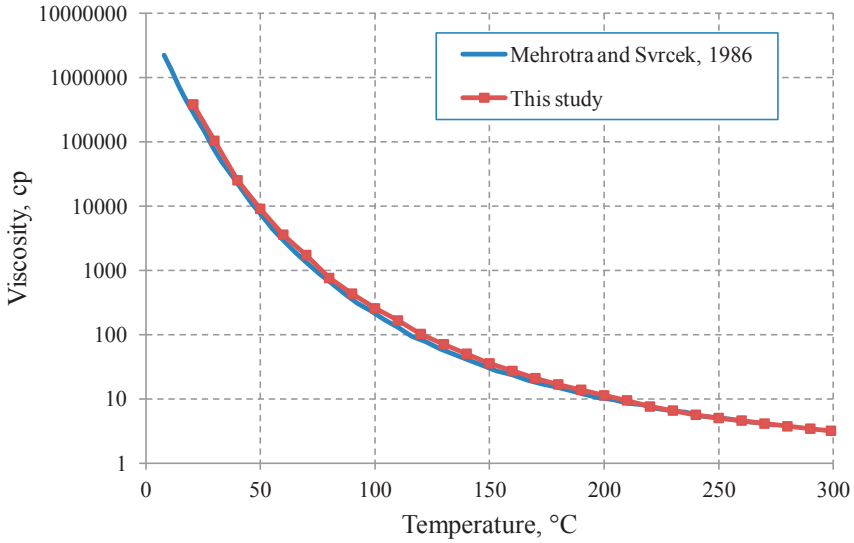

Figure 2.3 Viscosity of Athabasca bitumen versus temperature

$$\ln\ln(\mu) = c_1 \ln T + c_2 \tag{2.3}$$

In this equation μ is dynamic viscosity of heavy oil sample in "mPa.s" or "cp", at atmospheric pressure and temperature T (K). The constants c_1 and c_2 are empirical and can be found for each sample using experimental data. They can be determined using the least square parameter estimation technique. A graphical representation of double logarithm of viscosity versus logarithm of absolute temperature is presented in Figure 2.4. This figure compares laboratory measured viscosity data in this study with the viscosity correlation fit according to equation (2.3) for 4 different bitumen samples as given by Khan et al. (1984). They fit the viscosity data for 4 bitumen samples and presented the constant values of equation (2.3) as given in legends of Figure 2.3 as well as Table 2.1. The equation for the line, fitting our laboratory data points, is also shown in Figure 2.3, which is in good agreement with Khan et al. (1984) data. A comparison of the viscosity correlation constants can also be found in Table 2.1.

Table 2.1 Empirical constants of linear viscosity relation for our bitumen sample compared with the data given by Khan et al. (1984)

Sample No	C_1	C_2
1 (Khan et al., 1984)	-3.62722	23.2200
2 (Khan et al., 1984)	-3.57379	22.8379
3 (Khan et al., 1984)	-3.73360	23.8162
4 (Khan et al., 1984)	-3.56718	22.7823
This study	-3.59120	22.97600

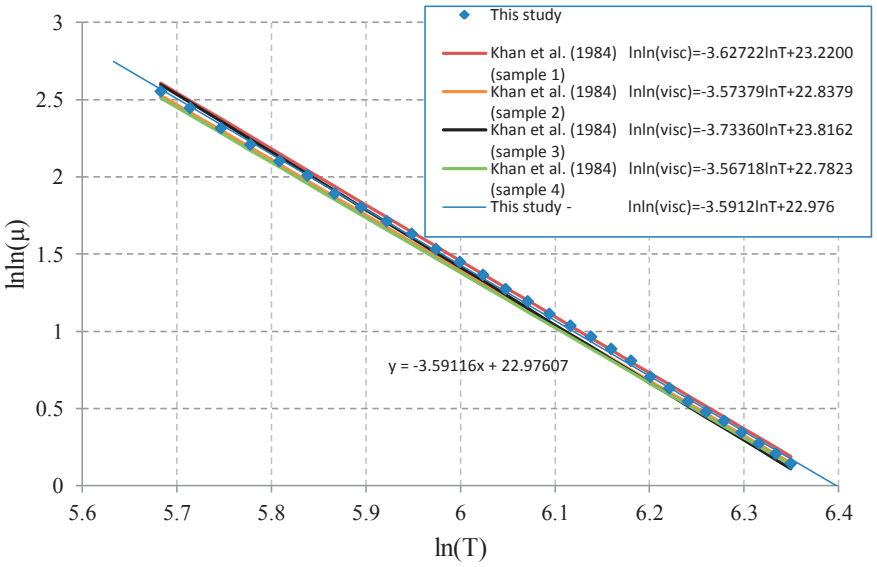

Figure 2.4 Bitumen viscosity correlation – double logarithm of viscosity shows straight line behavior versus logarithm of temperature

2.1.2 Oil dilution and diluted oil viscosity

In order to perform core flooding experiments investigating the effect of oil viscosity, Athabasca bitumen was diluted using normal-dodecane. Bitumen was added to n-dodecane in known amounts, and the mixture was stirred on a magnetic stirrer. Two types of oil were prepared. One sample is composed of 90% bitumen mixed with 10% n-C_{12}, and another which is 80 % bitumen and 20% n-C_{12} on a mass basis. These oils are referred to as OIL10 and OIL20 respectively. The properties of bitumen and these two oils are shown in Table 1. Molar mass and density of bitumen is measured experimentally, and will be presented in the other sections in this chapter.

Table 2.2 Oil properties for diluted oil samples OIL10 and OIL20

Component	Molecular Weight (g/gmole)	Density (g/cc)
Athabasca bitumen	534	1.0129
n-dodecane (n-C_{12})	170.34	0.748
OIL10	440.1	0.9783
OIL20	374.2	0.9459

The viscosities of these two oils are also measured using Brookfield viscometer as done for Athabasca bitumen. The viscosity measurements were done again in 10°C intervals,

and with sufficient time at each temperature step to read a steady viscosity reading. However, for OIL10 and OIL20, the measurements were done up to 70°C and extrapolated for higher temperature values. This was due to the possibility of n-dodecane evaporation at higher temperatures. The extrapolation was done using the empirical equation (2.3) given by Khan et al. (1984).

The values of empirical constants c_1 and c_2 for the bitumen, OIL10 and OIL20 are presented in Table 2.3. The viscosity versus temperature curve is also shown in Figure 2.5.

Table 2.3 Empirical constants of viscosity correlation (eq. 2.3) for Athabasca bitumen, OIL10 and OIL20

Component	c_1	c_2
Athabasca bitumen	-3.5912	22.976
OIL10	-3.4563	21.872
OIL20	-3.5094	21.905

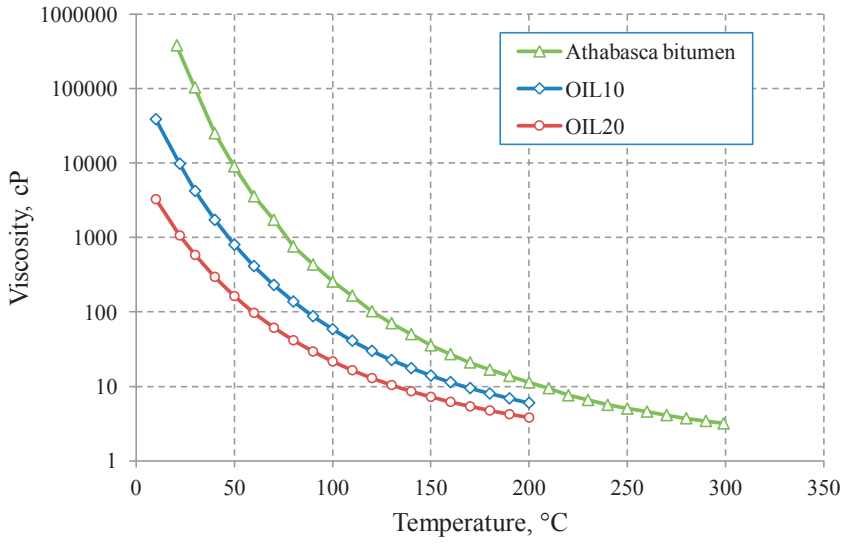

Figure 2.5 Viscosity of Athabasca bitumen compared to OIL10 and OIL20 versus temperature

2.2 Bitumen compositional analysis

The composition of the bitumen sample used in this study was determined using gas chromatographic (GC) analysis. The detailed GC analysis procedure and results can be found in the paper in Appendix A.1. The compositional analysis of the Athabasca oil is

presented in Table 2.4. The primary data obtained from GC analysis are the concentrations by weight. The weight percentages are given to three decimal places although the third decimal is uncertain. It is estimated that the results are accurate to the second decimal place. Molar concentrations are derived values calculated on the basis of the weight percentages, the Katz-Firoozabadi generalized properties (1978), and molar mass measured by cryoscopy (See section 2.3).

Table 2.4 Compositional analysis of Athabasca oil

Pseudo-component	Amount (Weight %)	Amount (mol. %)	Molar mass[a] (g/mol)	Density[a] (g/cm^3)
C_{10}	0.211	0.842	134.0	0.7780
C_{11}+C_{12}	0.948	3.286	154.0	0.7945
C_{13}+C_{14}	1.976	5.782	182.5	0.8165
C_{15}+C_{16}	3.006	7.501	214.0	0.8355
C_{17}+C_{18}	3.731	8.166	244.0	0.8495
C_{19}+C_{20}	4.068	8.075	269.0	0.8595
C_{21}+C_{22}	3.959	7.094	298.0	0.8695
C_{23}+C_{24}	3.759	6.186	324.5	0.8790
C_{25}+C_{26}	3.594	5.453	352.0	0.8870
C_{27}+C_{28}	3.602	5.048	381.0	0.8945
C_{29}+C_{30}	3.437	4.487	409.0	0.9005
C_{31}+C_{32}	3.265	3.989	437.0	0.9075
C_{33}+C_{34}	2.577	2.959	465.0	0.9130
C_{35}+C_{36}	2.599	2.815	493.0	0.9180
C_{37}+C_{38}	2.309	2.366	521.0	0.9230
C_{39+}	56.960[b]	25.950	11.72.1[c]	1.1474[d]
Total/Average	100.000	100.000	534.0	1.0129

a Molar mass and density for pseudo-components up to C_{38} are according to the Katz-Firoozabadi generalized properties (1978). Property values for combined fractions C_{11}+C_{12} to C_{37}+C_{38} represent averages.

b The C_{39+} fraction consists of characterized material (9.133 wt %) plus material unaccounted for in the analysis (47.827 wt %) (See Appendix A.1).

c Calculated using measured molar mass 534 g/mol (See section 2.3).

d Calculated using measured oil density 1.0129 g/cm^3 at standard conditions (1 atm, 60 °F) (See section 2.4).

2.3 Molecular weight measurement

Molar mass of the oil was measured by freezing point depression (cryoscopy) using a Roebling Kryometer. The freezing point of a solution is lower than that of the pure solvent, and for a dilute solution the freezing-point depression (ΔT) is directly proportional to the molar concentration of the solute. When the molar concentration is expressed as a molality, the proportionality constant is known as the cryoscopic constant (K_f) and is characteristic for the solvent. If w represents the mass fraction of the solute in solution, and assuming no dissociation of the solute, the molar mass is given by:

$$M = \frac{wK_f}{\Delta T} \tag{2.4}$$

The molar mass of the crude oil was determined by adding a known weight of crude oil to benzene and measuring the freezing point depression of the solution relative to the freezing point of pure benzene. The molar mass of Athabasca crude oil was measured to 534 ± 2 g/mol.

2.4 Bitumen density measurement

Oil density was measured by an Anton Paar density measuring cell for high pressure and high temperature. The instrument was calibrated by use of nitrogen gas and pure water at the temperatures for which oil density was measured. Due to the high viscosity of bitumen at room temperature, the cell was heated during the injection of bitumen. The cell was then cooled down to standard temperature (15.56°C). The density measurement was then performed at several pressures, namely 5, 10, 15, 20 and 25 bara (bar absolute). The reason for making measurements at higher pressures than atmospheric condition was very high viscosity of bitumen at standard condition (SC). This high viscosity causes the pressure readings to be less reliable at lower pressures. The results of density measurement at 15.56°C are shown in Figure 2.6. As depicted on this figure, the density shows a linear relation with pressure in the 5-25 bara pressure range. Extrapolation of this data to atmospheric pressure gives the density of bitumen at standard condition (1.01325 bara, 15.56°C) with a good accuracy. The resulted value is 1.0129 g/cm^3.

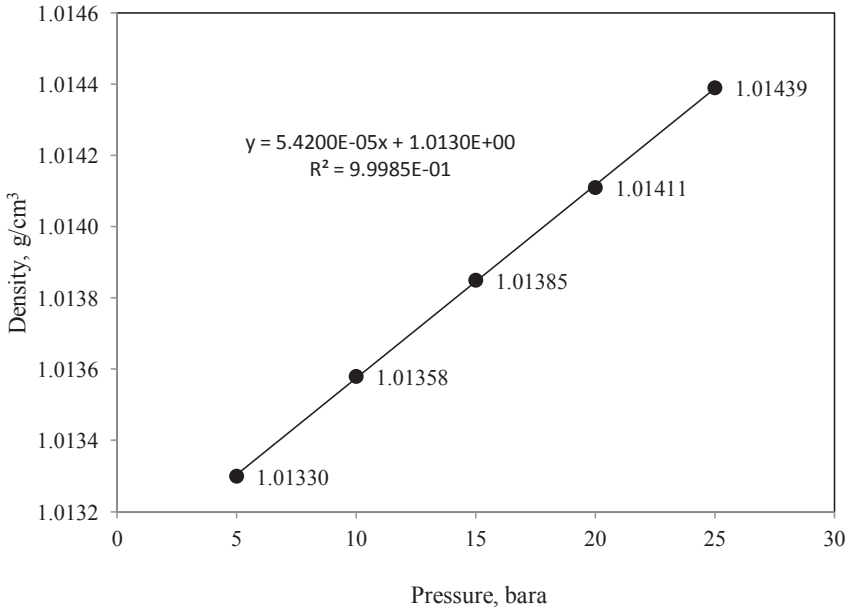

Figure 2.6 Density of Athabasca bitumen versus pressure at 15.56°C

The density measurement for the bitumen was also performed at the constant pressure of 20 bara and the temperatures of 120°C, 140°C, 160°C, 180°C and 195°C. This upper limit was due to heating limitations. Figure 2.7 shows these results. This pressure condition was the calibration pressure of the device. As seen on this figure (Figure 2.7) the oil densities measured are also showing a straight line behavior versus temperature.

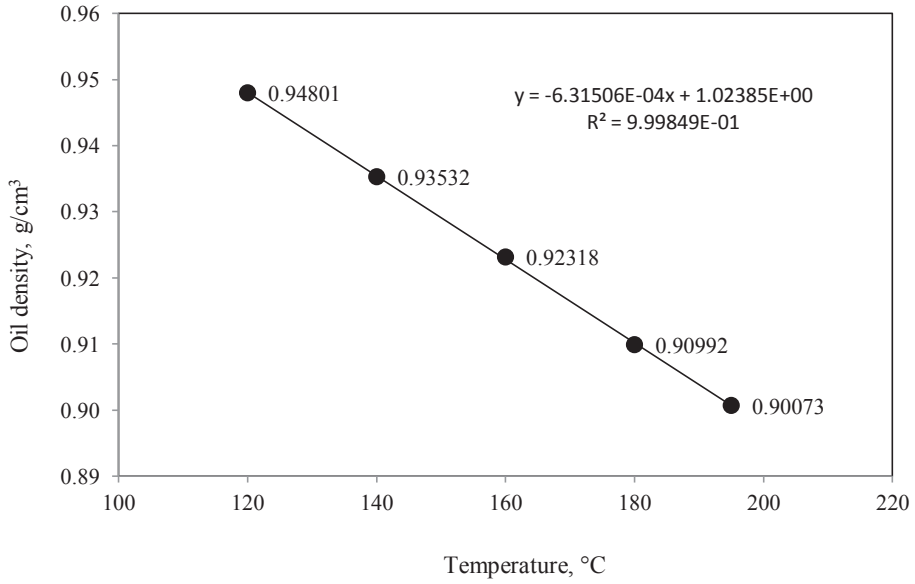

Figure 2.7 Density of Athabasca bitumen versus temperature at 20 bara

The measurement of density was also performed at the other pressures of 5, 10, 15 and 25 bara for the same temperature values as done for 20 bara. The oil density was found to have linear relationship with pressure at all temperature steps tested in this study. The slopes of these linear regression lines of density versus pressure are shown for each temperature value on Figure 2.8. These data also fall on a linear line function of temperature. The linearity of the data in Figures 2.7 and 2.8 suggested the following relationship for the density of Athabasca bitumen (ρ_o) versus temperature (T) and pressure (P), which is valid in the experimental temperature and pressure range studied (120-195°C, 5-25 bara):

$$\rho_o\left(T,P\right)=\rho_o\left(T,P_{ref}\right)+\left(\frac{\Delta\rho_o}{\Delta P}\right)_T\left(P-P_{ref}\right) \tag{2.5}$$

$$=\left[A\left(T-T_{ref}\right)+B\right]+\left[C\left(T-T_{ref}\right)+D\right]\left(P-P_{ref}\right)$$

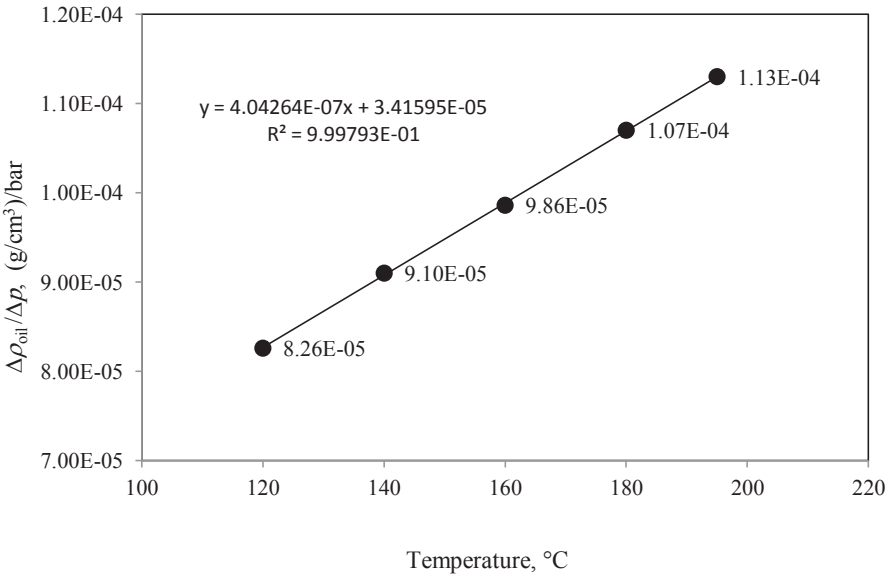

Figure 2.8 Pressure sensitivity of Athabasca oil density in the range 5-25 bara versus temperature

Where, T_{ref} is a reference temperature in the middle of the range 120-195°C, arbitrarily set to 160°C, whereas P_{ref} is the reference (calibration) pressure, 20 bara. Assuming that the density is given in units of [g/cm^3], temperature in [°C] and pressure in [bara], the constants A, B, C and D are given by:

$$A = -\left(6.32 \pm 0.04\right) \times 10^{-4} \qquad [\text{g/cm}^3/\text{°C}]$$

$$B = 0.9228 \pm 0.0001 \qquad [\text{g/cm}^3]$$

$$C = \left(4.04 \pm 0.03\right) \times 10^{-7} \qquad [\text{1/(bar.°C)}]$$

$$D = \left(9.88 \pm 0.01\right) \times 10^{-5} \qquad [\text{1/bar}]$$

Extrapolation of equation (2.5) to standard temperature of 15.56°C at the pressure of 20 bara yields the value of 1.0141 for the density, which is in excellent agreement with the value measured (Figure 2.6). Extrapolation of this density relation to lower temperature range is valid at the reference pressure, for which the pressure correction term is zero. However, we should mention that the pressure correction term is small compared to the dominating term (around three orders of magnitude), and the extrapolation to lower temperatures at other pressures will probably not result in a significant loss of accuracy. The density value estimation at SC (15.56°C, 1.01325 bara) from equation (2.5) is 1.0133 g/cm^3, which is in good agreement with the experimental value of 1.0129 g/cm^3, and the error is less than 0.04%.

2.5 Interfacial tension measurement

The interfacial tension analysis involved determination of the equilibrium shape of oil drops suspended at a needle tip surrounded by steam. The drop shape reflects the balance between IFT and gravity. Mathematically this balance is described by the Young-Laplace equation (which relates the pressure difference across a curved interface with the IFT). Given the density difference between oil and steam, the IFT is calculated by matching a numerical integration of the Young-Laplace equation to the observed drop shape. For details, see Jennings and Pallas (1988). The analysis was performed by use of in-house data analysis software. Details of the apparatus and the procedure used can be found in the paper in Appendix A.1.

The IFT between Athabasca crude oil and steam was measured in two measurement series A and B involving different samples of oil. Measurements were first taken at 160°C, 180°C, 200°C and 220°C (Sample A). For the second sample labeled B the IFT measurements were performed in steps of 20°C between 120°C and 200°C. The test drops are denoted by Series/Temperature/Number (e.g. A/160 °C/#1). Tabulated results for individual test drops are given in the paper in Appendix A.1.

The basic quantity measured by the drop shape method is the ratio between IFT and the density difference between drop and surrounding medium, (IFT/$\Delta\rho$). IFT values were calculated from the primary pendant drop data by use of oil density values given by equation (2.5) and steam density values calculated from the Wagner-Pruss (2002) equation of state, using in-house software. It is assumed that equation (2.5) can be extrapolated to 220 °C. It is further assumed that equilibration of oil and steam did not change either oil or steam densities significantly from the pure-substance values.

Average IFT values at the experimental temperatures of series A and B are presented in Table 2.5 and Figure 2.9. The error bars on the plotted average values in Figure 2.9 represent the standard deviation of the individual measurements (not that for the mean)

Table 2.5 Average initial and equilibrium interfacial tension values in Series A and B

Series	Average temperature (°C)	Average pressure (bara)	Initial IFT (mN/m)	SD[a] initial IFT (mN/m)	Equilibrium IFT (mN/m)	SD[a] Eq. IFT (mN/m)
A	159.95	4.29	23.17	0.08	19.31	0.31
A	180.03	8.56	22.82	0.16	19.00	0.18
A	199.95	13.71	21.17	0.51	19.39	0.21
A	220.11	20.32	20.60	0.11	18.30	0.28
B	120.03	1.86	24.80	0.17	25.19	0.60
B	140.08	3.01	24.80	0.66	23.10	1.21
B	159.94	5.51	23.79	0.38	22.63	0.14
B	179.88	8.22	22.82	0.19	21.16	0.11
B	200.02	14.11	21.48	0.09	19.62	0.02

a Standard deviation of individual measurements (not for the mean).

to indicate the spread of the data being averaged. Both oil samples yield similar results in the high-temperature range and the IFT does not change much during ageing of the oil/steam interface. At lower temperatures (below 200°C) the two samples yield quite different equilibrium IFT values although the initial values are quite similar. The IFT for sample A decreased during ageing of the oil/steam interface, however, the trend of IFT values were increasing for sample B during the aging of the drops. For detailed discussions and graphs showing the trends of IFT values over time refer to the paper in Appendix A.1. The two samples did probably differ in content of polar/surface-active components. The two measurement series may indicate a natural range of IFT variation. It is not possibly to say that one sample is more representative than the other. All that can be said is that the IFT value in the temperature range 120-220°C can be expected to fall between upper and lower bounds as indicated in the figure.

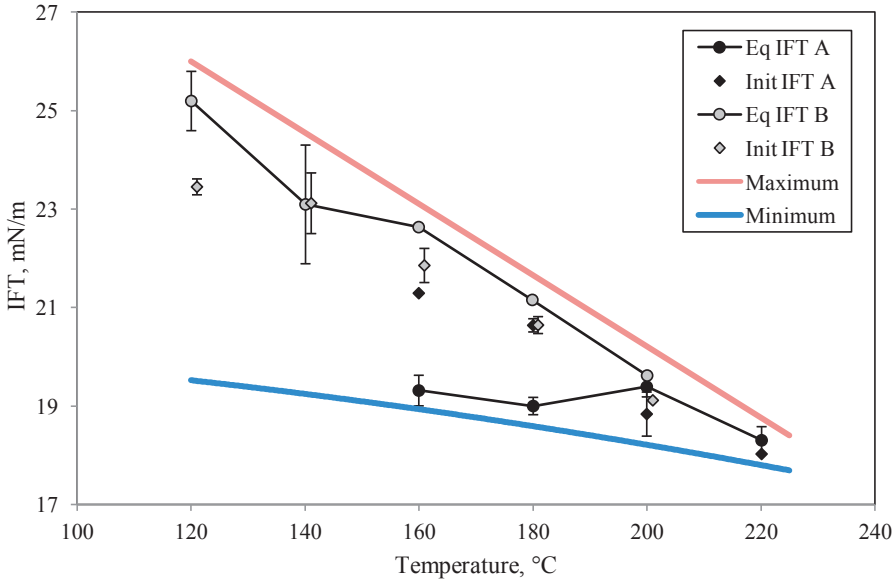

Figure 2.9 Initial and equilibrium interfacial tension between Athabasca oil and steam (some data points have been shifted slightly along the temperatures axis for clarity).

Chapter 3

Core Flooding Experiments and Relative Permeability Measurements

The following chapter contains the discussions regarding the relative permeability measurements conducted during this study. The core flooding experiments were aimed to study the effect of temperature on the resulting relative permeability curves. The procedures for packing and preparing artificial unconsolidated cores have been described. The laboratory set-up is presented, and the flooding sequences and procedures have been explained in details. The stability criteria for flooding are given and the relative permeability measurement method is discussed in this chapter. The chapter also includes the results of relative permeability measurements at different temperatures and using oils with varying viscosities. The results are compared and discussed at the end of this chapter. Although the chapter contains the main experimental results, the details can also be found in Appendices A.2 and A.3, where two main papers based on the laboratory experiments are presented.

3.1 Experimental procedures and apparatus

The procedures performed during core floodings and the laboratory set-up and equipment used are discussed in this section.

3.1.1 Porous media

Unconsolidated porous media was preferable as it better represents the oil sand reservoirs and the flooding of high viscous oil is much easier without building up high pressures at the injection side of the cores. Due to unavailability of preserved sand material from field, artificial core plugs made of sand and glass beads were used instead. The glass beads with two different size ranges were chosen to represent varying reservoir absolute permeabilities. One set of packs were prepared with 1 millimeter size glass beads, and another set were comprised of glass beads of size range 300-425 micron (μm). Sand packs were made of acid washed sand. For the simplicity we will name the glass bead packs as GB and the sand packs as SP. Two flooding experiments were also accomplished on sandstone core plugs. The type of sandstone was Bentheimer. These two flooding experiments, however, were conducted only using the lower viscous type of oil, as the pressure transducers used were sensitive and in the low pressure range.

3.1.2 Packing procedure

For preparation of the sand or glass bead packs, sand particles or glass beads of different size were packed inside a rubber sleeve. Two metal screens were placed on the top and bottom of the packed media inside the sleeve and in contact with end caps of core holder. These screens were used to obviously prevent the production or any movement of particles and at the same time evenly distribute the fluid at the injection port. The rubber sleeve was installed on the inlet end cap, and the metal screen was placed inside and in contact with the end cap face. They were then placed on an electric shaker. While the shaker was running the sand or glass beads were poured using a funnel until having a pack of desired length. The same packing procedure was always used to make sure we have a homogeneous medium. The diameter of the pack was 3.8 cm (1.5 inches) and the length was 21 cm. The inlet end cap was then installed on the core holder, the second metal screen was placed on top of the packed core, and the outlet end cap was installed and pressed firmly on the packed core. The metal screens were the same size as inside diameter of the sleeve, sitting there tightly and the combination of firm end caps on the packs and a high enough overburden pressure around the sleeve would make the movement of particles impossible. This was always investigated visually at the end of all experimental runs, and no movement of metal screens or disorder of the packed particles were observed at the end of any run.

3.1.3 Core flooding set-up

The flooding set up consists of different apparatuses and parts that will be presented in more details. A schematic view of the set-up is shown in Figure 3.1. It consisted of the following equipments.

3.1.3.1 Core holder

The core holder assembly was comprised of a stainless steel 48 cm long core holder that can withstand high temperatures up to 150°C. The core holder was installed on a metal frame stand that allowed the core holder to be placed in a horizontal or vertical position as required by the user. The length of the core holder was enough to allow the use of longer cores of size 21 cm. Both end caps of the core holder have one port for either injection or production of fluids, and the face of the end caps are equipped with flow distributors to allow an even injection or production at the whole area of the core. Both end pieces have a diameter of 3.8 cm (1.5 inches). A rubber sleeve of this ID (Inner Diameter) could be installed on these end caps. The annular space between the sleeve and core holder was filled with high viscosity paraffin, which was used to provide a constant overburden pressure on the core.

3.1.3.2 Overburden pressure equipment

The pressure around the rubber sleeve was maintained using viscous paraffin with a viscosity of around 120 cp at room temperature. The paraffin was stored in a cylinder

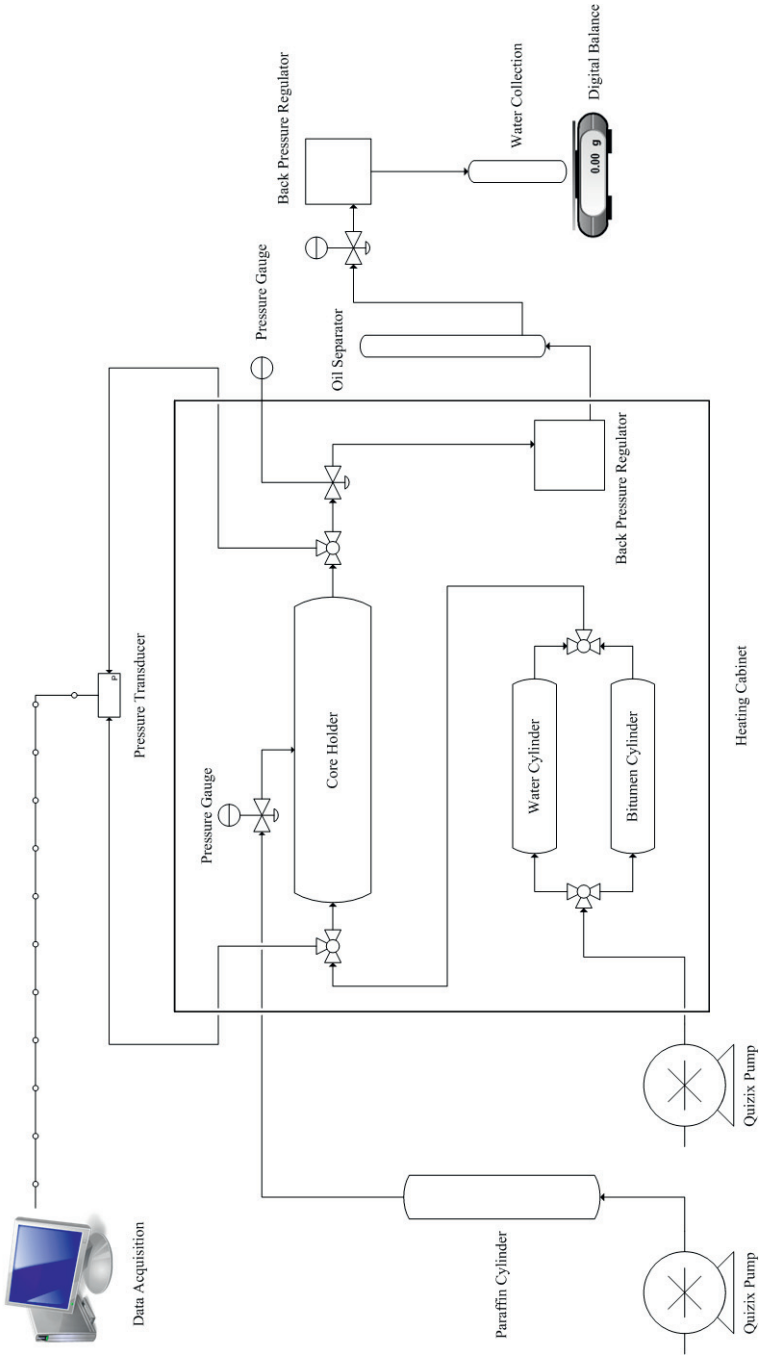

Figure 3.1 Schematic representation of core flooding setup used in this study

equipped with a floating piston. The pressure was provided by distilled water behind the piston using a Quizix positive displacement pump. The pump was a Q-5000-10k with the operating range of 0.000018ml/min – 15 ml/min. This pump could be set to operate at a constant pressure by either displacing or recovering the water. In this way it was possible to keep a constant overburden pressure by recovering the extra paraffin due to the expansion at higher temperatures during the experiments. A pressure gauge was placed on the paraffin line to the core holder to show the pressure.

3.1.3.3 Heating cabinet

Core holder was placed inside an oven to perform the core flooding tasks at the desired temperatures. The oven could operate at any desired temperature up to 300°C. The oven was equipped with window panels. Therefore the pressure gauge on the viscous paraffin line was visible, and it was possible to check the overburden pressure at all times. Another advantage of these panels was the possibility of checking the vessels for any leakage during the runs. Two fans were circulating the air which could provide a constant temperature inside the oven.

3.1.3.4 Injection equipments

The injection equipments consisted of cylinders and a pump. Two separate cylinders equipped with floating type pistons were holding the oil and water for injection purposes. These were placed inside the heating cabinet. The pistons were displaced by distilled water using a Quizix pump that could operate at either constant rate or pressure. The pump was a QX-6000 with operating range of 0.001 ml/min – 50 ml/min. The water and oil were stored inside the cylinder for a long enough time to allow them to expand and reach the constant desired temperature. The constant pressure mode of operation in the pump was used during these phases by recovering the expanded fluid. During the injection phases, however, the pump was operating at a constant rate.

3.1.3.5 Production equipments

The main part of the production collection system was an oil/water separator, which was placed outside the oven on the production line. The separator had a glass tube, which was graduated to make it possible to read the position of oil and water meniscus accurately. The separator was filled initially with water, and the effluent was entering the separator from the bottom through a tube which had been immersed further inside the separator, such that the oil drops were visible. The oil was collected on the top of the separator and the water was produced from a port at the bottom. The volume of oil produced could be read by visual inspection through graduated glass tube of the separator. Two back pressure regulators (BPR) were used in the set-up. One was placed inside the oven and before the separator. This BPR was maintaining the pressure inside the system at a high enough level to make sure the water is in liquid phase. Another BPR was placed outside the heating cabinet and after the separator. This BPR was regulated at a marginal pressure above the atmospheric condition to prevent evaporation

as the effluent was leaving the oven. The produced water was accumulated on a digital scale after leaving the second BPR.

3.1.3.6 Pressure measurement

The pressure drop across the core was monitored using a Keller pressure transducer that has a 0-3 bar operation range. The transducer was connected to a PC through a transmitter that comes with the transducer. It therefore made it possible to keep the track of pressure continuously and accurately. The pipe lines connecting the pressure transducer to the two sides of the system were always cleaned with solvents and were filled with Exxsol D-60 (a type of synthetic oil) before each stage of the experiments. All the efforts were made to prevent trapping of air inside these lines and have a continuous liquid phase for accurate pressure readings. These lines were connected to the set-up using 3-way valves on the injection and production lines. A pressure gauge on the production line was showing the pressure inside the system at all stages.

A view of the set-up is shown on Figure 3.2. The pumps and the separator are also shown in this figure.

(a) Heating Cabinet

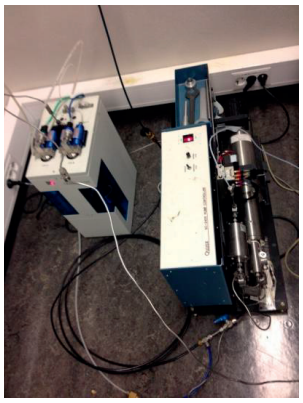

(b) Quizix Pumps

(c) Separator

Figure 3.2 Different parts of the core flooding set-up and apparatuses used in this study

3.1.4 Flooding sequence and procedures

The packed porous media was installed inside the core holder. After providing the overburden pressure of 25 bars, the packed porous media was saturated with distilled water using a vacuum pump. The porosity of the pack was calculated by doing a material balance on the amount of water left and knowing the exact value of the dead volume of pipes connected to the core.

The absolute permeability of the packed core was measured by flooding with water vertically upwards, and recording the pressure using Keller pressure transducer with the operational range of 0-3 bars. For absolute permeability measurement the core was flooded at different injection rates to make sure about the linearity of the pressure differential variations with the injection rate. The core holder was then placed inside the oven in horizontal position, and water injection was performed until reaching the desired temperature and pressure inside the core. For this condition to reach, the core holder was kept inside the oven overnight.

In the next step, oil was injected at a rate of 0.5 cc/min to initialize the core and calculate the initial water saturation (S_{wi}). Oil injection was continued at S_{wi} to measure effective oil permeability. The front was always sharp and no more water production was observed after the oil breakthrough. The graduated cylinder containing the produced water and oil on top was kept at a temperature of around 40°C for one or two days to make the meniscus clear, and make the produced water reading more accurate.

After initializing the core, the separator was connected and the imbibition process was initiated by injecting water at a rate of 0.8 cc/min. This rate was even less than 1 PV/h as recommended by Polikar et al. (1990). The injection rate used translates to a velocity of 1 m/day. During the water injection phase, the oil production was recorded versus time visually through the graduated glass tube of the separator, and the pressure differential across the core was monitored continuously. The mass of water accumulated on the digital scale represented the total oil and water production. The water injection was continued for almost 20 hours, which was enough to inject about 13 pore volumes (PV) of the packed core. After the experiment, the separator was disconnected and held at a temperature of 40°C for a few days in order for the oil/water meniscus to be separated completely and any possible adjustment to the final oil recovery to be done.

A complete experiment was conducted in almost a week, allowing the core to stay overnight at the constant temperature between each stage of the experiment.

3.2 Relative permeability calculation technique

In this section we will first talk about the stability criteria regarding the imbibition of water displacing the heavy crude and then the method used for relative permeability calculation will be discussed:

3.2.1 Stability criteria and stabilized flow consideration

The nature of heavy oil systems makes the displacement process more difficult. Very high viscosity of heavy oil results in unfavorable mobility ratios, when being displaced by a less viscous immiscible phase like water. Viscous fingering seems to be an inevitable phenomenon in such a system. Some researchers have studied the conditions that lead the initiation of viscous fingering in displacement tests (Peters & Flock, 1981; Bentsen, 1985). Peters and Flock (1981), for example, have presented the following dimensionless instability number to evaluate the onset of viscous fingering in core flooding experiments:

$$I_{sc} = \frac{(M-1)(v-v_c)\mu_w D^2}{C^* \sigma k_{wor}} \tag{3.1}$$

Where, I_{sc} is a dimensionless stability number, M represents the mobility ratio, v and v_c are the constant superficial and characteristic velocities, D is the core diameter, C^* is the wettability number determined experimentally, k_{wor} is the permeability to water at residual oil saturation, μ_w is water viscosity and σ represents the interfacial tension.

According to them, a core displacement test will be piston like and without viscous fingers, if the value of dimensionless instability number is less than 13.56. Maini and Okazawa (1987) stated that for a typical heavy oil reservoir, where the viscosity ratio is about 1000 to 10000, very low displacement velocities of 1 cm/day is necessary to achieve a stable front. Such a low frontal displacement velocity is extremely time-consuming to conduct in most of the laboratory applications. Very low displacement rate is not only hard to conduct, but also not practical in laboratory applications.

The low displacement velocity requirement for stability considerations is in conflict with the condition for stabilized flow. A displacement experiment needs to be done at a high enough rate to eliminate the capillary end effects and meet the criteria of being stabilized. The scaling coefficient for stabilized flow presented by Rapoport and Leas (1953) is $LV\mu_w$, which can be used to figure out the minimum injection rate to have the lowest possible capillary end effects. According to Rapoport and Leas (1953), there exists a critical value of scaling coefficient above which the breakthrough recovery becomes independent of this scaling coefficient. However, as already stated the requirements of stability and stabilized flow are in conflict, as the injection rate needs to be low to meet the former and at the same time be high enough to meet the latter. It seems to be impossible in heavy oil systems to meet both of these two criteria. In this work we have almost the same core dimensions and injection criteria close to the work of Polikar (1987). The core flooding seems to be stabilized, however, viscous fingering and instability of the front is not easy to prevent.

3.2.2 History matching method and relative permeability correlations used

As highlighted in the introduction, the calculation of relative permeabilities from displacement experiments data can be done by either explicit methods or implicit techniques. The explicit methods mostly used are the JBN (Johnson, Bossler & Naumann) technique (Johnson et al., 1959) and its modified version by Jones and Roszelle (1978).

Akin et al. (1998) generated hypothetical core flooding data at differing temperatures using a numerical simulator by assuming the relative permeabilities, and then tried to calculate the relative permeabilities by JBN method from the production data generated by simulation. They figured out that JBN and like techniques can lead to erroneous results. Due to the instabilities and viscous fingering in heavy oil systems, use of JBN technique results in a false temperature dependant behavior of relative permeabilities. Jones and Roszelle technique is based on differentiating the experimental data graphically which lead to some inaccuracies particularly if there is much scatter in the data (Polikar, 1987). This is the case when we are trying to displace the very viscous oil by lower viscous water phase, and the pressure differential data shows much more fluctuations compared to the lower viscosity oil displacement by water.

Due to the deficiencies mentioned above for the application of JBN and like methods to the heavy oil systems, we decided to use the implicit methods. The implicit method or history matching is based on numerical calculation. The relative permeability correlation parameters are adjusted to match the production and pressure differential data from core flooding experiments (Wang et al., 2006). The history matching of data was done using the core flooding simulator Sendra 2012. This software is a two-phase one dimensional black-oil simulation model used for analyzing SCAL (special core analysis) experiments. It is tailor made for revealing relative permeability and capillary pressure from two-phase and multi-phase flow experiments performed in the SCAL laboratory (Sendra user guide, 2012). This software acts as both a core flooding simulator and a history matching tool. Through history matching function, one can match the experimental data by adjusting the relative permeability curves. This is done by choosing the appropriate relative permeability correlation in the simulator. The software is then varying the empirical parameters in the function trying to match the experimental data. For the estimation method used in Sendra, refer to the software manual (Sendra user guide, 2012). There are several relative permeability correlations included in this simulator. Below is a review of these correlations. The normalized water saturation is used in all correlations:

$$S_w^* = \frac{S_w - S_{wi}}{1 - S_{wi} - S_{or}} \tag{3.2}$$

For simplicity, the formulations are given for oil-water systems; however they behave similar for oil-gas and water-gas systems (Sendra user guide, 2012).

3.2.2.1 Burdine Correlation

$$k_{rw} = k_{rw}^{0}\left(S_w^*\right)^{\frac{2+3\lambda}{\lambda}} \tag{3.3}$$

$$k_{ro} = k_{ro}^{0}\left(1-S_w^*\right)^{2}\left(1-\left(1-S_w^*\right)^{\frac{2+\lambda}{\lambda}}\right) \tag{3.4}$$

Where, the superscript 0 means the end point value in the relative permeability curves, superscript * means normalized value for water saturation as defined by equation (3.2) and λ is the pore size distribution index (Burdine, 1953).

3.2.2.2 Corey Correlation

$$k_{rw} = k_{rw}^{0}\left(S_w^*\right)^{N_w} \tag{3.5}$$

$$k_{ro} = k_{ro}^{0}\left(1-S_w^*\right)^{N_o} \tag{3.6}$$

In these equations the parameters N_w and N_o are the water and oil Corey parameters. These parameters show the curvature of water and oil relative permeability plots (Corey, 1954).

3.2.2.3 Sigmund & McCaffery Correlation

$$k_{rw} = k_{rw}^{0}\frac{\left(S_w^*\right)^{N_w} + AS_w^*}{1+A} \tag{3.7}$$

$$k_{ro} = k_{ro}^{0}\frac{\left(1-S_w^*\right)^{N_o} + B\left(1-S_w^*\right)}{1+B} \tag{3.8}$$

The exponents N_w and N_o are the same as Corey parameters. The constants A and B are small value constants that linearize the curves when relative permeability values approach zero. Note that these equations will be the same as Corey equation if the constants A and B are zero (Sendra user guide, 2012) (Sigmund & McCaffery, 1979).

3.2.2.4 Chierici Correlation

$$k_{rw} = k_{rw}\left(S_{or}\right)e^{-BR_w^{-M}} \tag{3.9}$$

$$k_{ro} = k_{ro}\left(S_{wi}\right)e^{-AR_w^{L}} \tag{3.10}$$

$$R_w\left(S_w\right)=\frac{S_w-S_{wi}}{1-S_{or}-S_w} \tag{3.11}$$

The water and oil relative permeability curves are estimated using different parameters in this equation. Note that in this equation R_w is used, which is different than the traditional normalized water saturation term. The S_{wi} in the denominator of normalized water saturation is replaced by S_w as seen in equation (3.11) (Chierici, 1984).

3.2.2.5 LET Correlation

$$k_{rw}=k_{rw}^0\frac{\left(S_w^*\right)^{L_w}}{\left(S_w^*\right)^{L_w}+E_w\left(1-S_w^*\right)^{T_w}} \tag{3.12}$$

$$k_{ro}=k_{ro}^0\frac{\left(1-S_w^*\right)^{L_o}}{\left(1-S_w^*\right)^{L_o}+E_o\left(S_w^*\right)^{T_o}} \tag{3.12}$$

In this equation only end point saturations and corresponding relative permeability values have physical meaning and the parameters L, E and T are empirical. The parameter L describes the shape of the curve in the lower parts, while the parameter T changes the top of the curves (Sendra user guide, 2012) (Lomeland et al., 2005).

For the analysis of data in this study, all the above mentioned correlations have been tried to come up with the best possible history matching of the experimental data.

3.3 Experimental conditions and experiments performed

The experiments were conducted on unconsolidated porous media. For simplicity we will refer to sand packs as SP, and to glass bead packs as GB. Two sizes of glass beads were used, 1 millimeter size and 300-425 micron size beads. Two more experiments were also performed using Bentheimer sandstone core plugs. All absolute permeability measurements for both consolidated and unconsolidated cores were done by injecting water vertically upwards. The absolute permeability was, however, used as an adjusting parameter in simulations by Sendra to match the experimental pressure drop observed. An overview of experimental parameters is listed in Table 3.1.

Different sets of experiments were run. These flooding experiments were designed to examine the effect of various parameters on flow behavior and relative permeability curves. Table 3.2 summarizes the experiments performed during this study.

Table 3.1 Experimental conditions

Core properties	
Length (Unconsolidated cores : SP / GB)	21 cm
Length (Sandstone cores)	20 cm
Diameter	3.8 cm
Permeability (1mm size GBs packs)	90 to 100 Darcies
Permeability (300-425 micron GBs packs)	40 to 45 Darcies
Permeability (Sand packs)	13.8 to 15.8 Darcies
Permeability (Core#1)	2.2 Darcies
Permeability (Core#2)	3.4 Darcies
Flooding Conditions	
Initial pressure in the system	5 bars
Overburden pressure	25 bars
Oil injection rate	0.5 cc/min
Water injection rate	0.8 cc/min

Table 3.2 Experiments performed during this study

Porous Media	Temperature °C	Oil Type	Porosity %	Pore volume cc	S_{wi} %
1 mm GBs	100	OIL20	30.06	71.6	19.55
	120	OIL20	30.27	72.1	15.95
	140	OIL20	30.90	73.6	16.30
	100	OIL10	31.95	76.1	11.83
	120	OIL10	31.53	75.1	21.30
	140	OIL10	31.32	74.6	28.15
300-425 micron GBs	100	OIL20	32.37	77.1	11.02
	120	OIL20	33.21	79.1	13.91
	140	OIL20	32.79	78.1	21.13
	100	OIL10	33.84	80.6	14.02
	120	OIL10	34.26	81.6	13.48
	140	OIL10	34.05	81.1	17.88
Sand Pack	100	OIL20	30.65	73.0	22.60
	120	OIL20	31.07	74.0	29.05
	140	OIL20	29.81	71.0	31.69
	100	OIL10	30.44	72.5	17.93
	120	OIL10	29.60	70.5	21.28
	140	OIL10	30.48	72.6	27.55
Bentheimer core	120	OIL20	21.00	47.5	28.36
	140	OIL20	20.88	47.2	30.07

3.4 Experimental results and discussions

As mentioned earlier, the method of relative permeability calculation was history matching the production curves and pressure differential data using Sendra simulator. No capillary pressure was considered as the porous media is very high permeable. Different relative permeability correlations were tested, and the parameter estimation was done by the software to get the best match. Fig. 3.3 shows some of the pressure differential and production curve matches obtained as some examples.

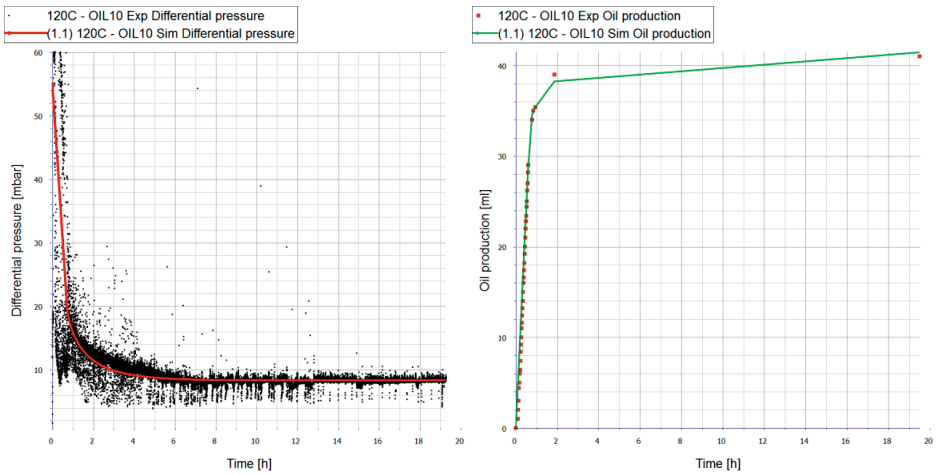

(a) Sand pack experiments – OIL10 – 120°C

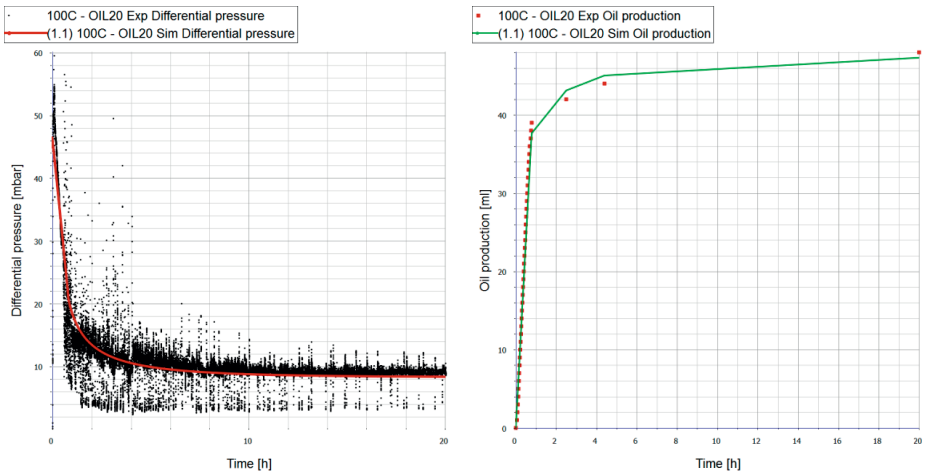

(b) Sand pack experiments – OIL20 – 100°C

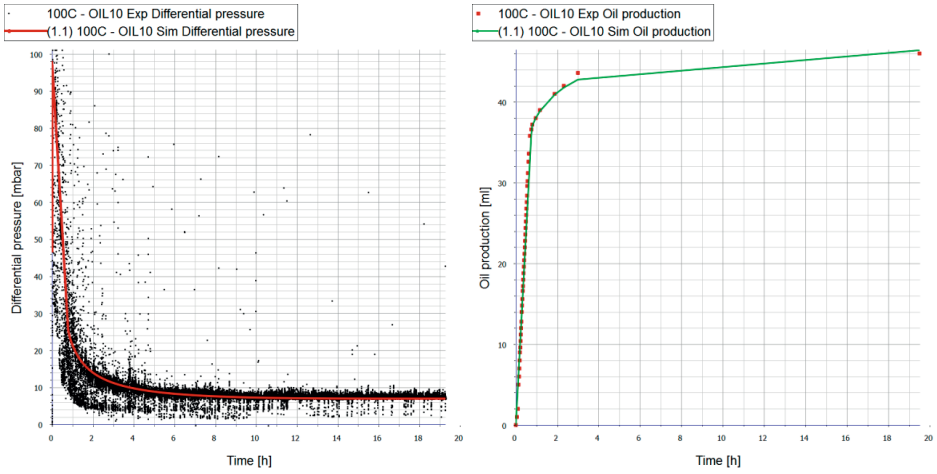

(c) Sand pack experiments – OIL10 – 100°C

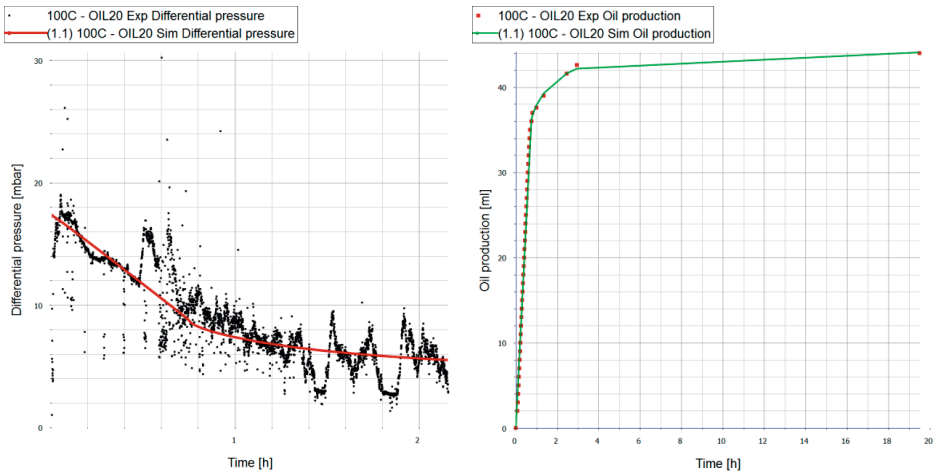

(d) Glass bead experiments 300-425 micron – OIL20 – 100°C

Figure 3.3 Pressure differential and oil production curve matches obtained by adjusting relative permeability curves using Sendra. Dots represent the experimental values and the continuous curves show the simulator matches.

The relative permeability curves for the experiments performed on 1 mm size glass beads (GBs) using OIL20 are shown on Figure 3.4. Note that the values of water relative permeability are magnified for better visibility on part (a) of this figure. The plots are shown on Figure 3.4.b as normalized relative permeability curves. Both water saturation and relative permeabilities are normalized on this figure to only show the difference in curvature of the data. Table 3.3 summarizes the relative permeability correlation parameters obtained for the curves shown on Figure 3.4. The correlations

matching the data best were LET for 100°C and Corey for both 120 and 140°C for these sets of experiments.

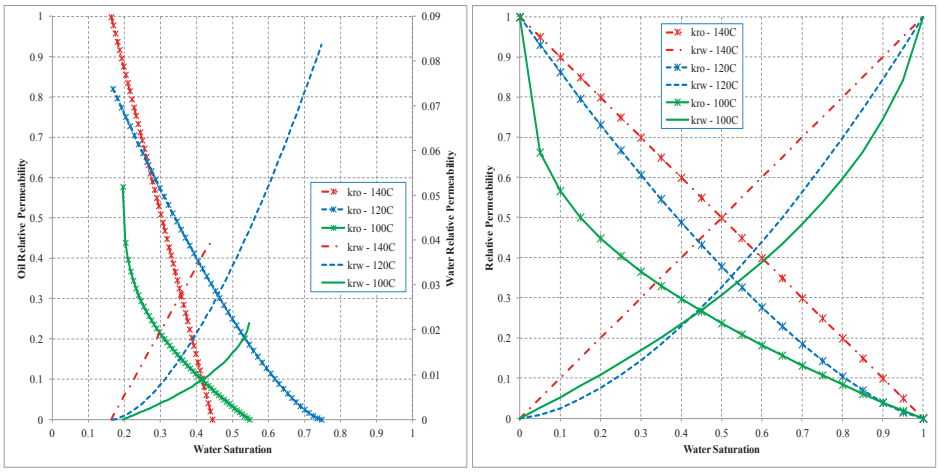

(a) **(b)**

Figure 3.4 Relative permeability curves for the experiments done on 1 mm size GBs using OIL20. Normalized values are shown on Figure (b)

Table 3.3 Relative permeability correlations matching the experimental data and corresponding parameter values for the experiments 1 mm GB – OIL20

Temperature °C	Relative permeability correlation	Parameters		
100	LET	$L_w = 1.001$	$E_w = 1.96474$	$T_w = 0.8$
		$L_o = 1.07434$	$E_o = 2.16229$	$T_o = 0.501$
120	Corey	$N_w = 1.61003$		$N_o = 1.40167$
140	Corey	$N_w = 1.001$		$N_o = 1.001$

The relative permeability curves obtained for the experiments on 1 mm GBs media using OIL10 are shown in Figure 3.5 with the normalized values on the part (b) of the figure. For these sets of experiments Corey correlation gave the best history match results for 100 and 140°C, and the experimental data at 120°C were best matched when Sigmund and McCaffery correlation were used to represent relative permeabilities. It seems that there is no unique trend and definite temperature dependency, as the curves have sometimes increased from one temperature to another and then decreased as the temperature has further been increased. The relative permeability curves obtained for the experiments on 300-425 micron size GBs using OIL10 are shown on Figure 3.6. Part (a) of the figure shows normal plots of relative permeability versus water saturation. In part (b), however, normalized relative permeability values are plotted against normalized water saturation.

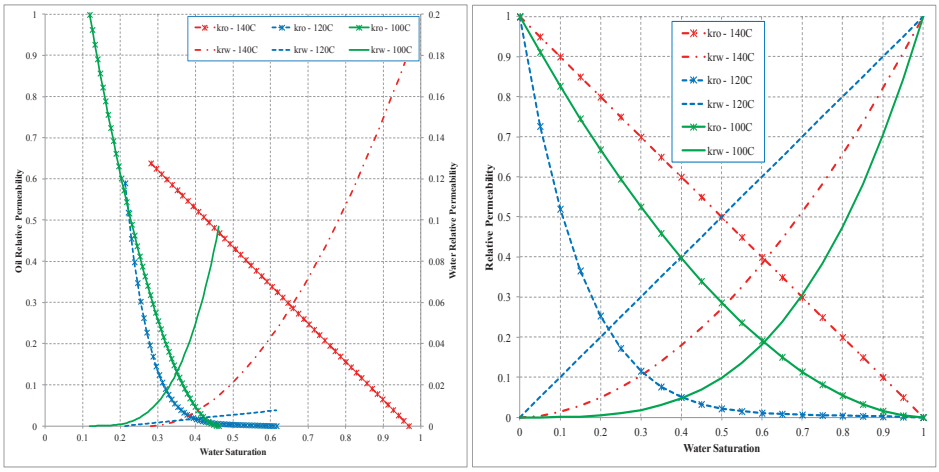

(a) (b)

Figure 3.5 Relative permeability curves for the experiments done on 1 mm size GBs using OIL10. Normalized values are shown on Figure (b)

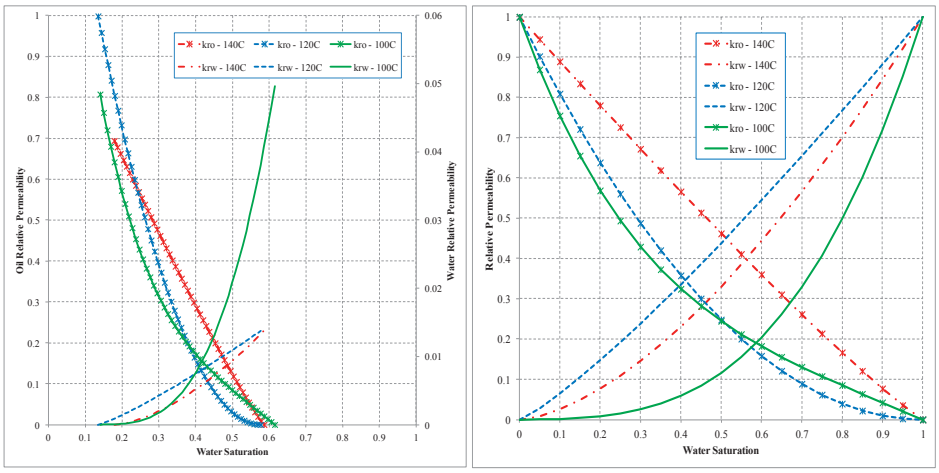

(a) (b)

Figure 3.6 Relative permeability curves for the experiments done on 300-425 micron size GBs using OIL10. Normalized values are shown on Figure (b)

The experimental runs using OIL20 performed on the core plugs of smaller sized GBs, namely 300-425 micron, have been analyzed and the resulting relative permeability curves are revealed in Figure 3.7.

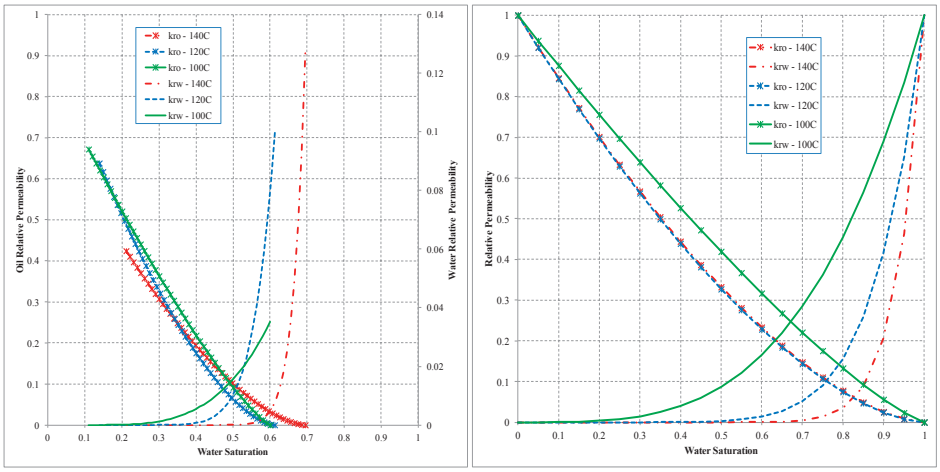

(a) **(b)**

Figure 3.7 Relative permeability curves for the experiments done on 300-425 micron size GBs using OIL20. Normalized values are shown on Figure (b)

In the experiments performed on 300-425 micron GBs, the best history matching of the data was achieved with Corey correlation except in one case. The correlation parameters are shown on Table 3.4 for OIL10 experiments.

Table 3.4 Relative permeability correlations matching the experimental data and corresponding parameter values for the experiments 300-425 micron GB – OIL10

Temperature °C	Relative permeability correlation	Parameters	
100	Sigmund & McCaffery	$N_w = 3.15676$	$N_o = 4.1142$
		$A = 0.01$	$B = 0.732672$
120	Corey	$N_w = 1.18993$	$N_o = 2.01199$
140	Corey	$N_w = 1.59629$	$N_o = 1.\ 11373$

As per the effect of temperature on relative permeability curves, we were not able to determine a unique trend in our experimental results. Dependency of either oil or water relative permeability on temperature is not justified in any of the experiments performed on glass bead packs. The spread in relative permeability variation by temperature is even more adverse in the tests with higher permeable GBs (1 mm size). This further suggests that the variations seen can be attributed to viscous instabilities. This has also been reported by several authors. (Sufi et al., 1982; Miller and Ramey, 1985)

As already mentioned, some core flooding experiments were accomplished using artificial unconsolidated core plugs made of sand instead of glass beads. Sand packs showed lower absolute permeabilities than glass bead packs due to smaller size of sand

particles. The oil recovery factor versus cumulative number of pore volumes of water injected (W_i) are shown on Figure 3.8. The breakthrough recovery factors and the corresponding value of W_i at which the breakthrough happened are shown in Table 3.5. As depicted on Figure 3.8 the residual oil saturation (S_{or}) was not reached during the flooding experiments, due to volume limitation of the water injection vessel. The value of S_{or} was therefore a matching criterion, and was allowed to be adjusted by the simulator. Proximity of the S_{or} values forecasted by the simulator to the values already obtained experimentally, indicated that around 13 pore volumes of water injected has been almost enough to produce the recoverable oil, and further injection will not increase the ultimate recoveries dramatically.

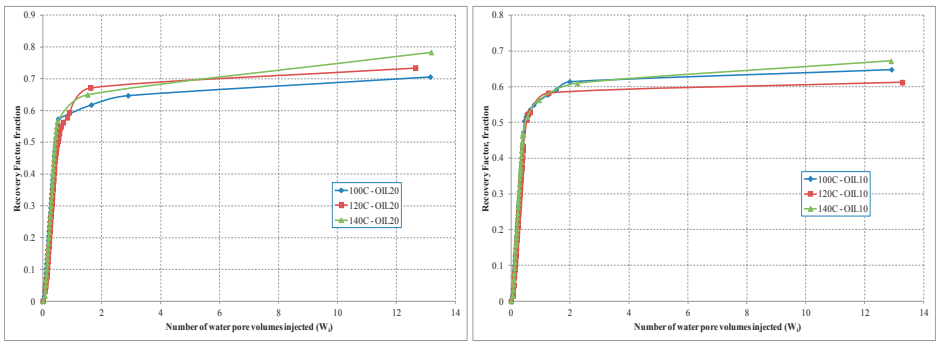

Figure 3.8 Oil recovery factor (RF) versus number of cumulative pore volumes of water injected (W_i) during the experiments on sand packs

Table 3.5 Recover factor (RF) at breakthrough and the corresponding value of pore volumes injected (W_i) during sand pack experiments

Oil type used	OIL20			OIL10		
T, °C	100	120	140	100	120	140
W_i , fraction	0.37	0.39	0.37	0.42	0.41	0.39
RF at breakthrough, fraction	0.44	0.42	0.43	0.47	0.43	0.47

The relative permeability curves for sand pack experiments performed using lower viscous oil (OIL20) and higher viscosity alternative (OIL10) are shown on Figures 3.9 and 3.10 respectively. An overview of the correlation parameters that matched the experimental data best is provided in Table 3.6. The experiments performed on sand packs were best history matched using Corey type relative permeabilities.

Again, the same as glass bead pack experiments, the variations in the shape and curvature of the curves are not conclusive and not following a unique increasing or decreasing trend versus temperature. The relative permeabilities are sometimes rising

Table 3.6 Relative permeability correlation parameters matching the experimental data best for sand pack experiments

Oil Type	Temperature °C	Relative permeability correlation	Parameters	
			N_w	N_o
OIL20	100	Corey	4.03051	1.34961
OIL20	120	Corey	2.0567	1.001
OIL20	140	Corey	3.87943	2.56457
OIL10	100	Corey	5.38172	1.001
OIL10	120	Corey	4.13469	1.07344
OIL10	140	Corey	3.87387	1.36534

with temperature and sinking again as the temperature is further increased, and in some cases not showing any sensitivity to temperature at all. This suggests that the variations seen can be due to artifacts present in the flooding experiments. This has been the topic of an argument in the literature that the reason behind the apparent temperature dependency of relative permeability curves might be the instabilities and viscous fingering and not a fundamental flow property. (Sufi, 1982) (Miller and Ramey, 1985) (Maini and Okazawa, 1987) (Polikar et al., 1990)

The increase of initial water saturation (S_{wi}) versus temperature has been spotted generally, although not present in all the experimental results. We believe in those experiments we might have been inside the experimental error margin. Generally the

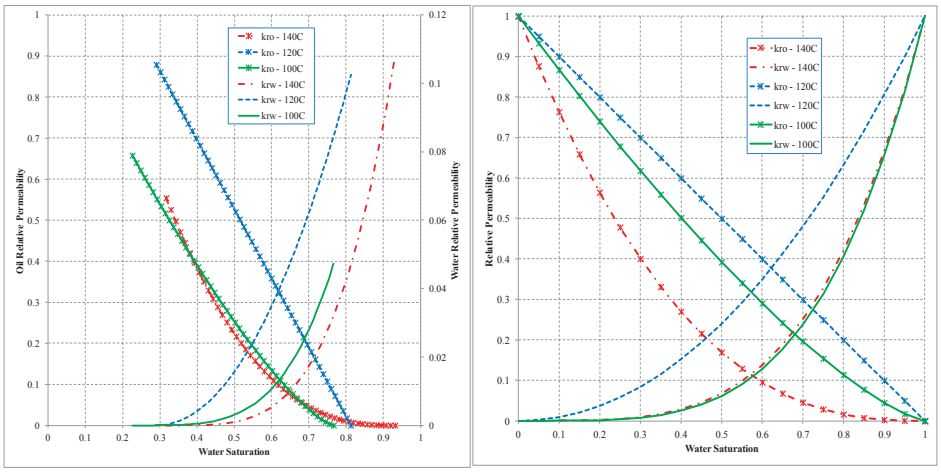

(a) **(b)**

Figure 3.9 Relative permeability curves for the experiments done on sand packs using OIL20. Normalized values are shown on Figure (b)

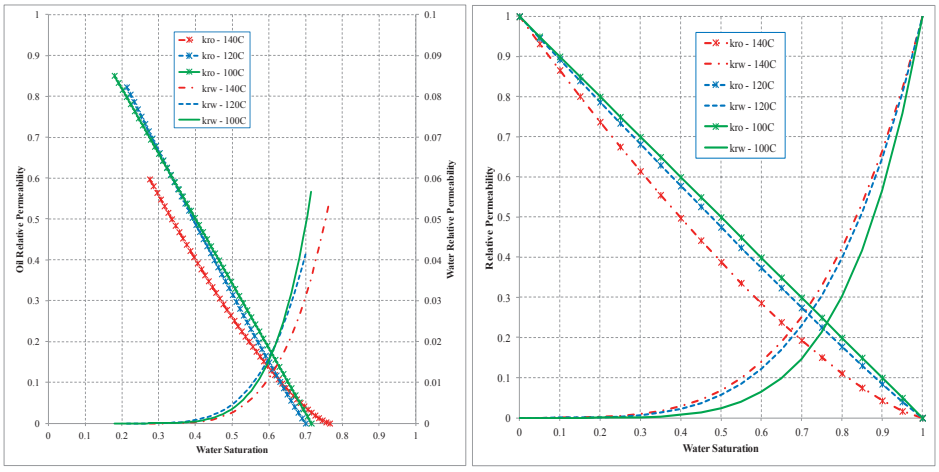

(a) **(b)**

Figure 3.10 Relative permeability curves for the experiments done on sand packs using OIL10. Normalized values are shown on Figure (b)

increase in S_{wi} as the temperature increases is expected. During the initialization of core samples, oil is displacing water. As the oil viscosity drops much more than water viscosity with temperature, the viscosity ratio of water to oil increases and will result in an unfavorable displacement of water by oil during this stage. During the water flooding of oil saturated core, the same interpretation should apply regarding the residual oil saturation (S_{or}). As the temperature increases the viscosity ratio of oil to water drops, and this results in a more favorable mobility ratio and S_{or} is expected to decrease. However, this was not the case in some of the experiments. We think this could have happened due to viscous instabilities and possible viscous fingering in core flooding experiments. Viscous fingering seems to be inevitable in such an adverse mobility ratio condition, even at low injection rates.

Two experiments performed on Bentheimer sandstone core plugs of length 20 cm showed the same trend for S_{wi} and S_{or}. The corresponding relative permeability curves are shown in Figure 3.11. Part b of the figure shows a semi log plot of the obtained relative permeabilities. Due to the lower absolute permeability of core plugs compared to unconsolidated porous media, we only performed the experiments using the lower viscous oil (OIL20) and two highest temperatures of 120 and 140°C. The relative permeability correlation that could best match the experimental data for these core floodings was again the Corey correlation.

A comparison of relative permeabilities at the same experimental temperature, highlighting the effect of oil viscosity, reveals changes in the water saturation range similar to the temperature effect. Displacing an oil of lower viscosity under the same

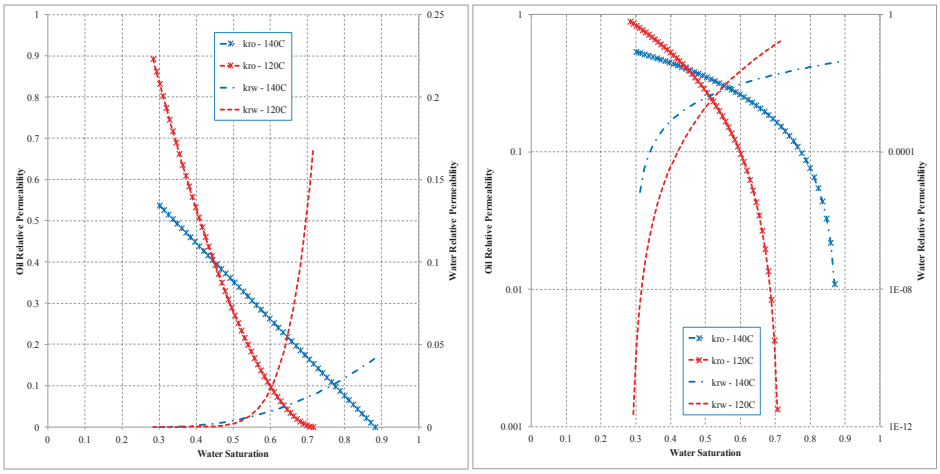

(a) **(b)**

Figure 3.11 Relative permeability curves for the experiments done on Bentheimer sandstone core plugs using OIL20. Semi-log plot on Figure (b)

temperature condition shifts the relative permeabilities to higher saturation range, increasing S_{wi} and decreasing S_{or}. This has been depicted on Figure 3.12 for some of the experimental runs. In almost all of the cases, the shift to higher water saturation range is observed without any rising or falling trend for the shape of the relative permeability curves.

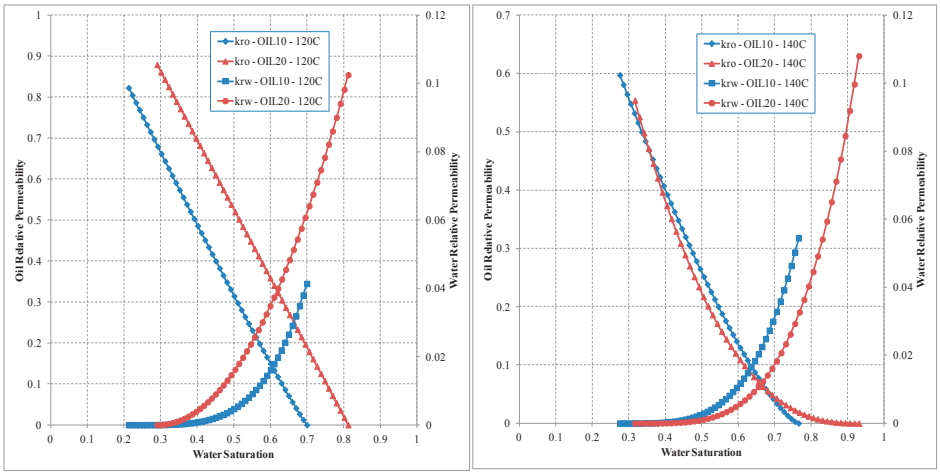

(a) sand pack experiments at 120°C **(b) sand pack experiments at 140°C**

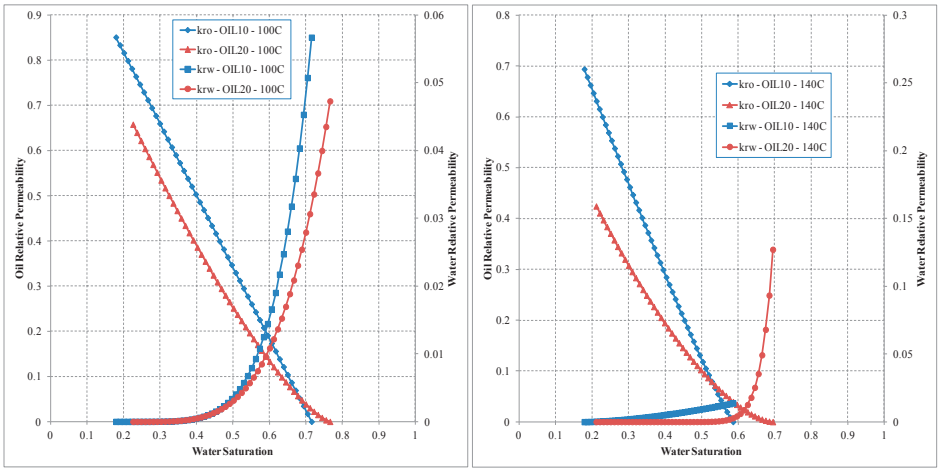

(c) sand pack experiments at 100°C **(d) 300-425 micron GB – 140°C**

Figure 3.12 Comparison between relative permeabilities for some of sand pack and glass bead experiments – highlighting the effect of oil viscosity

Akin et al. (1998) also reported that the variations observed in the relative permeability curves by changing the temperature is related to the decrease in oil/water viscosity ratio as the temperature rises.

Our experimental results confirm that at least for the types of porous media and oil we have used and the specified conditions of temperature, the variations seen are probably related to either viscosity changes or viscous instabilities.

The general trend observed in our experimental results was an increase in initial water saturation (S_{wi}) and a decrease in residual oil saturation (S_{or}) as the temperature rises or the viscosity of oil drops. During the initialization of the core, oil is displacing the water and the mobility ratio is proportional to the water/oil viscosity ratio. Because the oil viscosity is dropping much more than the water viscosity, this ratio grows in value with temperature resulting in a less favorable displacement. Therefore the amount of S_{wi} rises with temperature. In water flooding phase, however, the mobility ratio becomes more favorable at higher temperatures. In this stage of the experiments, the displacing agent is water and the displaced phase is the higher viscous oil. The mobility ratio will be proportional to the oil/water viscosity ratio, which makes the displacement quite unfavorable. The mobility ratio drops, however, at higher temperatures which results in a better sweep of oil by water and a lower value for the S_{or}.

The experiments not following the increasing trend of S_{wi} was believed to be affected by experimental error. Also the trend for S_{or} has sometimes been ruled out. We believe in

those cases the experiments might have been influenced by viscous fingering and instabilities, which seemed to be inevitable in such an adverse mobility ratio condition.

No conclusion can be made regarding the temperature dependency of relative permeability curves, and any possible effect of temperature on either value or shape of these curves is not justified. The spread in relative permeability curves is even higher in the case of highest permeable cores. The possible reason for that is the presence of viscous instabilities and fingering issues as reported in the literature as well. Sufi et al. (1982) and Miller and Ramey (1985) have concluded that the variations in relative permeability with temperature are probably not related to fundamental flow properties and they are rather related to experimental artifacts. Maini and Okazawa (1987) have also concluded that due to several artifacts involved in the experiments no effect of temperature could be justified. Polikar et al. (1990) also stated that it is not possible to predict theoretically what the effect of temperature on relative permeabilities could be, and the results are system specific.

The relative permeabilities are functions of a complex mixture of several contributing parameters including interfacial tension, wettability, viscosity of fluids, pore shape and pore size distribution. Several of these parameters are affected by variations in temperature. It is, however, not clear what the overall contributing effect of all these parameters are on the relative permeability curves as the temperature rises. The increase in relative permeability value caused by variation of one of these parameters can totally be masked by the effect of another parameter, leaving no overall variation of data.

Comparing the curves at the same values of temperature and under the conditions when the oil viscosity is the only variable, reveals the same results as the temperature effect; that is a shift to higher water saturation range. This further indicates the possible interrelation between the temperature dependency issue and the viscosity changes resulted by variations in temperature. Akin et al. (1998) have reported the same finding that the possible cause of temperature dependency of relative permeabilities is the drop in oil/water viscosity ratio with temperature.

Chapter 4

Numerical Investigation of Steam Flooding in a Heterogeneous Porous Media Containing Heavy Oil

This chapter presents the results of some numerical simulation studies on steam flooding in one-dimensional porous media. The porous media is considered to represent a core flooding case. The material presented in this chapter is the content of SPE conference paper 144168, and deals with the steam flooding in a heterogeneous core containing heavy oil. The content of the paper is, however, presented with some editions to prevent repetition in this thesis. This paper is the extension of the simulation work performed on a fractured core. The content of the paper dealing with steam flooding in a fractured core is presented in Appendix B.1.

4.1 Abstract

Thermal recovery methods and especially steam flooding have long been considered as the most effective methods to unlock heavy oil reservoirs. These highly viscous hydrocarbon deposits are proven to constitute a huge proportion of total world oil reserves. Large volumes of heavy oil are located in heterogeneous porous media containing high permeable wormholes or non-permeable shale barriers. High permeable zones can be the results of sand migration in loose and unconsolidated sandstones. There is a question of how these non-homogeneities can possibly enhance or hinder the flow of high viscous oil, steam and condensed water under a steam injection process.

This paper addresses experimental and simulation study of steam flooding in heterogeneous porous media that contains Athabasca heavy oil. Some PVT properties of Athabasca crude oil have been measured experimentally and simulation study was accomplished using a numerical thermal reservoir simulator (For PVT properties refer to chapter 2). A horizontal layer of high porosity and permeability was assumed in the middle of a core to verify the performance of steam injection in a 20 cm long sandstone core with a permeability of 640 mD saturated with Athabasca heavy crude. High permeable zone had a permeability of 5 D. Different shale barrier configurations were also considered to examine the effect of these no flow layers. Considering a heterogeneous system, sensitivity analyses were focused on the effect of injection rate, porosity, permeability contrast and thickness of high permeable zone. Different steam temperature and quality cases for core flooding experiment in this system were also investigated.

The most important conclusion is that there is an optimum steam temperature and quality for most efficient steam injection. It was figured out that shale barriers in the model can hinder the flow of oil and cause high residual oil, but their impact is dependent on permeability distribution in the core.

The permeability contrast between the high and low permeable layers should be smaller considering both oil production and steam oil ratio (SOR), which is a measure of economy. Although core permeability of 640 mD provides satisfactory recovery and SOR, higher permeability can cause faster recovery and lower SOR, since the injection can stop earlier. Porosity of the model is found to have an inverse relation with the oil recovery and SOR. Results also clearly show that higher injection rates improve the oil recovery. However, SOR should also be considered at the same time. There is a trade-off between recovery and SOR. It is also clear that lower thickness for the high permeable zone results in better recovery while causing high injection pressure at the inlet. This corresponds with lower permeability contrast case.

4.2 Introduction

The work presented in this paper is two parts, experiments and reservoir simulation studies. In the experimental part, PVT properties of Athabasca bitumen like viscosity versus temperature were measured in the laboratory. In addition gas chromatography and compositional analysis, density versus temperature and interfacial tension between bitumen and steam at different temperatures were measured experimentally. Numerical simulations were then conducted to examine the effectiveness of steam injection in a heterogeneous core sample containing high permeable layers and shale barriers. A sandstone core is assumed to be saturated with high viscous bitumen. A horizontal layer with higher porosity and permeability than the core is considered in the middle of the core. Permeability and porosity of a sandstone core sample measured in the laboratory were used in the simulation studies. Different injection schemes were simulated with varying operating and reservoir parameters.

The results of these sensitivity analyses and discussions are given in this chapter; however, some of the experimental PVT properties results have been excluded to prevent repetition. Properties of the bitumen can be found in chapter 2 or in the paper in Appendix A.1.

4.3 Asphaltene precipitation experiment

A bulk experiment was performed to determine the weight percentage of asphaltene precipitation when mixing particular solvents with Athabasca heavy oil. The purpose of the experiment was to investigate if there is any connection between the mole fraction of solvent and the amount of asphaltene precipitation. The solvents used in this test were n-pentane, n-hexane and n-heptane. Different solvent loadings were added to the

oil, which was heated up to 60 °C to provide some mobility. The mixtures were stirred and left at room temperature for about 20 hours. The mixtures were then filtered using a vacuum pump and the precipitations were weighted. The results are shown in Figure 4.1. The experiments have shown that lighter n-alkanes lead to more solid precipitation from heavy oil than heavier n-alkanes. Also, increasing the mole fraction of solvent will increase solid precipitation. The onset of precipitation is at about 85% mole fraction of n-pentane, roughly 86% for n-hexane and 87% for n-heptane. Mole fractions of solvent should be kept below these values to avoid issues such as asphaltene induced formation damage. Microscopic images of asphaltene particles are shown in Figure 4.2.

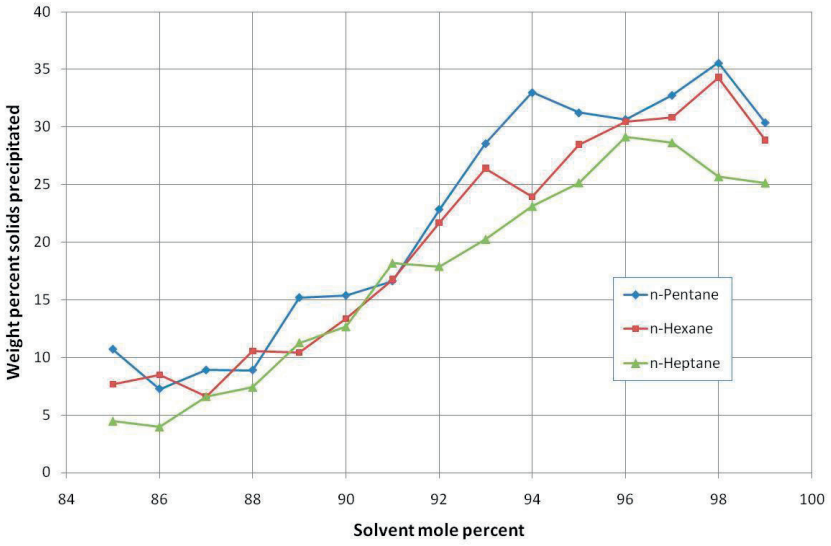

Figure 4.1 Asphaltene precipitation versus different solvent loadings

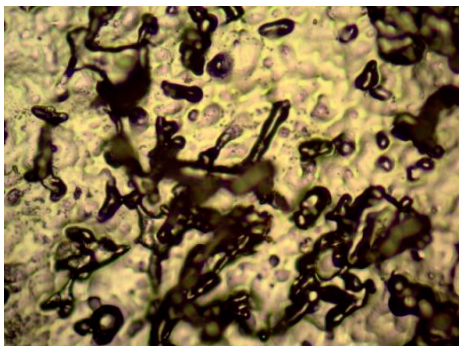

a – Mix with n-C5 – 20x magnification

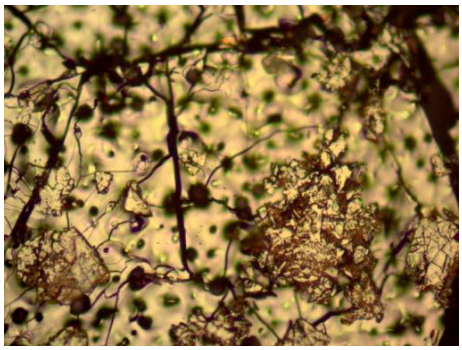

b – Mix with n-C5 – 20x magnification

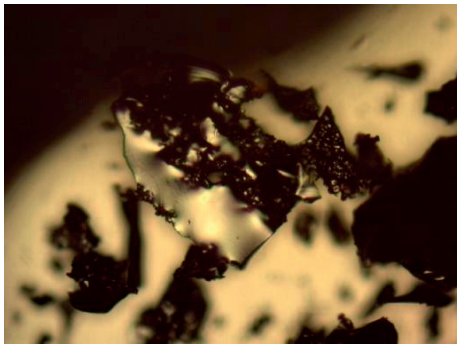

c – Mix with n-C6 – 10x magnification

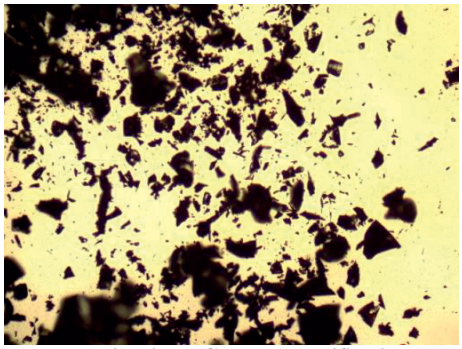

d – Mix with n-C7 – 5x magnification

Figure 4.2 Microscopic images of asphaltene particles precipitated after mixing with different solvents

4.4 Numerical simulation study

Numerical simulation was accomplished on a heterogeneous core to investigate effectiveness of steam injection. Different shale barrier configurations were examined to see the effect of these no flow layers. Considering a heterogeneous system, sensitivity analyses were focused on the effect of injection rate, porosity, permeability contrast and thickness of high permeable zone. Different steam temperature and quality cases for core flooding experiment in this system were also investigated.

4.4.1 Numerical model

The core is sandstone with a measured permeability of 640 mD, and the model contains a tiny horizontal highly porous and permeable layer in the middle. The simulation study was performed using CMG STARS thermal simulator, typical reservoir properties of Athabasca oil sand reservoirs and some laboratory measured fluid properties.

A Cartesian coordinate system is used so that the squared cross-sectional area of the cubic model is equal to the cross-sectional area of the core. The numerical model considered is shown in Figure 4.3.

It is a 20×10×11 grid block model. The grid block length is 1 cm in x-direction and 0.33588 in y- and z-directions. A tiny horizontal layer of 1mm width is considered in the middle to represent a high permeable channel. Porosity of this layer is considered to be 0.5 and the permeability is 5 Darcies. The model, reservoir and fluid properties used are given in Table 4.1. The relative permeability data were taken from steam flooding case by Coats et al. (1974).

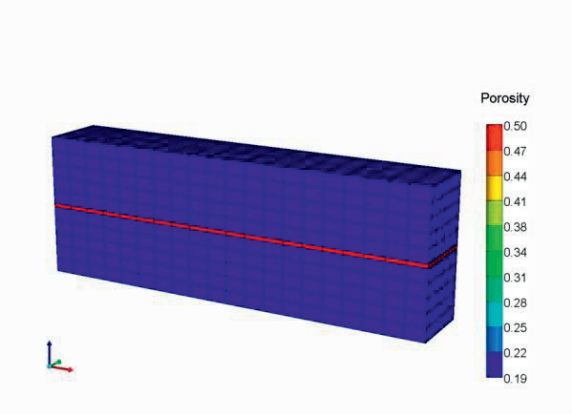

Figure 4.3 Numerical model

Table 4.1 Numerical simulation parameters used in this study: Rock properties and fluid properties are taken from literature except bitumen molar mass and density which were measured in the laboratory (Law et al., 2000), (Chow, 1993) and (Yang and Gates, 2009)

Model properties		Thermal properties	
Width	3.3588 cm	Formation heat capacity	2.39E+06 J/(m3.°C)
Height	3.3588 cm	Rock thermal conductivity	1.469E+05 J/(m.day.°C)
Length	20 cm	Water thermal conductivity	5.35E+04 J/(m.day.°C)
Permeability	640 mD	Oil thermal conductivity	1.34E+04 J/(m.day.°C)
Porosity	0.19	Gas thermal conductivity	2.60E+03 J/(m.day.°C)
Initial temperature	21°C	Water's first coefficient of thermal expansion	2.657E-04 °C-1
Oil saturation	0.95	Bitumen's first coefficient of thermal expansion	7.85E-04 °C-1
Water saturation	0.05		

4.4.2 Numerical simulation results and discussions

Different steam injection conditions are examined in this heterogeneous core model. Steam temperature and quality were the parameters examined. Increasing the temperature of injected steam will cause more energy input into the model, which results in better viscosity reduction and improved cumulative oil production. As can be seen in Figure 4.4 the ultimate recovery is increased as the temperature of injected steam is raised from 180 °C to 221 °C. However, the difference in terms of recovery is not so big between 200 °C (91.35 % recovery) and 221 °C (91.86 % recovery). Having in mind that the higher the steam temperature the higher the cost of steam generation and the higher energy consumption, one might suggest that 200 °C steam temperature would be satisfactory. To operate beyond this temperature would not be economical as we are injecting more heat, while enhanced oil produced is insignificant.

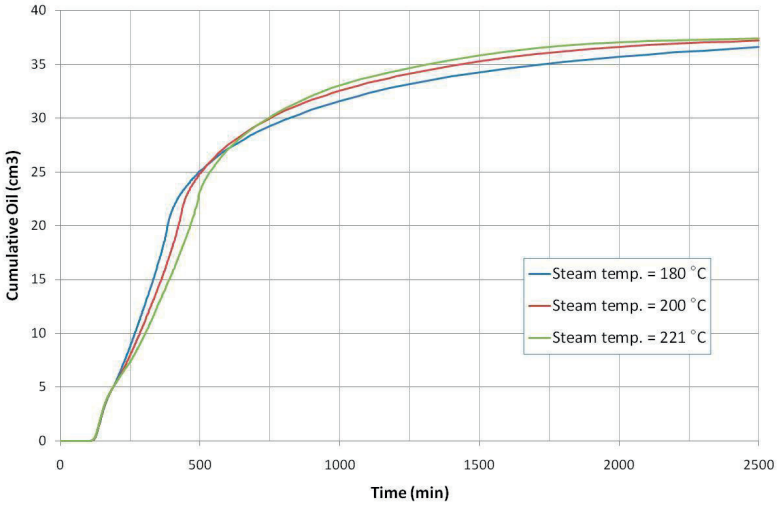

Figure 4.4 Cumulative oil production for different steam injection temperatures at 85% steam quality

The temperature 200 °C was chosen as the steam injection temperature in the rest of the simulation runs and the effect of different steam qualities on the final oil production was examined. Steam with qualities of 50, 75, 85, 95 and 100%, on a molar basis, was injected in the system. Cumulative oil production curve is shown in Figure 4.5. Injecting steam with higher quality will introduce more heat content in the porous media, and as the result the process will be more effective with increased cumulative production. This is what can be seen in the earlier times in Figure 4.5. However, a closer look at the later times reveals some other behavior. The late production times are magnified in Figure 4.6. The figure shows that up to the steam quality of 85% the increased recovery as a result of higher steam quality is apparent. As the quality is further raised to 95 and 100%, however, the effect vanishes and less ultimate oil production is observed. Similar behavior was observed when steam injection was performed with different steam temperatures.

An investigation into snapshots of the saturation distribution inside the core shows what is happening at very high steam qualities. Snapshot of the core at a late time showing oil and water saturations are shown in Figure 4.7. The left column in this figure shows snapshots when the injected steam had 85% quality and the snapshots for 100% quality are shown in the right column. When steam of quality of 100% is injected, the liquid water saturation is lower especially at the inlet face of the core. This is due to the lower liquid content of the injected steam, which even causes some evaporation of interstitial water at the inlet face of injection. As the water saturation is even below the initial water saturation, residual oil saturation is higher in these grid blocks compared to the rest of the blocks.

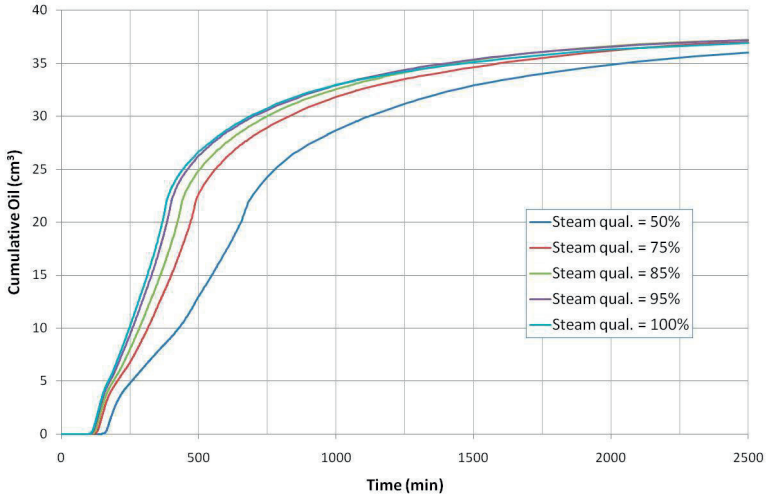

Figure 4.5 Cumulative oil production for different steam qualities at 200 °C steam temperature

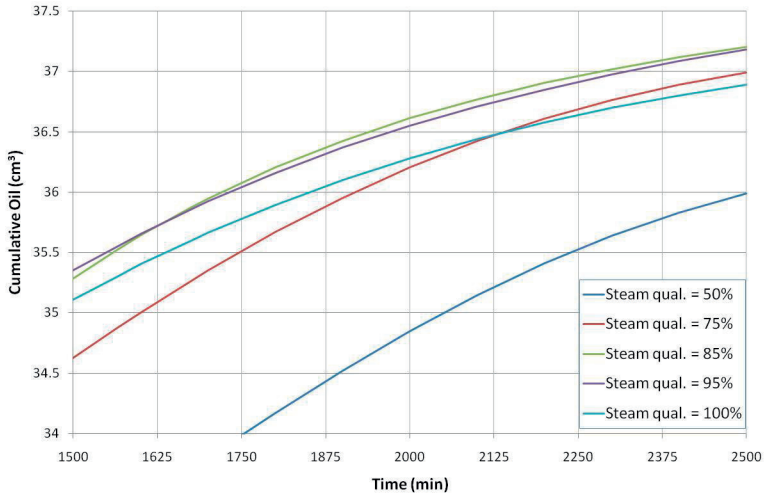

Figure 4.6 Cumulative oil production for different steam qualities at 200 °C steam temperature – magnified at later times

Depending on the relative permeability data in every system, this behavior could be seen at different intensities. What is apparent in saturation distribution snapshots is that injecting dry steam will cause very low water saturation at inlet. The conclusion is that in steam injection processes, it is better not to have very high steam quality. There is an optimum quality of steam which for this case was found to be around 85%.

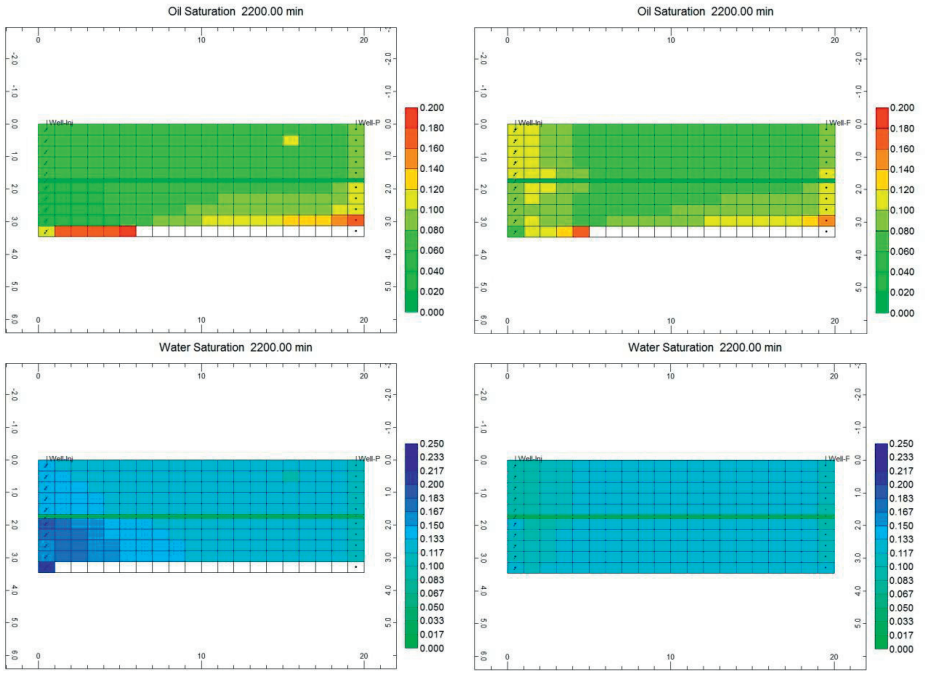

Figure 4.7 Saturation distribution at 2200 min for steam injection at 200 °C and different steam qualities (steam quality of 85% on the left column and steam quality of 100% on the right column)

In order to see the effect of shale barriers that could be present inside the core sample, some scenarios are considered with different shale barrier configurations in this heterogeneous core sample. Two horizontal shale barrier, two vertical shale barrier and one randomly distributed shale barrier cases are considered. These configurations are shown in Figure 4.8. In horizontal shale barrier – scheme 1 (HS-1), the shale layers are extended horizontally inside the core from injection face to the production face. In horizontal shale – scheme 2 (HS-2), however, the extent is limited inside the core and not to the outer faces. Random shale barrier scheme contains a combination of both horizontal and vertical shale barriers.

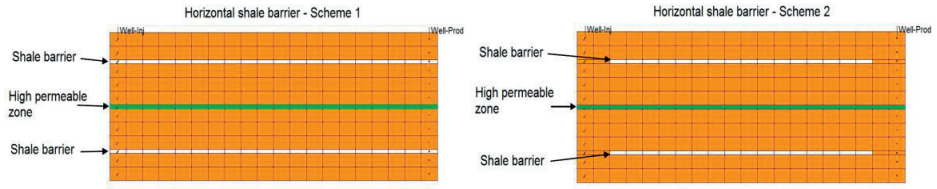

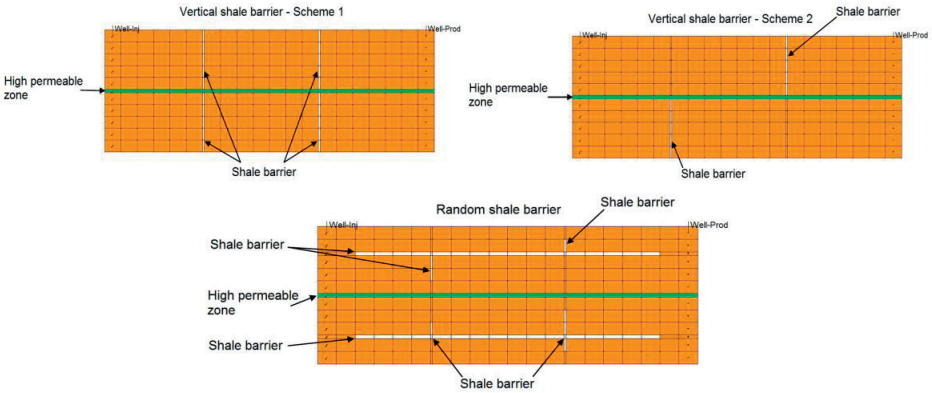

Figure 4.8 Schematic representations of different shale barrier schemes

Steam was injected at a temperature of 200 °C and a quality of 85% in these different shale barrier schemes. The result is shown in Figure 4.9 in terms of recovery percent. The lowest oil recovery was obtained in horizontal shale – scheme1 (HS-1).

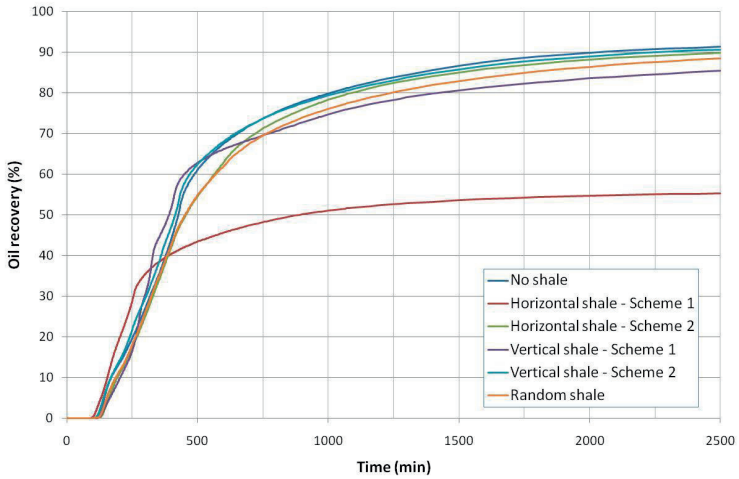

Figure 4.9 Oil recovery for different shale barrier schemes

In this scheme as can be seen in Figure 4.10.a some areas of the core are almost intact. These areas are completely isolated by shale layers and are not in communication with high permeable zone in the middle. The significance of having good communication with the high permeable zone is that steam flows easily inside this zone and transfers thermal energy to the cold oil inside the lower permeable parts. Shale barriers, however, prevent this heat communication in HS-1 case. The top and bottom portions of the core do not get enough thermal energy and the oil in these regions does remain viscous. The injectivity in these two regions is therefore still low and almost no oil is produced from these areas (Figure 4.10.a). In Figure 4.10.b, which depicts the oil saturation distribution

at the end of run for randomly distributed shale barrier, lower residual oil is left in the core, since no part of the core is completely isolated. The conclusion is that shale layers can limit the flow of oil, but their impact is dependent on permeability distribution in the core.

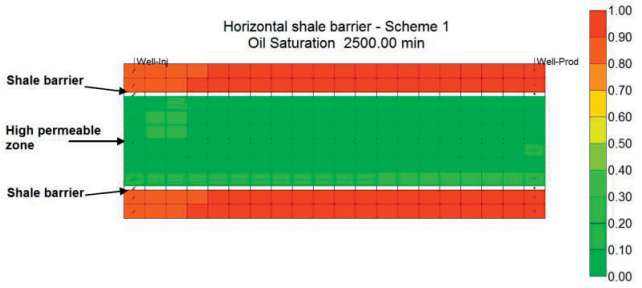

Figure 4.10.a – Snapshot of core showing residual oil saturation for horizontal shale barrier case

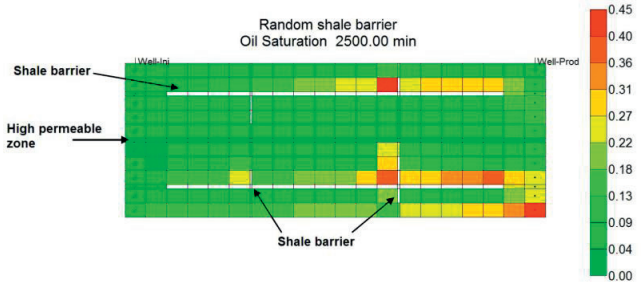

Figure 4.10.b Snapshot of core showing residual oil saturation for random shale barrier case (combination of vertical and horizontal shale barriers)

The permeability contrast between the higher and lower permeable zones in the model was examined for possible impact on production from the core. For this purpose, the permeability of high permeable zone is called kH and the permeability of the core itself is referred to as kL. Different permeability values are examined and the results are compared based on the ratio of high to low permeability (kH/kL). Figure 4.11 shows cumulative oil produced for different (kH/kL) values. In this case, however, only kH is changed and the results are analyzed. Figure 4.11 indicates that when the permeability ratio is decreased, having lower kH values, more oil production is achieved. This happens because higher kH values result in early steam break through, not enough heat communication with the oil inside the core and higher residual oil saturation. Lowering the permeability of the high permeable channel, however, results in a buildup of pressure at the inlet face of the core as shown in Figure 4.12.

Changing the value of kL, results in almost the same kind of behavior. Figure 4.13 shows cumulative oil production for different (kH/kL) values as well, but here only the

kL values are varied with constant kH. Again lower (kH/kL) ratio, higher kL value, is desirable and results in higher oil production. Higher permeability causes more mobility and higher and faster cumulative oil production. At the same time it results in lower instantaneous steam oil ratio (SOR) values considering that the process can stop much earlier, say around 800 min for (kH/kL) of 1 (Figure 4.14). The curve corresponding to (kH/kL) value of 7.8 represents the base simulation case with permeabilities of 5 D and 640 mD as kH and kL respectively. It can be concluded that lower permeability contrast between the high and low permeable layers is desirable.

Porosity of the model is varied to investigate the effect of this parameter on steam injection in this model. Two porosity values of 30 % and 40 % are compared with the original case of 19 %. Oil recovery and SOR curves are shown in Figures 4.15 and 4.16. The porosity is found to have an inverse relation with the oil recovery and SOR. Initial volume in place is lower for lower porosity value and consequently the amount of heat which is required to reduce the viscosity of oil is lower. So for the same amount of steam injection rate, the model with the lowest porosity value shows the best recovery factor.

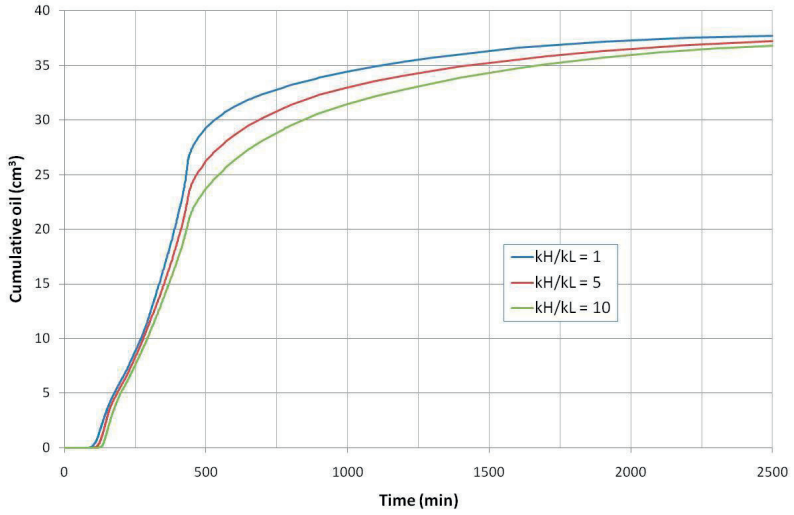

Figure 4.11 Cumulative oil production for different permeability ratios – changing kH only

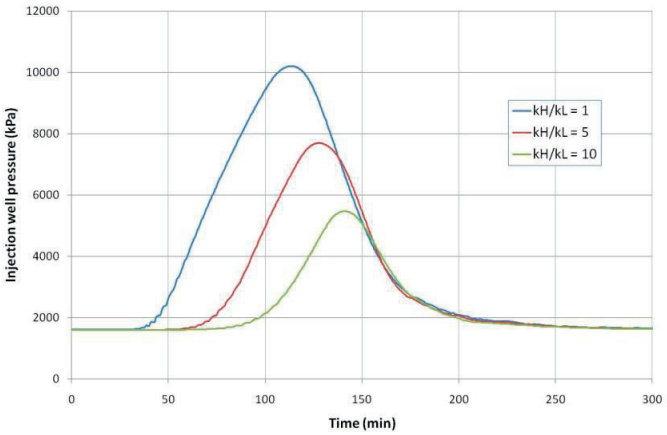

Figure 4.12 Pressure at the injection face of the core for different permeability ratios

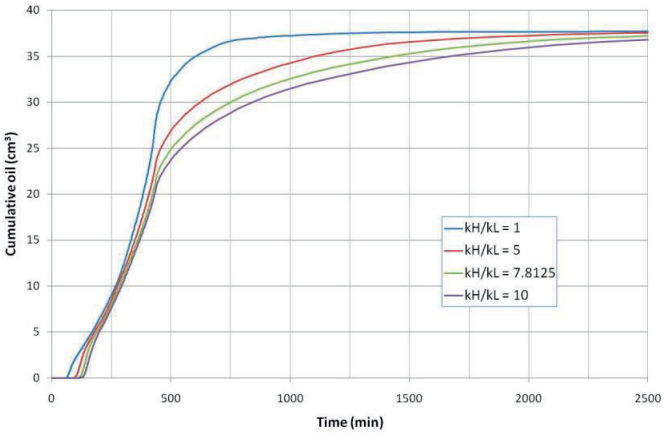

Figure 4.13 Cumulative oil production for different permeability ratios – changing kL only

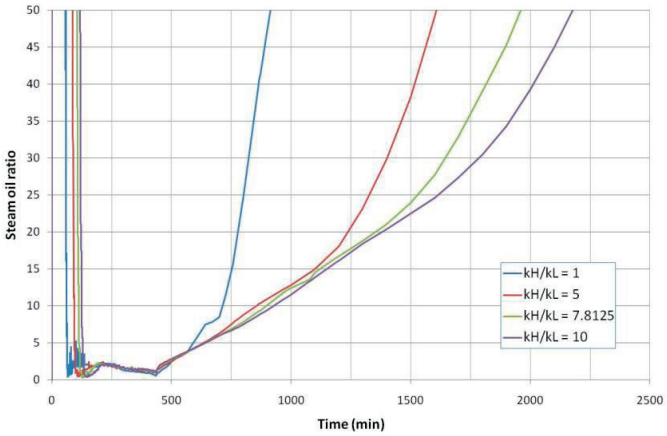

Figure 4.14 Instantaneous steam oil ratio for different permeability ratios – changing kL only

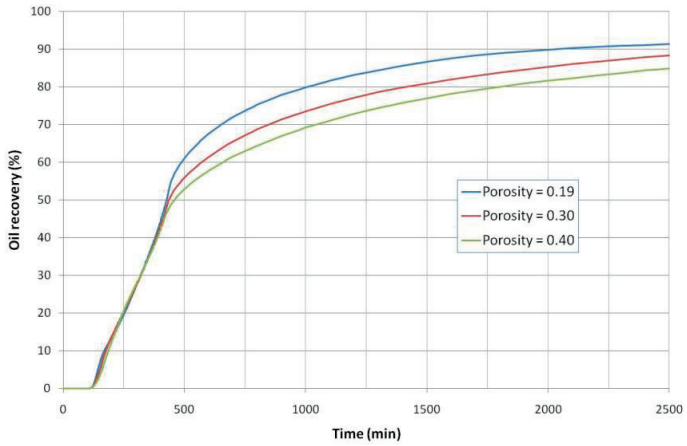

Figure 4.15 Oil recovery for different porosity values

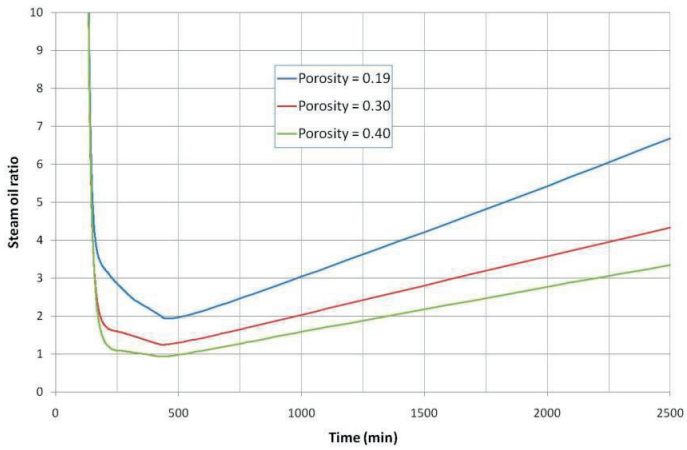

Figure 4.16 Steam oil ratio for different porosity values

The rate of steam injection is varied, and the response is shown in Figures 4.17 and 4.18. Although higher injection rate results in faster recovery, one should consider the very high SOR associated with it. Figures 4.17 and 4.18 clearly show that injecting with a rate of 0.1 cc/min is the best choice. Although the oil recovery is not so fast for this rate of injection, the ultimate recovery is the same as for other higher injection rates. One should note, however, that SOR with this injection rate is far more economic.

Another sensitivity parameter considered was the thickness of the high permeable layer in this heterogeneous core. Changing the thickness of this layer has an effect similar to varying its permeability. Lower layer thickness corresponds to lower kH and vice versa. This can be seen in Figure 4.19. Having lower layer thickness increases the oil recovery. This is the same as what results from lowering kH values, and happens since the high permeable layer will be filled with the drained oil, which in turn causes the blockage of

steam and better heat communication with the oil in the lower permeable blocks. It should also be noted that setting very low thickness for the horizontal high permeable layer results in huge pressure build up at the injection face of the core (Figure 4.20).

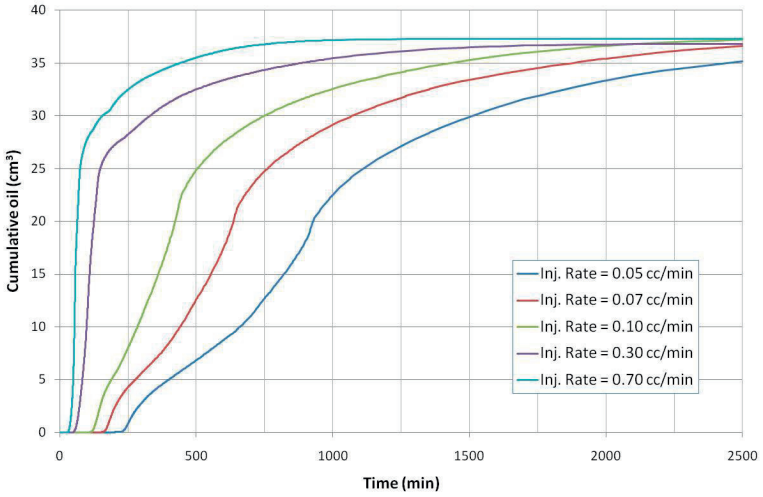

Figure 4.17 Cumulative oil production for different steam injection rates

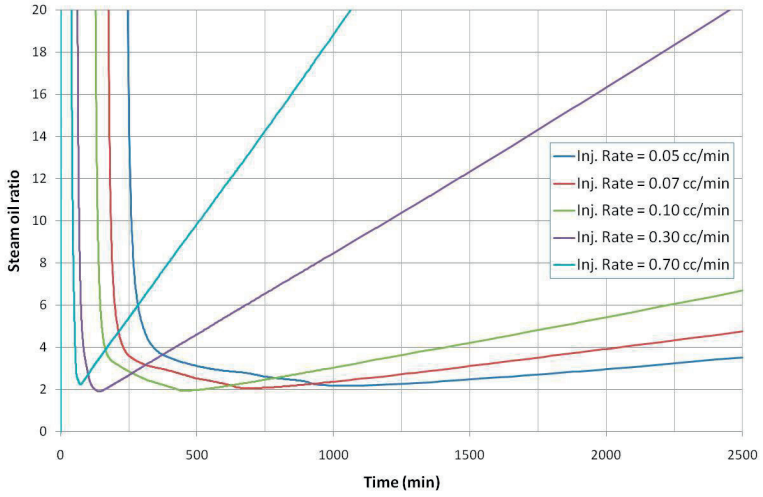

Figure 4.18 Steam oil ratio for different steam injection rates

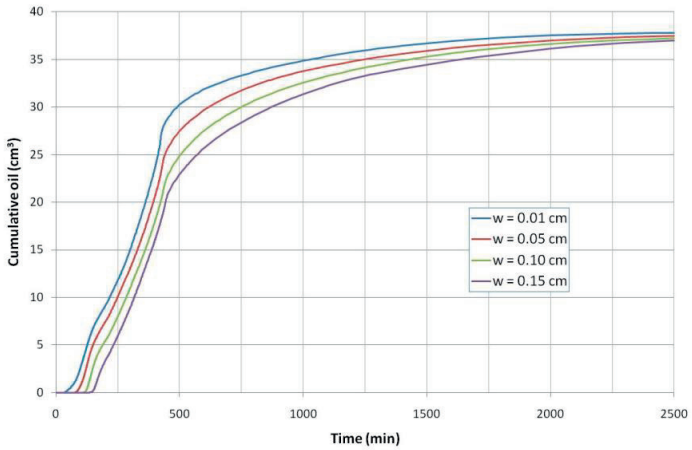

Figure 4.19 Cumulative oil production for different high permeable layer thickness cases

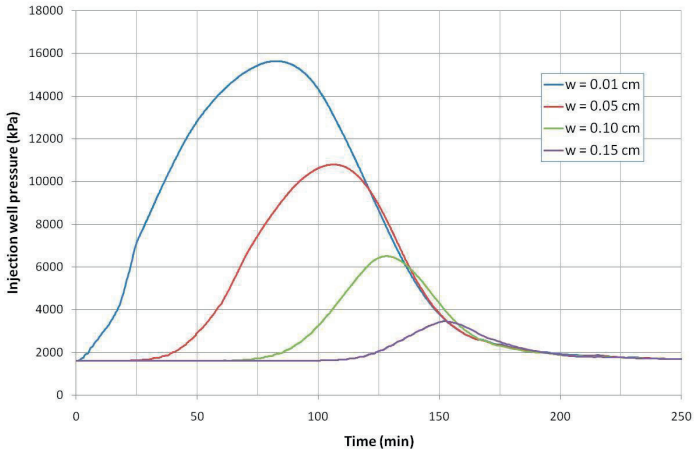

Figure 4.20 Pressure at the injection face of the core for different high permeable layer thickness cases

4.5 Conclusions

The performance of steam injection in heterogeneous porous media containing Athabasca heavy crude was studied numerically. The core was assumed to have a high porous and high permeable layer in the middle. Considering a heterogeneous system, sensitivity analyses were focused on the effect of steam temperature and quality, different shale barrier configurations, permeability contrast in the core, porosity of the model, injection rate and thickness of the high permeable zone in the middle of the core. The following conclusions can be drawn from this study.

- There is an optimum steam temperature and quality regarding efficiency of steam injection. In our case the best steam temperature was 200 °C and steam quality of 85% resulted in a better oil recovery response. Higher steam temperature introduces more energy into the porous media, while the extra oil recovery is insignificant. Increasing steam quality, however, reduced oil recovery as there will be lower water saturation than interstitial water due to evaporation at the inlet face and higher residual oil saturation.
- Considering different shale barrier configurations in the core revealed that shale layers can limit the flow of oil and cause high residual oil saturation, but their impact is dependent on permeability distribution in the core. Having good communication with the high permeable zone in the core is significant since steam flows easily inside this zone and transfers thermal energy to the cold oil inside the lower permeable parts.
- The permeability contrast between the high and low permeable layers should be smaller considering both oil production and SOR. Higher permeability in the core can cause faster recovery and lower SOR, since the injection can stop earlier.
- Porosity of the model is found to have an inverse relation with the oil recovery and SOR.
- Higher injection rates improve the oil recovery. However, SOR should also be considered at the same time. There is a trade-off between recovery and SOR.
- Lower thickness for the high permeable zone results in better recovery while causing high injection pressure at the inlet. This corresponds with lower permeability contrast case.

Acknowledgement

The authors would like to thank Statoil ASA for providing financial support and acknowledge SINTEF Petroleum Research for collaboration in PVT properties analyses of Athabasca bitumen.

Nomenclature

GC	Gas chromatography analysis
HS-1	Horizontal shale barrier – Scheme 1
HS-2	Horizontal shale barrier – Scheme 2
IFT	Interfacial Tension, mN/m
kH	High permeable zone permeability
kL	Low permeable zone permeability
SAGD	Steam Assisted Gravity Drainage
SOR	Steam Oil Ratio
T	Temperature, K
w	Thickness of high permeable zone, cm
μ	Dynamic viscosity, cp

Chapter 5

Numerical Simulation Study of Field Scale SAGD and ES-SAGD Processes Investigating the Effect of Relative Permeabilities

This chapter is a paper accepted for publication in the Energy and Environment Research Journal. It is presented as an application of the experimental work on relative permeabilities. The content of the paper is presented with only a couple of minor revisions.

5.1 Abstract

Steam Assisted Gravity Drainage (SAGD) has been proved to be an effective method in producing from extra heavy oil or bitumen resources. The main recovery mechanism in this process is viscosity reduction by introducing heat into the reservoir. The Solvent Co-Injection processes (SCI) or Expanding Solvent SAGD (ES-SAGD) are alternative methods to the conventional SAGD. In these processes reduction in the oil viscosity is achieved by a combination of latent heat from steam and dissolution of solvents into bitumen. These alternative methods lower the steam requirements and associated costs with it as well as the amount of carbon dioxide emission into the atmosphere caused by steam generation process.

In this work some numerical simulations were conducted to examine the effect of relative permeability data on the performance of SAGD and ES-SAGD processes. Temperature dependant relative permeability data, that shows variation of end points with temperature, was tested against fixed relative permeabilities. Oil production was found to be strongly dependant on the end point relative permeability data. It is suggested to use temperature dependant relative permeabilities in numerical simulations. This must be considered as a matching criterion, when trying to history match field data.

Solvent co-injection showed promising results both in terms of improved recovery factor and reduced steam oil ratio as an economical criterion. In addition, the high solvent recoveries of 97-100% in all solvent co-injection runs make the process even more economically interesting. Injecting only 2% on a molar basis of pentane, hexane or heptane as solvent, boosted the oil rates up.

Keywords: Steam Assisted Gravity Drainage, Solvent Co-Injection, Expanding Solvent SAGD, Bitumen, End point relative permeabilities

Nomenclature

CWE	Cold Water Equivalents		
ES-SAGD	Expanding Solvent Steam Assisted Gravity Drainage		
HSor	High residual oil saturation relative permeability data set		
K	K-value		
k_r	Relative Permeability		
LSor	Low residual oil saturation relative permeability data set		
N	Oil or water Corey exponents in Corey relative permeability equation		
P	Absolute Pressure, kPa	S	Fluid saturation
SAGD	Steam Assisted Gravity Drainage	SCI	Solvent Co-Injection
SOR	Steam to oil ratio	T	Absolute Temperature, K
TD	Temperature dependant relative permeability data set		
$VISC$	Fluid viscosity, cP		

Subscripts

o	Oil	w	Water
i	Initial value	r	Residual value

Superscript

0	End point value	*	Normalized value

5.2 Introduction

The idea of Steam Assisted Gravity Drainage (SAGD) process was introduced by Roger M. Butler in late 1970s as a thermal in-situ heavy oil recovery process. The procedure is applied to multiple well pairs. In this process, two horizontal wells separated by a vertical distance are placed near the bottom of the formation. The top horizontal well is used to inject steam, which rises forming a large steam chamber above the well, and the bottom well is used to collect the produced liquids (formation water, condensate, and oil). The rising steam condenses on the boundary of the chamber, heating and entraining the oil to the production well. The process leads to a high recovery and high oil rate at economic steam oil ratios (SOR) (Butler, 1981). This process, however, suffers from high energy requirements in order to produce steam. Access to water resources is crucial and generation of steam emits huge amount of carbon dioxide into the atmosphere. The energy requirement is expressed in terms of SOR, which is defined as the ratio of injected steam to the produced oil in this process.

In order to improve the energy efficiency of SAGD, some hybrid processes were introduced. These processes, usually known as Solvent Co-Injection (SCI) or Expanding Solvent Steam Assisted Gravity Drainage (ES-SAGD), are based on co-injection of limited amount of solvents together with steam (Nasr and Isaac, 2001). These

hydrocarbon solvents or solvent mixtures dissolve into the heated oil at the boundary of the steam chamber and will further reduce the bitumen viscosity.

Chow (1993) simulated the laboratory experiment of SAGD that was performed by Chung (1988). He was able to history match spreading steam chamber phase of his experiment using linear relative permeability curves, as the model had a very high absolute permeability. He mentioned, however, that the simulator was not able to fully match the rising steam chamber phase due to not having the capability of modeling oil and water emulsification that occurs as a result of counter current flow.

Kamath et al. (1999) modeled SAGD in two dimensions for heterogeneous layered oil sand reservoirs to study the effect of heterogeneity on the growth of steam chamber and the process performance. The effect of various reservoir parameters such as porosity, permeability, initial mobile water saturation, Dykstra-Parson's permeability variation, reservoir anisotropy and shale barriers on the SAGD process performance was investigated.

Later Kisman and Yeung (1995) performed a similar study with a two-dimensional numerical model which considers the relative effects of permeability, relative permeability, wettability changes, oil viscosity, thermal conductivity, flow barriers and solution gas.

Albahlani and Babadagli (2008) performed a critical review of the attempts in the literature to model the SAGD process and improve its performance. Their paper contains an intensive review highlighting the important parameters affecting the operation of SAGD. These parameters include porosity, thickness of the layer, gas saturation, permeability of the formation, viscosity and API of the bitumen, wettability of the rock and heterogeneity of the formation.

Deng et al. (2010) presented the results of a laboratory ES-SAGD process that uses diluents as the co-injected solvent to the steam. They highlight that use of a solvent mixture (such as diluents / naphtha) is superior to pure hydrocarbons due to its availability and reduced cost. They stated that the solubility of the solvent used in the ES-SAGD process needs to be determined in the bitumen sample experimentally, and the operating condition of the process must be tuned accordingly for a successful simulation of the experiments.

Yazdani et al. (2012) performed field scale simulation of the ES-SAGD process using normal alkanes C_3 to C_7 as solvents added to steam stream. According to them uncertainty in relative permeability data can have a significant effect on the performance of different solvents in the simulation study. It is recommended to use a solvent that follows the steam condensation behavior at the reservoir temperature and pressure condition (Yazdani et al., 2012).

5.3 Numerical simulation study

In order to investigate the effect of temperature dependency of relative permeabilities on the field performance of SAGD and ES-SAGD, a numerical simulation study was conducted. Below is a summary of the model.

5.3.1 3-D numerical model

The model considered for this study was a 3-deminsional section of a reservoir. Due to symmetry of the SAGD process, only half of the area covered by the two wells is modeled. The section of the reservoir is 47m in thickness, and the two horizontal wells are stretched all the way through 300m length of the section in y-direction. The spacing between horizontal well pairs is 100m. Therefore the width of the section considered is 50m. The grids are 25×3×26 in x, y and z-directions respectively. The spacing between the horizontal injector and producer is 10m, and the producer is located 1.5m above the formation base. Figure 5.1 illustrates the cross-sectional view of the model in two directions.

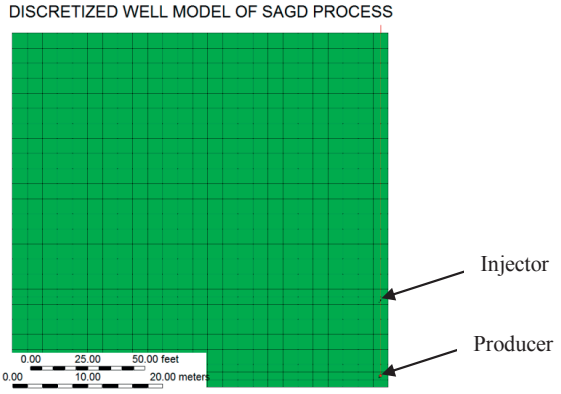

(a) I-K view of the simulation model

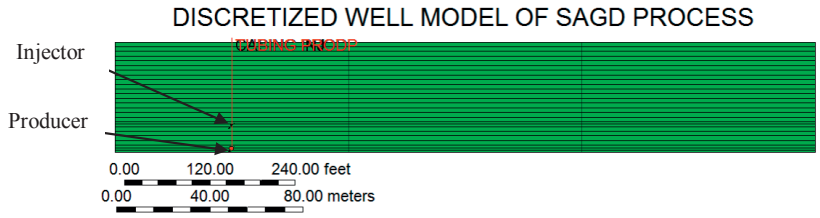

(b) J-K view of the simulation model, injector and producer extend through 3 layers in y-direction

Figure 5.1 Cross-sectional view of the simulation model showing the position of injection and production wells

5.3.2 Discretized well model option

In order to be able to model the preheating period at the start of the SAGD process, a discretized well model approach was chosen. This option is being provided by CMG reservoir simulator to be able to model the well flow more accurately. The well is then considered as a casing or annulus space with tubing in the middle. Steam is injected through the tubing and flows into the open wellbore at the end of the tubing. The stream flows into the reservoir through perforations and the extra steam is produced to the surface through the annulus space. (CMG-STARS user's guide, 2012)

5.3.3 Rock and fluid properties

In the fluid characterization part of the model, the bitumen was considered as a pseudo component with defined properties. It was the only component in the oil phase with no solution gas. The PVT properties of the Athabasca bitumen such as density, molecular weight and viscosity behavior versus temperature, measured in the laboratory, were used in the fluid characterization model (Ashrafi et al., 2011). Figure 5.2 shows the viscosity variation by temperature used in this simulation study.

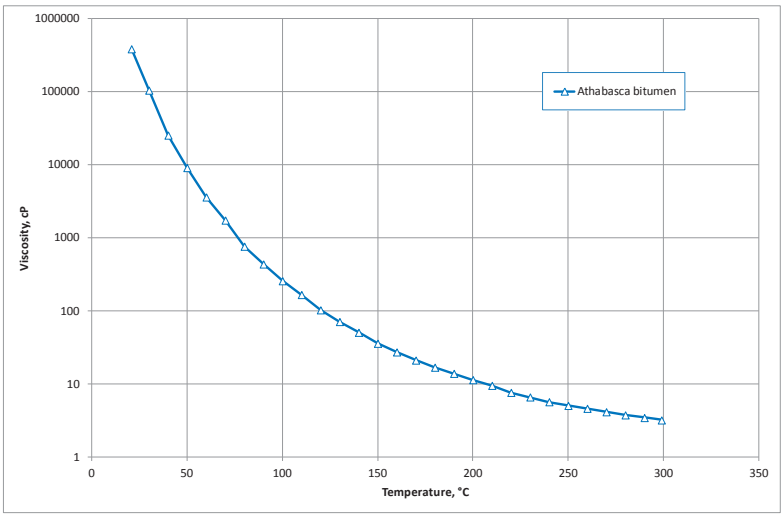

Figure 5.2 Viscosity of Athabasca bitumen versus temperature (Ashrafi et al., 2011)

For the viscosities of the solvents used in ES-SAGD process simulations, the internal liquid viscosity correlation for some selected normal alkanes presented in STARS manual was used. This equation is as follows (CMG-STARS user's guide, 2012):

$$VISC = AVISC \times exp(BVISC/T) \quad (5.1)$$

Where values of the coefficients $AVISC$ and $BVISC$ are given for selected components in STARS manual, $VISC$ is viscosity and T is absolute temperature.

The advantageous effect of adding solvents to the steam in any solvent co-injection process is the viscosity reduction of bitumen as a result of solubility. Solubility of the solvents in bitumen is reflected in K-values of the solvents. K-values are the ratios of the mole fraction of each solvent in vapor phase to that in liquid phase at thermodynamic equilibrium condition. K-values are therefore temperature, pressure and concentration dependant. In this study the K-values of the solvents versus temperature and pressure were estimated using the following equation provided in STARS manual (CMG-STARS user's guide, 2012):

$$K = (KV1/P) \times exp(KV4/(T - KV5)) \tag{5.2}$$

Where coefficients *KV1*, *KV4* and *KV5* are component dependant and presented in STARS manual for selected components. *P* and *T* are pressure and absolute temperature respectively.

Other fluid and rock properties used in this study are listed in Table 5.1.

Table 5.1 Rock and fluid properties used in the simulation study

Reservoir properties		Thermal properties	
Horizontal permeability	7000 mD	Rock heat capacity	3.52×10^{6} J/(m^3.°C)
Vertical permeability	2100 mD	Rock thermal conductivity	2.164×10^{5} J/(m.day.°C)
Porosity	0.33	Water thermal conductivity	5.357×10^{4} J/(m.day.°C)
Reservoir temperature	11°C	Oil thermal conductivity	1.296×10^{6} J/(m.day.°C)
Reservoir pressure	2200 kPa	Heat capacity of overburden and underlying layers	2.39×10^{6} J/(m^3.°C)
Oil saturation	0.9	Thermal conductivity of overburden and underlying layers	1.69×10^{5} J/(m.day.°C)
Water saturation	0.1		

5.3.4 Relative permeability data

Previous laboratory core flooding experiments by the authors have indicated the dependency of the end point relative permeabilities on the temperature (Ashrafi et al., 2012). Therefore it was decided to examine different relative permeability data to check the sensitivity of model to these data. The option to include the temperature dependant end point relative permeability data is provided by CMG-STARS simulator. The basic shape of the relative permeability curves considered was Corey type (Corey, 1954) as follows:

$$k_{rw} = k_{rw}^{0}\left(S_w^*\right)^{N_w} \tag{5.3}$$

$$k_{ro} = k_{ro}^{0}\left(1 - S_w^*\right)^{N_o} \tag{5.4}$$

Where, S_w^* is normalized water saturation:

$$S_w^* = \frac{S_w - S_{wi}}{1 - S_{wi} - S_{or}} \tag{5.5}$$

The same type of equation form applies to the liquid-gas relative permeability curves. All the Corey type exponents (N) were considered to be equal to 1.5 arbitrarily. One set of relative permeability data is referred to as HSor (High residual oil saturation) in which the residual oil saturation is considered to be 0.38. This set of data was used in simulations as a basic case for comparison. In another set of simulation runs, the same relative permeability data as HSor was used together with the temperature dependant end points option. It was assumed therefore that the initial water saturation is rising and the residual oil saturation is decreasing as the temperature increases. A third relative permeability data set is considered with a lower residual oil saturation of 0.25. This set is referred to as LSor (Low residual oil saturation). This was used as a control check to see the difference in having a fixed S_{or} or a temperature dependent S_{or}. Figure 5.3 shows both HSor and LSor relative permeability data sets.

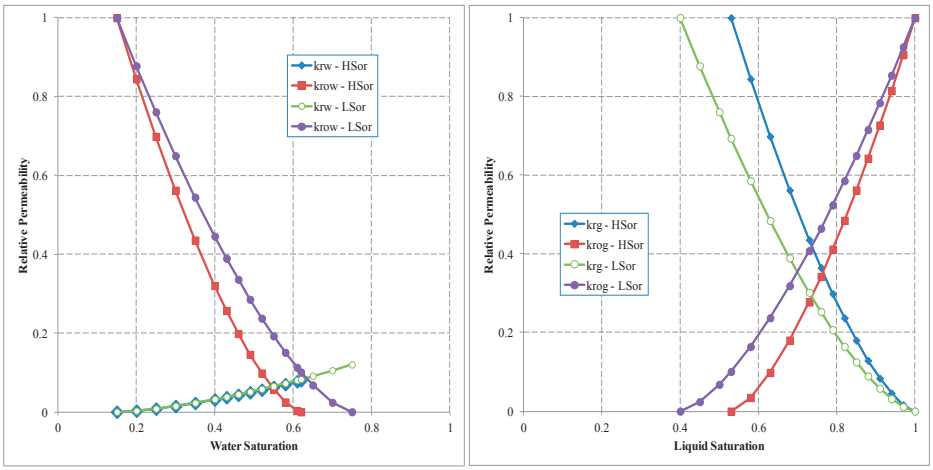

Figure 5.3 Relative permeability data sets HSor (High S_{or}) and LSor (Low S_{or})

The case of temperature dependant relative permeability data uses the same data as HSor together with the temperature dependant values listed in Table 5.2.

Table 5.2 Temperature dependant relative permeability data parameters

Temperature, °C	S_{wr}	S_{orw}	S_{gr}	S_{org}	k_{rwiro}	k_{rocw}	k_{rgcw}
15	0.15	0.40	0	0.38	0.08	1	1
105	0.20	0.34	0	0.32	0.10	1	1
195	0.25	0.28	0	0.25	0.12	1	1

Where:

S_{wr} Irreducible water saturation

S_{orw} Residual oil saturation for water injection

S_{gr} Critical gas saturation

S_{org} Residual oil saturation for gas injection

k_{rwiro} Relative permeability to water at irreducible oil saturation for water injection

k_{rocw} Relative permeability to oil at connate water and zero gas saturation

k_{rgcw} Relative permeability to gas at connate liquid

5.3.5 Operation scenario

This simulation study was conducted to represent a field scale SAGD process. It consisted of several injection phases. The discretized injector and producer wells defined are used to circulate steam of temperature 325°C and 0.8 quality in a 3 month period. This pre-heating period is simulated to represent the circulation phase in an actual SAGD project. The goal is to warm up the space between the well pairs and establish an initial communication between the wells. After the pre-heating period, the high pressure SAGD phase starts when the temperature of steam is 325°C and the quality is 0.9. The steam was injected with a rate of 100 m^3/day for a 2 month period, and then with a reduced injection rate of 50 m^3/day for 1.5 month as a depressurization phase. The normal SAGD phase was then initiated at 6.5 month from the start of the whole process until the end. The whole simulation run was about 9-10 years depending on the oil rate at final stages, as the process was set to stop if the oil rate dropped to 2 m^3/day. The well constraints in SAGD phase was a maximum pressure of 5500 kPa and maximum injection rate of 250 m^3/day for the injector and a minimum bottom hole pressure of 5200 kPa for the producer. The injected steam had a temperature of 270°C and a quality of 0.9. There was a maximum liquid rate of 150 m^3/day for the producer at the first year of SAGD process, which was then raised to 250 m^3/day. The maximum steam production rate was also considered for the producer to prevent the production of live steam. During the ES-SAGD runs, the process was turned to solvent co-injection after about one year from the beginning of the SAGD phase. This was set at the same time as the jump in the maximum production rate for the producer well. The ES-SAGD phase lasted for 5.25 years, and then turned to SAGD when the oil production rate was dropping in order to produce back as much of the solvent as possible.

5.4 Numerical simulation results and discussions

Three SAGD cases were simulated using three sets of relative permeabilities described earlier. These base cases were considered to figure out the behavior of the model mainly with respect to variable end points. The case HSor has a higher residual oil saturation (S_{or} = 0.38) than LSor (S_{or} = 0.25). These two permeability sets were fixed, however, the third set was a temperature dependant set. It was basically the same as HSor at reference temperature and gradually shifting towards LSor at higher temperatures especially in terms of S_{or}. The recovery factors are compared in Figure 5.4. As the figure shows the ultimate oil recovered in both LSor and Temperature dependant cases are about the same, however, the rate of recovery is higher when using temperature

dependant relative permeability data. The oil production rates for these three cases are also depicted on Figure 5.5 for comparison.

In lack of actual field production data, it is really hard to judge which relative permeability set is matching the reservoir behavior best, but this clearly shows the sensitivity of the SAGD production data to this important piece of data, namely relative permeabilities. Previous work by the authors (Ashrafi et al., 2012) has shown the dependency of end points on the temperature, and it seems crucial to consider this fact as a matching criterion when one is trying to match SAGD field data with a numerical reservoir simulator.

The two relative permeability sets of HSor and temperature dependant (TD) were chosen for the rest of the runs to examine the effect of solvent co-injection in the model. Three normal alkanes were added to the model as solvents to help reduce the viscosity of Athabasca bitumen. Normal pentane, normal hexane and normal heptane were tested as solvents in the ES-SAGD process.

Different simulation runs indicated that the best scenario was to start the injection of solvent at about 1.75 years from the start of the simulations (1 year after the start of normal SAGD phase), when the process is mature, and the steam chamber almost hits the top of the formation. Starting the injection of solvent before this time was not increasing the recovery while spending valuable solvent. The injection of solvent continued for 5.25 years and was stopped at the end of the 7th year. Injecting solvent with steam beyond this time was also not beneficial as there was no more increased recovery. Starting from 7th year until the end of the simulation runs was a normal SAGD operation to help produce as much of the oil and solvent in place as possible.

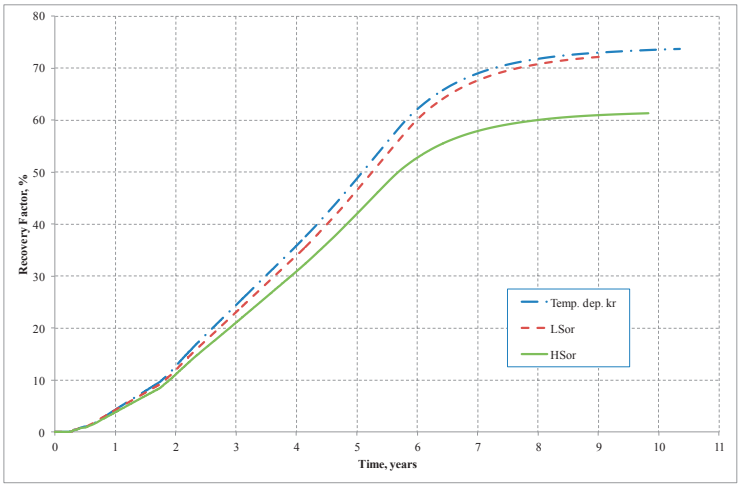

Figure 5.4 Recovery factors for the three different relative permeability sets: Temperature dependant, Low S_{or} and High S_{or}

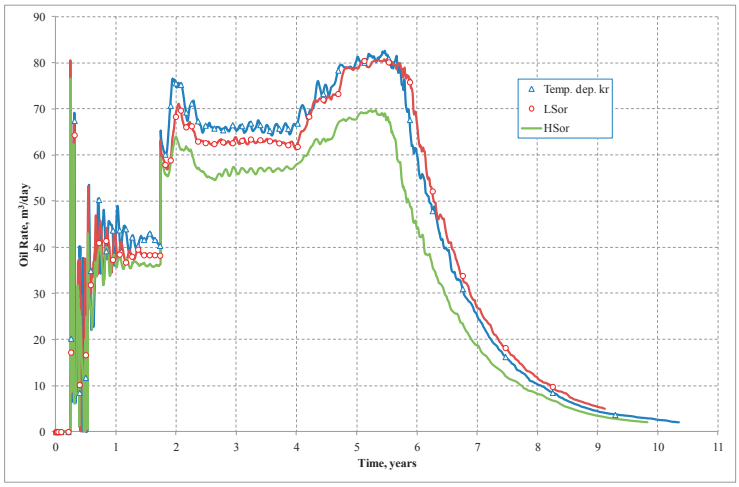

Figure 5.5 Oil production rate for the three relative permeability sets

Figure 5.6 compares the recovery factors of SAGD and ES-SAGD processes for the temperature dependant relative permeability (TD) case. The amount of solvents co-injected is 1% molar based in this case.

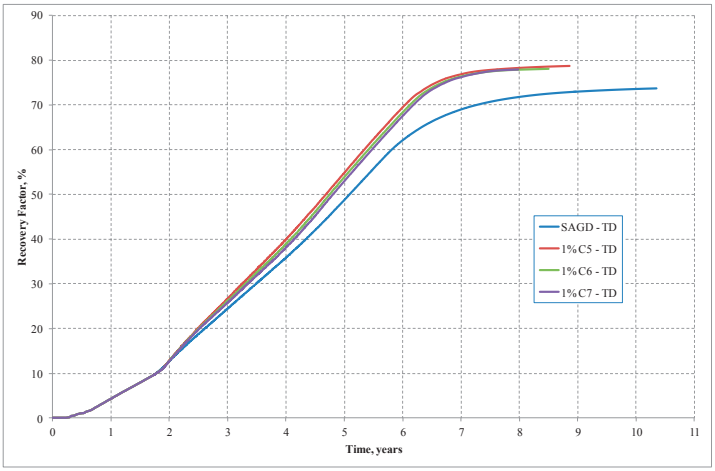

Figure 5.6 Oil recovery factor for the TD (Temperature Dependant k_r) case – Co-injecting 1% solvent

As seen on the figure there is a minor difference between C_5, C_6 and C_7 in terms of increasing the oil recovery factor. In all the three solvent cases the recovery is higher than SAGD by about a 5% increase.

The co-injection of solvent together with steam seems to be quite efficient in terms of solvent recovery. Figure 5.7 shows the amount of solvent in place expressed in standard

cubic meters. Knowing that total amount of injected solvents are 20003 Sm^3, 22922 Sm^3 and 25849 Sm^3 of C_5, C_6 and C_7 respectively, the solvent recovery is 98.3% for both pentane and hexane co-injection and 97.2% for heptane co-injection case.

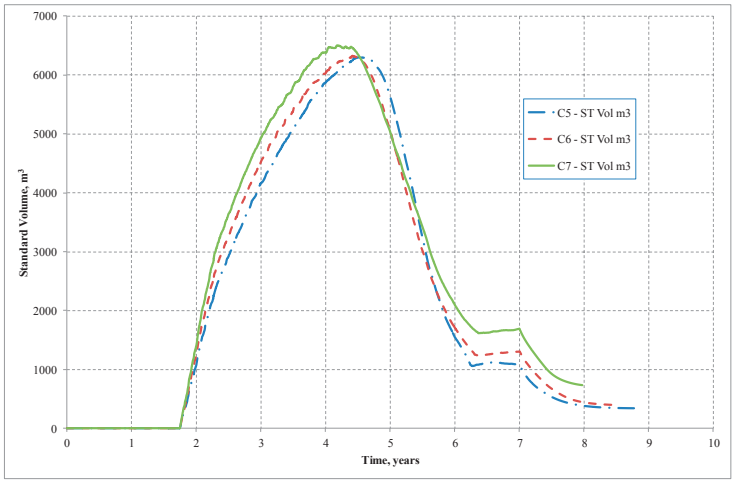

Figure 5.7 Solvent in place in terms of standard volume for 1% solvent ES-SAGD – TD case

The increase in oil recovery factor by co-injecting solvents seems to be more pronounced in the case of HSor relative permeability set. The recovery factors are revealed in Figure 5.8. Again the three solvents are acting about the same, pushing up the ultimate recovery by about 10.5-11% compared to pure SAGD. The oil rate comparison between SAGD and ES-SAGD is shown on part b of Figure 5.8. The oil rate for the co-injection of pentane is only compared against base SAGD case, as it was almost the same for the other solvents. The period of time during which solvent is co-injected into the reservoir together with steam is quite visible on this figure. The oil rate during this period is higher. At the end of the 7^{th} year, when the injection of solvent is stopped and the process is changed back to normal SAGD, the oil rate drops below the base SAGD case. The positive effect of solvent in reducing the viscosity by dissolving in bitumen is the cause of higher oil rates. The solvent co-injection (SCI) process is improving the economy of the oil production operation by reducing the steam oil ratio (SOR). SOR is defined as the ratio of injected steam in terms of cold water equivalents (CWE) to the amount of oil produced. SOR is considered as an economical parameter when comparing different operations to recover viscous oils. As depicted on Figure 5.8.c, the cumulative SOR is reduced when solvent is added to steam. The energy lost to over and under-burden layers during the operations are compared on part d of Figure 5.8. There seems not to be a big difference between SAGD and SCI processes in terms of energy loss.

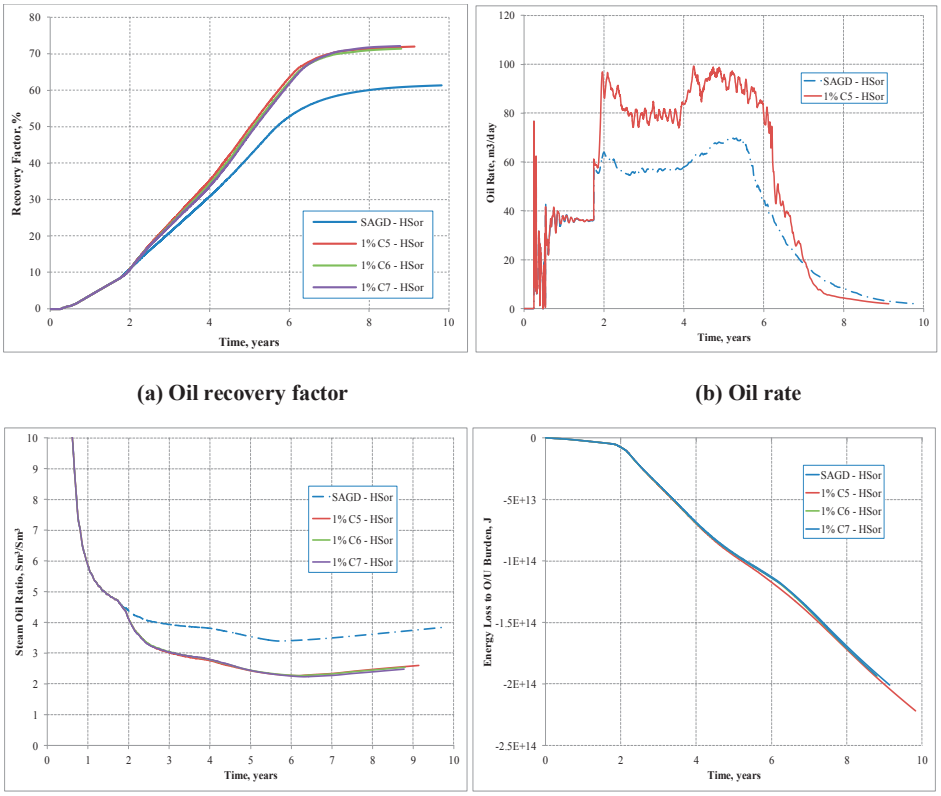

(a) Oil recovery factor **(b) Oil rate**

(c) Cumulative steam oil ratio **(d) Energy loss to over/under-burden**

Figure 5.8 Comparison between SAGD and ES-SAGD for the HSor (High S_{or}) case – Co-injecting 1% solvent

Another set of simulation runs were accomplished to figure out how much more oil can be recovered by doubling the amount of solvent used. As such 2% of solvent was added to the steam on a molar basis. The rise in recovery factors was considerable compared to 1% solvent case. The recovery factors are shown in Figure 5.9.a for temperature dependant relative permeabilities (TD) case. The recovery factor rises to about 86.6% for 2% pentane co-injection and 89.1% and 89.6% for 2% co-injection of hexane and heptane respectively. The recovery factor improvements are even more dramatic for the HSor (High S_{or}) relative permeability case, which is not temperature dependant. They show an increase of about 22.8-25.8% for the three tested solvents compared to the base SAGD run (Figure 5.9.b). On parts c and d of Figure 5.9 production oil rates are demonstrated. The comparison is depicted only for the case of heptane co-injection with steam. The impact of injecting 1 or 2% of solvent on a molar basis is clearly visible on boosting the oil rates up during the co-injection phase of the operation as compared to the pure SAGD process. Injecting only 1 or 2% of normal alkanes as solvent together

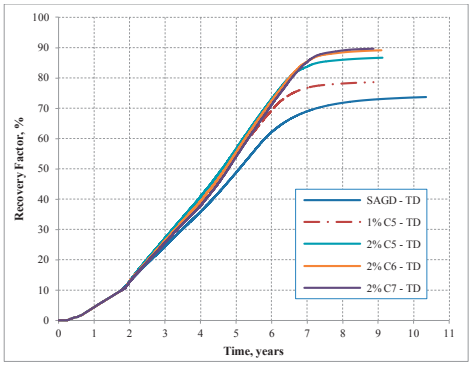

(a) Recovery factor – TD rel. perm. data set

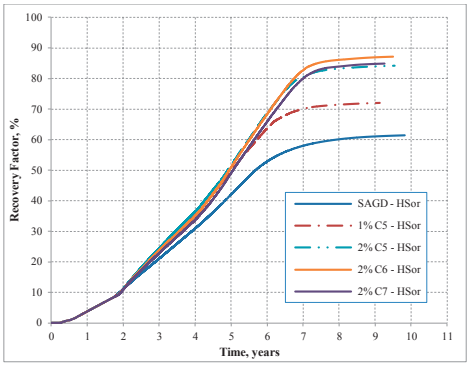

(b) Recovery factor – Hsor rel. perm. data set

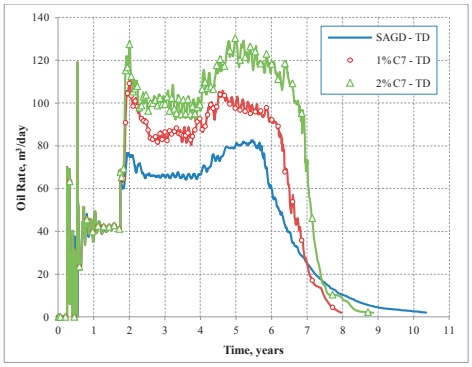

(c) Oil production rate – TD rel. perm. data set

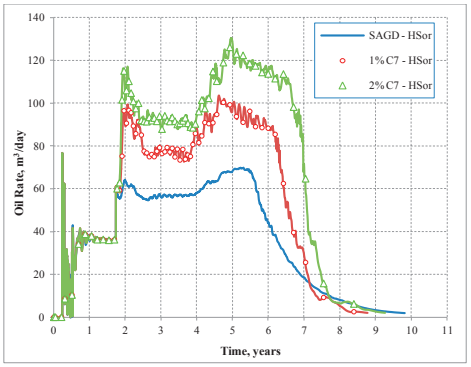

(d) Oil production rate – Hsor rel. perm. data set

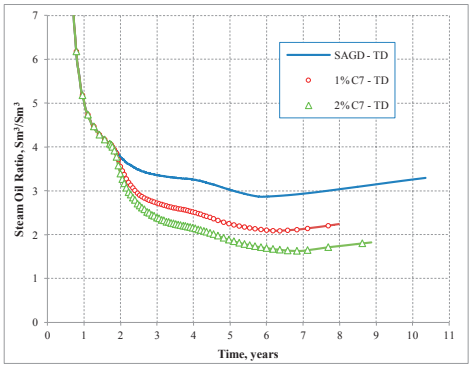

(e) Cumulative steam oil ratio – TD rel. perm. data set

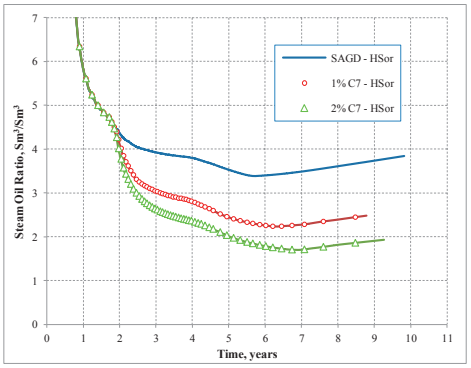

(f) Cumulative steam oil ratio – Hsor rel. perm. data

Figure 5.9 Comparison between SAGD and ES-SAGD with two different solvent loadings of 1% and 2% molar based for the two different permeability data - TD (Temperature Dependant k_r) and HSor (High S_{or})

with the steam not only improves the final amount of oil recovered, it also makes the whole operation less polluting. As can be seen on parts e and f of Figure 5.9, the amount of cumulative steam oil ratio drops as a result of both higher oil production and lower steam injection. Generating and injecting lower amount of steam is beneficial to the environment as well as the economy of the operation, as steam production requires burning of valuable hydrocarbons. This, however, raises some questions about the value of the injected solvents and its effect on the cost of operations. It is beyond the scope of this study to consider the costs of operation, however, as it will be shown later, most of the injected solvents are recoverable during the SCI process.

Figure 5.10 compares the cumulative volumes of solvent injected and produced for some of the simulation runs. When the injection of solvent begins, it takes some time for the solvent to accumulate inside the reservoir and diffuse into bitumen. That causes the production of solvents to occur late as seen on Figure 5.10 plots. However, almost the whole amount of solvent that is injected in each run is produced at the final stages.

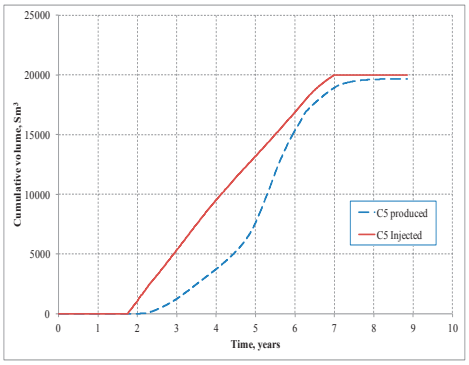

(a) 1% C_5 Co-injection – TD rel. perm. data set

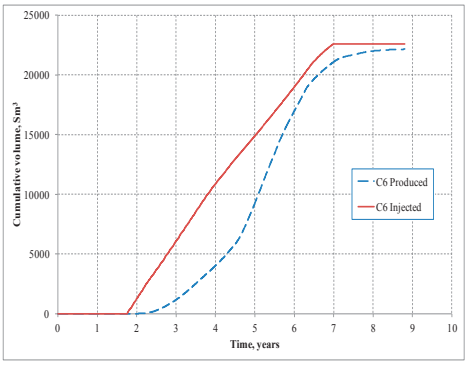

(b) 1% C_6 Co-injection – Hsor rel. perm. data set

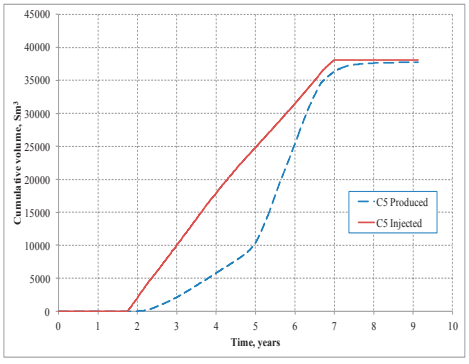

(c) 2% C_5 Co-injection – TD rel. perm. data set

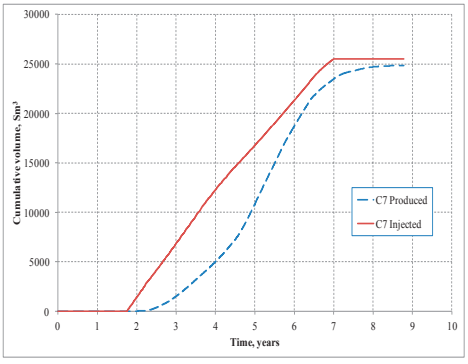

(d) 1% C_7 Co-injection – Hsor rel. perm. data set

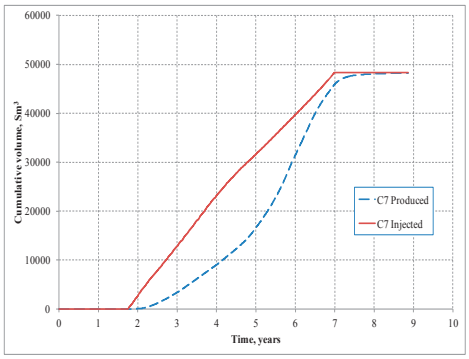

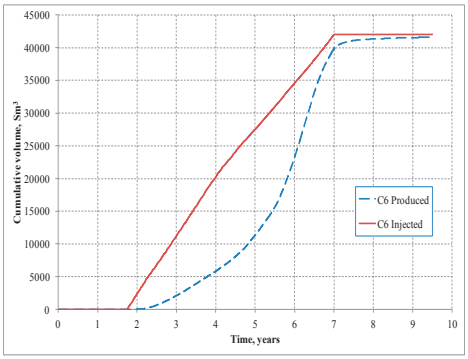

(e) 2% C_7 Co-injection – TD rel. perm. data set **(f) 2% C_6 Co-injection – Hsor rel. perm. data set**

Figure 5.10 Cumulative volume of solvent injected and produced expressed in standard condition volume

The plots on Figure 5.11, showing the solvent recovery, demonstrate the ratio of solvent production to injection. At the end of the operation about 97- 100% of the injected solvent was recovered in all the cases. The final SAGD phase starting at the end of 7th year in particular was effective to recover any amount of solvent left inside the reservoir. High solvent recovery indicates the privilege of ES-SAGD process compared to normal SAGD operation, because less amount of steam is needed and the extra solvent used is also recovered.

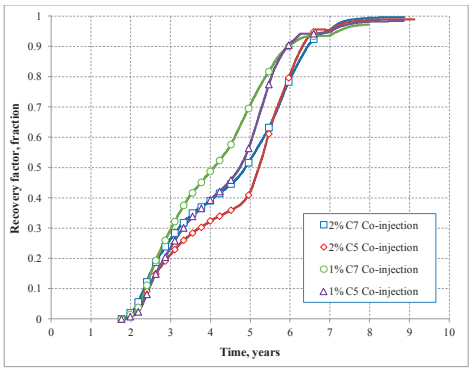

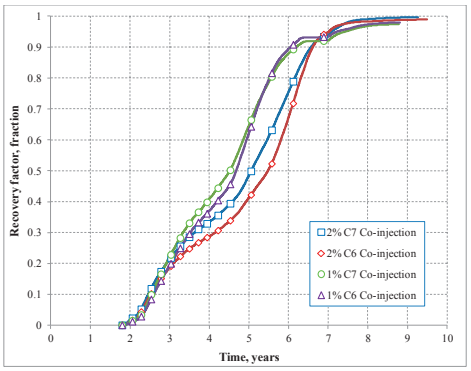

(a) Temperature dependant rel. perm. data set **(b) High S_{or} rel. perm. data set**

Figure 5.11 Instantaneous solvent recovery factor for the two relative permeability data set simulations

5.5 Conclusions

Numerical simulation study was conducted to test the effect of relative permeability data on the performance of SAGD and ES-SAGD or SCI (Solvent Co-Injection) processes. Oil production was found to be strongly dependant on the end point relative

permeability data. As the results of previous work by authors (Ashrafi et al., 2012) justify the dependency of endpoint data on temperature, it is therefore suggested to use temperature dependant relative permeability data in numerical reservoir simulations. Comparing the use of fixed relative permeability data with shifting data between the two end points shows different outcomes in terms of oil production curve. This must be considered as a matching criterion, when field data are available.

Using different relative permeability data with and without varying end points, the SAGD and ES-SAGD processes were compared. In both cases solvent co-injection showed promising results both in terms of improved recovery factor and reduced steam oil ratio. ES-SAGD process seemed to be superior to SAGD from economical point of view as well, since between 97 to 100% solvent recovery was achieved in all solvent co-injection runs. Injecting only 2% on a molar basis of pentane, hexane or heptane as solvent together with the steam, boosted the oil rates and showed increased recovery factors. At the end of the operation, normal SAGD was conducted to produce back any amount of solvent trapped inside the reservoir.

Acknowledgements

The authors would like to acknowledge Statoil ASA's financial support during the course of our research. We also thank Computer Modeling Group for providing us the license to CMG reservoir simulator.

Chapter 6

Numerical Simulation Study of SAGD Experiment and Investigating Possibility of Solvent Co-Injection

In this chapter the results of numerical simulation studies conducted on a two-dimensional model of SAGD is presented, and the sensitivity analysis is performed on different operating and reservoir parameters. The content of this chapter is taken from SPE conference paper 145013 with some minor revisions. An earlier version of this work is presented in a paper in Appendix B.2.

6.1 Abstract

Bitumen resources constitute a high portion of the total world oil resources. The main recovery mechanism for these high viscous fluids is to reduce their viscosity by the application of heat, mostly by introducing steam.

Among different steam injection schemes, steam assisted gravity drainage (SAGD) has become the method of choice applicable to bitumen and oil sand reservoirs. In these extra heavy oil resources, the reservoir has almost no injectivity due to high oil viscosity, and therefore conventional steam flooding is hard to conduct. SAGD, however, reduces the viscosity of bitumen in place and the heated bitumen drains due to gravity forces towards the production well and is then being produced. Recently hybrid processes are attracting more attentions in the industry. These processes benefit from co-injection of a solvent together with steam. The solvent can diffuse into the bitumen and make it even lighter by reducing the viscosity.

Our simulation study is based on the experimental work done by Chung (1988) and the simulation model of this experiment by Chow (1993). Chung′s physical experiment was a 2-D model to simulate SAGD experiment in laboratory. The Chung′s experiment was done with Cold Lake crude oil. A reservoir simulation model was built using a numerical thermal reservoir simulator. The model was then tested and validated with Chung′s physical model. Having a valid model, sensitivity analysis was run to examine the effect of different simulation parameters on recovery and steam oil ratio.

The sensitivity parameters tested are steam temperature and quality, the porosity of the model, different well placement schemes, and the effect of shale barrier. Different steam temperatures and qualities were examined. The best injection condition was found to be 130 °C and 90% quality, beyond which no increased recovery was achieved. Different

injector and producer placements were tested. Placing injector and producer diagonally in the model showed the best horizontal sweep efficiency in the laboratory model. Horizontal shale barrier had a dramatic negative effect on the oil recovery. Vertical shale, however, had a smaller effect. This is because in horizontal case the steam chamber cannot reach to the top layers. Porosity was found to be inversely proportional to the oil recovery and steam oil ratio. Results showed that solvent can help to improve oil recovery and steam-oil ratio. In addition most of the injected solvent could be recovered from production stream. Sensitivity analyses on solvent type and concentration indicated significant effects on performance of process. Among the solvents used in this study, hexane showed the best recovery performance.

6.2 Introduction

There are some attempts in the literature to simulate the SAGD process in order to provide a better understanding of the sensitivity of the process to various operational parameters. Kamath et al. (1999) developed a two-dimensional numerical model of the steam assisted gravity drainage process with a pair of horizontal wells (SAGD) for heterogeneous layered oil sand reservoirs to study the effect of heterogeneity on the growth of steam chamber and the process performance. The effect of various reservoir parameters such as porosity, permeability, initial mobile water saturation, Dykstra-Parson's permeability variation, reservoir anisotropy and shale barriers on the SAGD process performance was investigated. The SAGD performance improves significantly with high steam injectivities, low mobile water saturation near the producer, absence of continuous shale barriers, high vertical to horizontal permeability ratio and optimum injector-producer vertical spacing. The lateral well spacing affects the early period of oil production and the project life.

Later Kisman and Yeung (1995) performed a similar study with a two-dimensional numerical model which considers the relative effects of permeability, relative permeability, wettability changes, oil viscosity, thermal conductivity, flow barriers and solution gas.

Elliot and Kovscek (1999) simulated a single-well SAGD (SW-SAGD) and performed a sensitivity analysis to improve the process performance at early times. The sensitivity analysis performed indicates that SW-SAGD is most applicable to heavy oils with initial viscosity below 10 Pa-s (10000 cp). Additionally, the reservoir must be sufficiently thick to allow significant vertical steam chamber growth. The sensitivity analysis also indicates that the presence of relatively small amounts of solution gas aids the recovery process by enhancing volumetric expansion of the oil on heating. They concluded that cyclic steam injection was the most efficient pre-heating method for SW-SAGD.

Akin and Bagci (2001) made an experimental investigation and optimization of startup procedure for single-well steam-assisted gravity drainage. They compared two methods

of continuous and cyclic steam injection and concluded that cyclic steam injection yields better results for SW-SAGD. They simulated the process with CMG (STARS), however, their numerical model was heated up more slowly than in the experiment and therefore a good match was not achieved.

Barillas et al. (2006) determined the optimum steam injection rate for a homogeneous reservoir whose sole heterogeneity was barriers using CMG (STARS). They noted that vertical permeability has a significant role on oil recovery. Parameters like horizontal permeability and viscosity have negligible effect on optimum steam injection rate. They also studied the effect of reservoir thickness.

Bagci (2006) made experimental and simulation studies on 3-D SAGD process in both homogeneous and fractured reservoirs. The shape and growth of the steam chamber in a fractured pack are different from those observed in the uniform permeability pack without fracture. An elongated steam chamber is observed for the fractured case while the homogeneous model had almost a circular steam chamber. Good results were obtained for the history matching of the experimental data. The author also investigated the effects of fracture orientation and different well configurations. He concluded that the horizontal well pair scheme gave higher recovery of original oil in place as expected. Existing or induced vertical fractures could be used to improve initial oil production rates. However, higher steam-oil ratios were observed in both vertical and horizontal fractures than in the conventional homogeneous model.

Chen et al. (2006) investigated the effects of heterogeneity on SAGD performance. The heterogeneity includes the effect of a hydraulic fracture either vertical or horizontal. For the case with a vertical fracture, the main oil production period starts shortly after steam injection and exhibits a much greater average oil rate, more than twice the oil rates of horizontal fracture and the base case without fracture. The observed different effects of horizontal and vertical fractures are explained by examining how the steam chamber profile is affected by the presence of fractures.

Swapan Das (2007) conducted a simulation study to investigate the possibility of the application of thermal techniques in fractured carbonate heavy oil reservoirs. He found that the SAGD method shows better performance in the case of high viscosity heavy oil fractured reservoirs whereas Cyclic Steam Stimulation (CSS) or Staggered SAGD may yield better recovery and production rates in the case of lower viscosity oil fractured reservoirs. He also concluded that the success of thermal techniques in fractured carbonate reservoirs depends strongly on the spontaneous imbibition of water and expulsion of the oil from the matrix.

Mollaei and Maini (2010) presented a review of important issues such as effect of temperature on physical properties of heavy oils and rocks and the thermo-chemical alteration of crude oil in their studies based on the context of steam injection through

naturally fractured reservoirs. They concluded that the differential thermal expansion between the pore volume and the oil is the most important oil recovery mechanism in the matrix. The reduction of viscosity ratio due to steam injection is the governing mechanism in fractures during steam injection process in naturally fractured reservoirs.

Oil rate improvement, reduction of SOR (Steam-oil Ratio), lowering energy consumption and water requirements are the most important advantages of solvent co-injection with steam over a conventional SAGD process. Govind et al. (2008) performed a 3-D field scale simulation to study ES-SAGD process. They reported that effective parameters that control ES-SAGD process are the solvent type, concentration, operating pressure and the injection strategy. They also concluded that ES-SAGD results in higher production rate, lower SOR, reduction in water consumption and fuel required for generating steam.

Ivory et al. (2008) conducted an experiment and simulations to investigate ES-SAGD process at a lower pressure. They found out that at 1500 kPa minimum production pressure and 10 °C sub-cool, co-injection of solvent with steam increased the average oil rate while reducing the SOR. Also they recommended considering the effects of solvent concentration, minimum production pressure and sub-cooling simultaneously in ES-SAGD process because they impact each other.

6.3 Physical model

A 2-D experimental model was used by Chung (1988) to carry out scaled physical model tests of SAGD using Cold Lake bitumen. The experimental apparatus used by Chung (1988) was composed of the physical reservoir model, the steam injection system, the production (effluent) handling system and the data monitoring system. The reservoir model used was of 35 cm width, 22 cm height and 3 cm thickness. Five sides of the model were constructed of reinforced phenolic resin, and the sixth large side was of transparent Plexiglas. The model was assumed to represent a vertical section through the reservoir. The Plexiglas side allowed observation and photography of the growth of the steam chamber and the flow pattern of the heated bitumen. The entire model was insulated, except the 35 cm x 22 cm transparent Plexiglas side. Forty-two copper-constantan, T-type thermocouples were planted to monitor the temperature distribution in the model.

The reservoir model was scaled to the field condition by using the method described by Butler et al. (1981). The porous media in the reservoir model was a glass bead pack, where the beads had a diameter of 2 mm. The model was initially saturated completely with the Cold Lake bitumen. Two procedures were considered in the experiments; namely rising steam chamber and spreading steam chamber. For conducting the rising steam chamber procedure, a horizontal steam injection well was located 1 cm above a horizontal production well which was at the bottom of the formation. In order to

consider the spreading steam chamber procedure, the injector well was placed near the top of the formation.

6.4 Numerical model

The model used in this simulation study is a 2-D Cartesian model. A 10×1×8 grid block configuration model is considered to provide sufficiently accurate results. This model is shown below in Figure 6.1. The producer well is placed in the bottom most layer and the injector is placed in the layer directly above it for the rising steam chamber case and in the top most layer for the spreading steam chamber case.

The vertical grid block dimension of 2.75 cm is assigned for all 8 layers. The horizontal dimensions of the 3 blocks at and near the wellbore are 0.5, 1 and 1 cm respectively. For the blocks farther from the well, the horizontal dimension is 2 cm each. It is considered to be 3 cm for the grid block farthest away from the wellbore. The increase in the horizontal grid size from the wellbore toward the boundary areas will improve computing efficiency since the degree of resolution required is higher near the wellbore and less at the boundaries of the model.

To simulate Chung's experiment (Chung, 1988), two well configuration schemes are considered. For the rising steam chamber scheme, the horizontal producer well is assigned into cell block (1, 1, 1), and the injector is in cell block (1, 1, 2), 1 cm above the producer well. In the spreading steam chamber scheme, the producer is in the same spot, while the injector well is assigned into cell/block (1, 1, 8). Please note that the Z direction in this model is from bottom to the top i.e. (the layer number 1 is the bottom layer of the model).

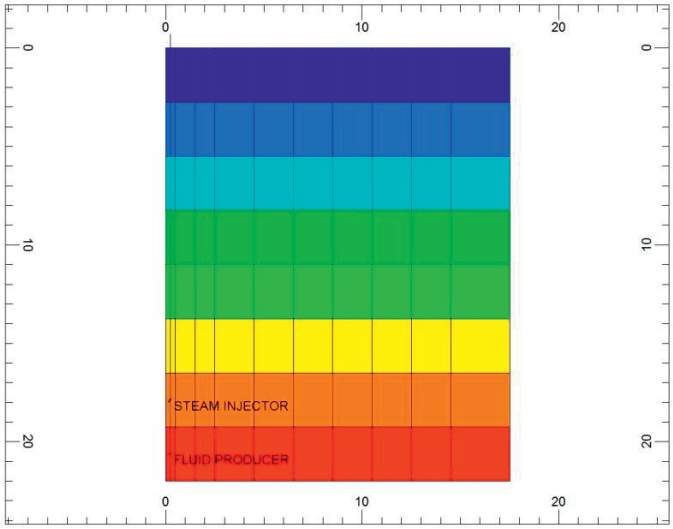

Figure 6.1 Numerical model illustration showing well positions for rising steam chamber case

Furthermore, in order to have more efficient simulation runs with respect to time, the numerical model is designed to simulate only half of the reservoir. This is possible since the steam chamber is symmetrical around the production and injection wells. In this case, only the right half of the physical portion of the experiment is selected for simulation. Multiplication of results by a factor of 2 will give the total production of the full well. Steam of 99% quality at 105 °C is injected under constant pressure of 153 kPa in the base simulation case. This constraint ensures that a liquid leg will be maintained between the injection and production wells. This liquid leg prevents excessive and premature steam breakthrough to the production well, and the effect is referred to as steam trap control.

The reservoir simulation parameters required are listed in Table 6.1. The viscosity data for the two cases of rising steam chamber and spreading steam chamber is assumed to be different at higher temperatures as shown in Figure 6.2 (Chow, 1993). The reason for having different viscosities is that when the steam chamber is rising upwards, we have a counter current flow of oil and steam and condensate. This will cause the formation of condensate emulsion inside the oil phase, which causes the viscosity to be higher than the oil phase viscosity.

Linear relative permeability curves, according to Table 6.1, independent of temperature are assumed in this study.

Table 6.1 Numerical simulation parameters used in this study (Chow, 1993)

Model properties		
	Width	17.5 cm
	Height	22 cm
	Thickness	3 cm
	Horizontal permeability	2360 D
	Vertical permeability	1880 D
	Porosity	0.392
	Initial pressure	101.3 kPa
	Initial temperature	25°C
	Oil saturation	0.99
	Water saturation	0.01
Rock properties		
	Rock compressibility	7.30E-06 kPa^{-1}
	Rock heat capacity	17.8 J/(gmole.°K)
	Rock thermal conductivity	0.628 J/(cm.min.°C)
	Insulation volumetric heat capacity	0.99 J/(cm^3.°C)
	Insulation thermal conductivity	0.0533 J/(cm.min.°C)
	Plexiglas volumetric heat capacity	0.99 J/(cm^3.°C)
	Plexiglas thermal conductivity	0.1 J/(cm.min.°C)

Fluid properties

Bitumen compressibility	7.00E-07 kPa^{-1}
Water thermal conductivity	0.372 J/(cm.min.°C)
Oil thermal conductivity	0.090 J/(cm.min.°C)
Gas thermal conductivity	0.018 J/(cm.min.°C)
Bitumen heat capacity	2093 J/(kg.°C)
Bitumen's first coefficient of thermal expansion	6.00E-04 $°C^{-1}$
Molecular weight of bitumen	500 g/gmole
Bitumen density	992 kg/m^3

Relative permeability data

S_w	k_{rw}	k_{row}	S_l	k_{rg}	k_{rog}
0.10	0.00	1.00	0.10	1.00	0.00
0.15	0.03	0.94	0.15	0.94	0.05
0.20	0.07	0.88	0.20	0.88	0.11
0.30	0.22	0.76	0.30	0.76	0.22
0.40	0.32	0.64	0.40	0.64	0.32
0.45	0.39	0.58	0.45	0.58	0.39
0.50	0.44	0.52	0.50	0.52	0.44
0.60	0.55	0.42	0.60	0.42	0.55
0.70	0.66	0.30	0.70	0.30	0.66
0.80	0.78	0.18	0.80	0.18	0.78
0.90	0.88	0.06	0.90	0.06	0.88
0.95	0.94	0.00	0.95	0.00	0.94
1.00	1.00	0.00	1.00	0.00	1.00

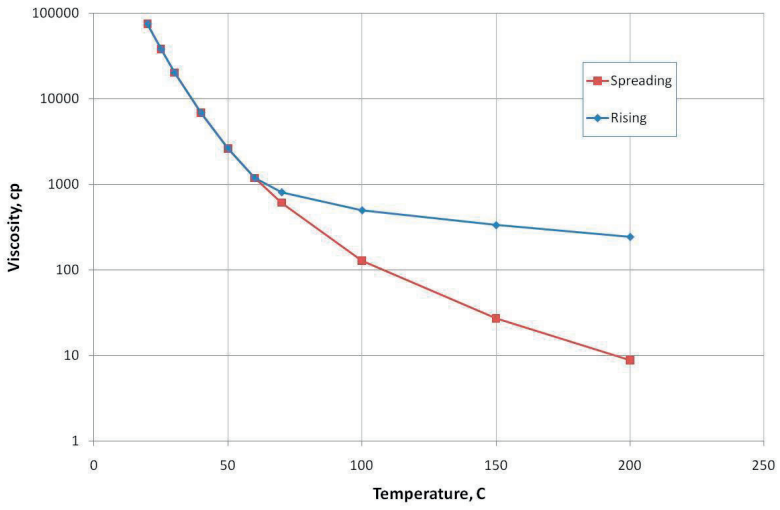

Figure 6.2 Cold Lake bitumen viscosity versus temperature for rising and spreading steam chamber schemes (Chow, 1993)

6.5 Numerical simulation results and discussions

As discussed earlier, in order to simulate the spreading steam chamber situation, the injector was placed on top of the formation above the producer, which is at the bottom of the formation. Cumulative oil produced during the spreading steam chamber simulation is compared with the experimental results of this procedure presented by Chung (1988). As can be seen in Figure 6.3 the simulation results are in good agreement with the experiment.

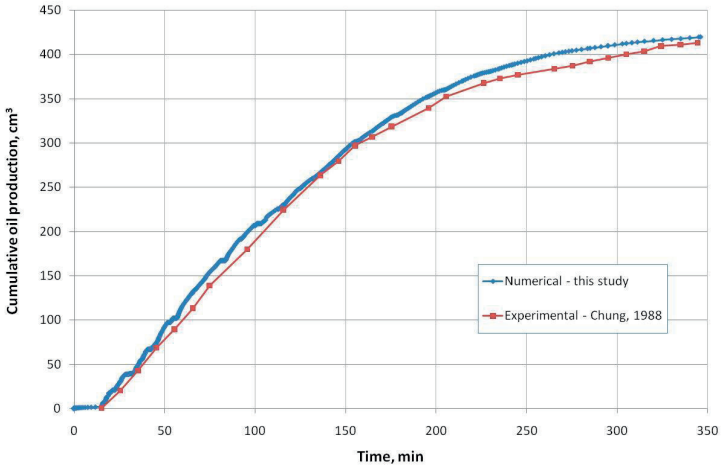

Figure 6.3 Cumulative oil production – Numerical versus experimental – Spreading steam chamber

A simulation case was considered under the spreading steam chamber case to see the effect of numerical dispersion. The original simulation file had 10 grid blocks in the x-direction and 8 in the z-direction. The refined case had 18 grid blocks in both x- and z-directions.

In the original SAGD data file, the injector is placed above the producer on top of the formation for the spreading steam chamber case. Another scenario was considered, where the injector was placed on top but on the other side of the model. The injector and producer are therefore placed on a diagonal line in the model. Since it was not possible in the model to place heaters to set up the initial communication between the two wells in the staggered model, the base case was also run without the initial heater between the injector and the producer, and the results are then compared. The results of the comparison are presented in Figures 6.4 and 6.5.

When the injector is placed diagonally with respect to the producer, there may be a better horizontal sweep than the case where the injector is placed above the producer.

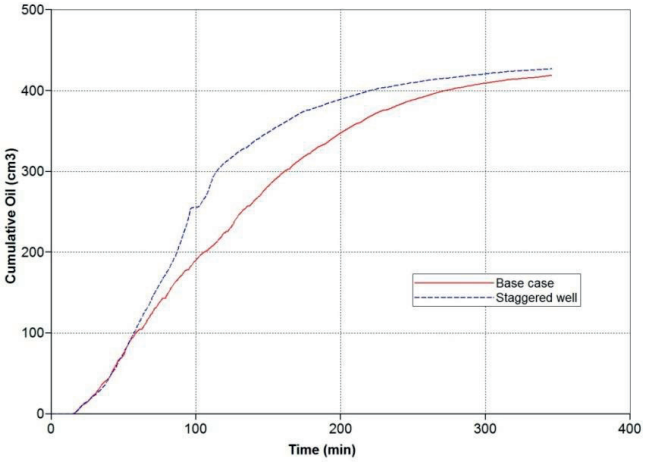

Figure 6.4 Cumulative oil production for spreading and staggered cases

This will cause an earlier oil production response for the staggered case compared to the base case of spreading steam chamber. Ultimate recovery however, is not that much different, since SAGD process is quite efficient in this case and the ultimate recoveries are in the range of above 90%. Lower water oil ratio at earlier times is also due to higher oil production for the staggered case.

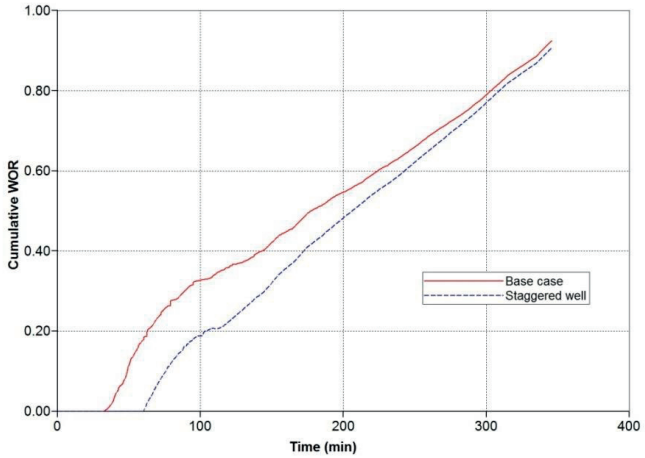

Figure 6.5 Cumulative water oil ratio for spreading and staggered cases

In order to simulate the rising steam chamber part of the SAGD process, the injector was placed directly above the producer near the bottom of the formation. This case is equivalent to the actual SAGD well placement. The cumulative oil production for the base case is compared with the experimental results of Chung (1988) in Figure 6.6. Knowing again that the developed simulation data file is matching the results of

experiments, some sensitivity analyses were accomplished. Two scenarios were considered for steam injection with a higher temperature than the original case. In the base simulation case, the temperature of steam was 105 °C. Two other cases of 130 and 140 °C were studied and are compared with the original case.

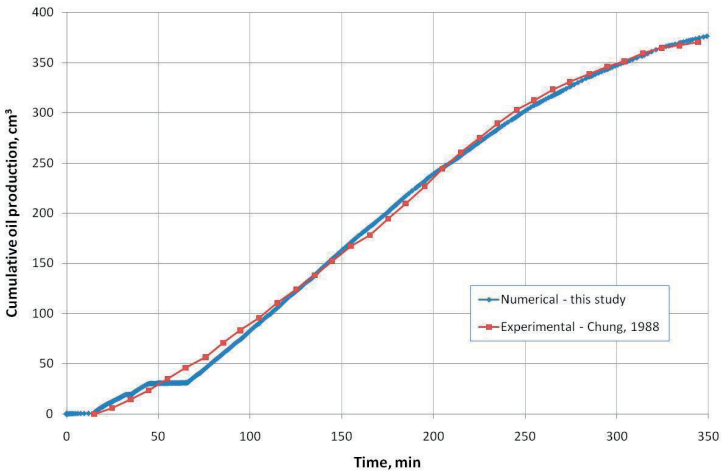

Figure 6.6 Cumulative oil production – Numerical versus experimental – Rising steam chamber

As can be seen from the cumulative oil production graph (Figure 6.7), increasing the temperature of injected steam will ultimately increase the amount of oil produced. However, there is an optimum temperature which seems to be 130 °C. Higher injection temperature of 140 °C has no substantial effect on the amount of oil produced. At earlier times of simulation, however, we got lower oil production at higher steam temperatures. Investigating the saturation changes in the 3-D model revealed the reason. At an early time, say 100 min. in Figure 6.7, the saturations in the model indicate that when the temperature of injected steam is higher there is more water and less steam in the steam chamber than in the lower temperature case. This is because it takes more time to heat up the grid blocks to higher temperatures. This will cause the process of oil drainage at earlier times to be slower. Cumulative WOR for different steam temperature cases is shown in Figure 6.8.

The sensitivity of the model with respect to the steam quality was also examined. In the original case of rising steam chamber, the quality of steam was considered to be 0.99. Two other cases were considered with lower steam qualities of 0.9 and 0.7. Figures 6.9 and 6.10 show the oil production and water oil ratio for these cases respectively. Apparently, when the quality of steam is lower, there is less heat content in the injection stream and therefore less energy is injected into the reservoir. This will cause lower oil production and results in higher water oil ratio for lower steam quality. Steam quality of 90 %, however, seems to be high enough, as there is no big difference between oil recovery for 90 % and 99 % steam quality cases.

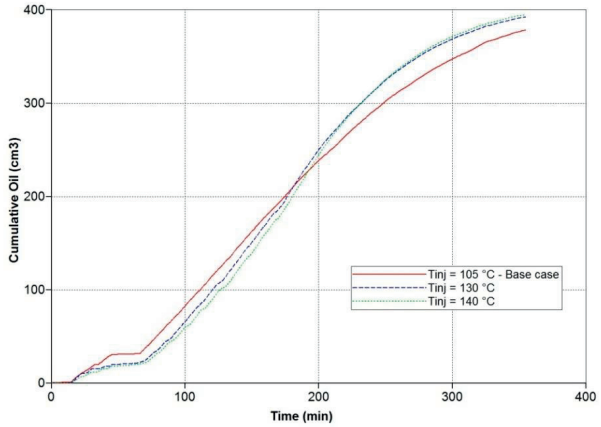

Figure 6.7 Cumulative oil production – rising steam chamber – different steam temperature cases

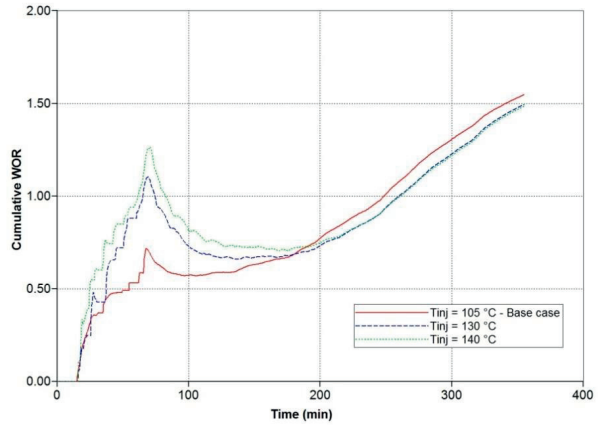

Figure 6.8 Cumulative water oil ratio – rising steam chamber – different steam temperature cases

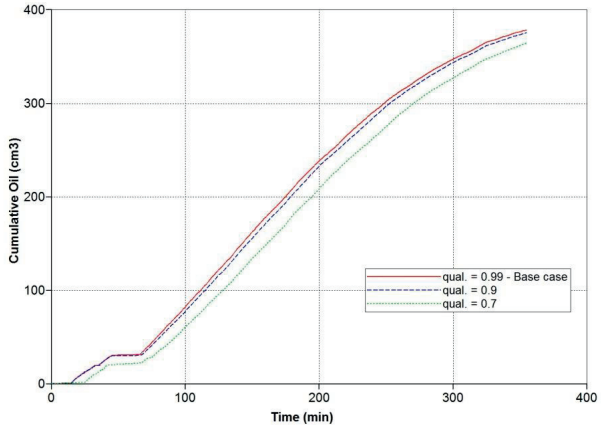

Figure 6.9 Cumulative oil production – rising steam chamber – different steam quality cases

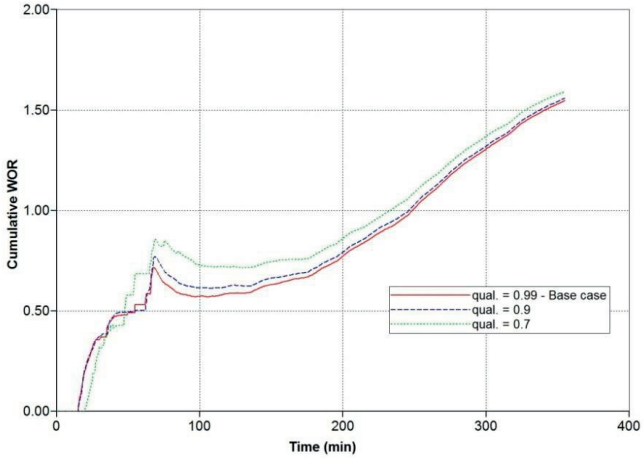

Figure 6.10 Cumulative water oil ratio – rising steam chamber – different steam quality cases

In order to see the effect of having different injector positions, the distance between the injector and the producer was changed. The injector well was placed in the block (1, 1, 2) in the original case. In the other two cases it was placed in the blocks (1, 1, 3) and (1, 1, 4). Placing the injector higher above the producer will cause a better recovery as can be seen in Figure 6.11. This is perhaps due to the fact that when the injector is placed higher in the formation, the steam chamber hits the top of the formation earlier and we will have a better top down sweep thereafter.

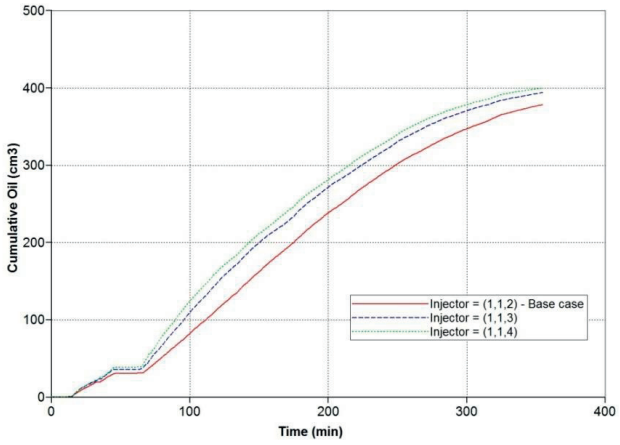

Figure 6.11 Cumulative oil production – rising steam chamber – different well spacing cases

To investigate the effect of porosity on SAGD performance, two other cases were considered where the porosity values of the models were different than the original case. The base model porosity is 39.2%. Two other porosity values of 45% and 30% were selected for comparison. Results show that recovery factor and WOR have inverse

relation to porosity. The lowest value of porosity has the best recovery factor, while it has the worst WOR. Figures 6.12 and 6.13 show results for recovery factor and cumulative WOR respectively. Initial volume in place is lower for lower porosity value and consequently the amount of heat which is required to reduce viscosity of oil is lower, so for the same amount of steam injection rate the lowest porosity case shows the best recovery factor.

The presence of shale layers in reservoir is a serious problem in SAGD process which can limit the growth of steam chamber. In order to study the effect of shale barrier, three different schemes were selected to represent horizontal, vertical and random shale barriers. These three schemes are depicted in Figures 6.14.a, 6.14.b and 6.14.c respectively.

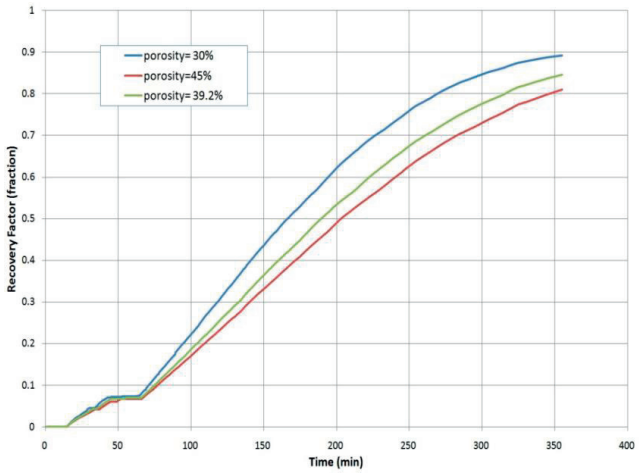

Figure 6.12 Oil recovery factor- rising steam chamber – different porosity values

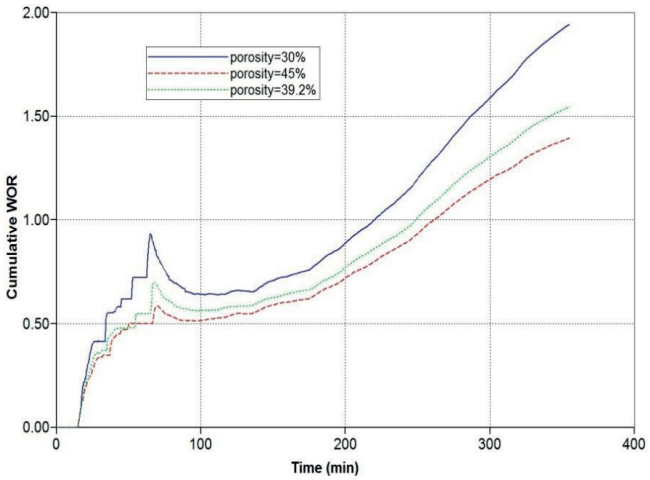

Figure 6.13 Cumulative water oil ratio – rising steam chamber – different porosity values

The growth of steam chamber is hindered by shale barriers especially in the case of horizontal shale layers. In this case the upper layers remain intact since the shale layers are acting like an obstacle, preventing the bitumen in top of the model from being touched by steam. Consequently the most dramatic drop in the oil recovery is observed for the case of horizontal barrier. Figures 6.15 and 6.16 compare effects of shale barrier on oil recovery factor and WOR respectively.

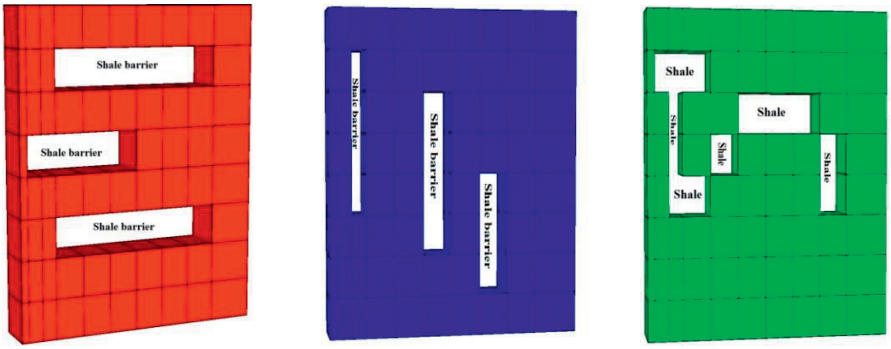

a) Horizontal shale barrier **b) Vertical shale barrier** **c) Random shale barrier**

Figure 6.14 Shale barrier configurations

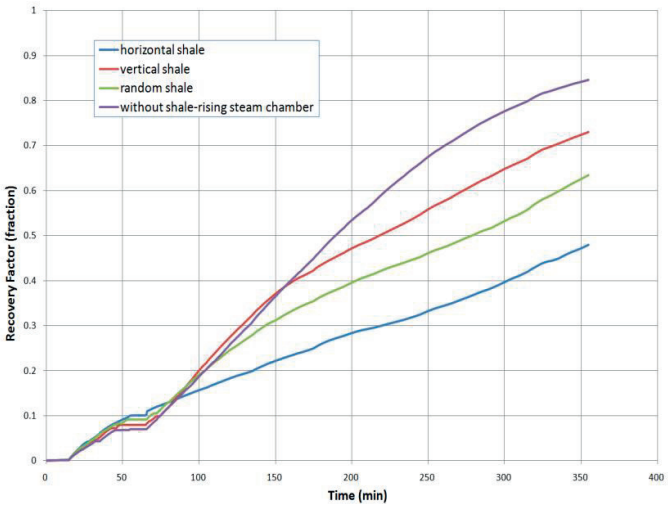

Figure 6.15 Oil recovery factor – rising steam chamber – different shale barrier configurations

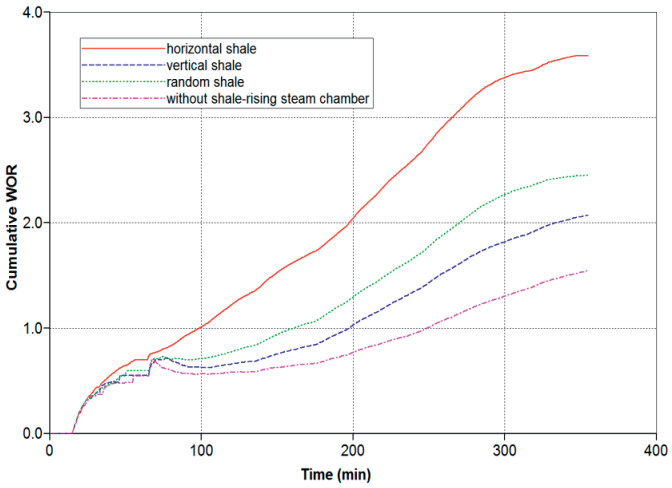

Figure 6.16 Cumulative water oil ratio – rising steam chamber – different shale barrier configurations

Adding solvent to steam in order to reduce the cost of steam generation in SAGD, reduce the green house gas emissions and take the advantage of reduction in oil viscosity due to diffusion of solvent into the bitumen is considered as an improvement for SAGD process.

The possibility of solvent co-injection was investigated in this model by selecting normal butane, normal pentane and normal hexane as solvents for injection together with steam. 95 % by volume of injected fluid was steam and the rest was solvent. The pseudo-liquid viscosities for these three solvents were obtained using CMG WINPROP (Table 6.2). The diffusivity coefficient of 3×10^{-4} cm^2/min is used for all of these three solvents. (Salama and Kantzas, 2005)

Table 6.2 Pseudo-liquid viscosity data versus temperature for solvents (WINPROP, 2010)

Temperature (°C)	Butane viscosity (cp)	Pentane viscosity (cp)	Hexane viscosity (cp)
20	19.565	22.190	25.152
25	15.636	17.688	20.014
30	12.798	14.442	16.312
40	8.9991	10.108	11.378
50	6.7733	7.5744	8.4995
60	5.4591	6.0796	6.8020
70	4.6144	5.1190	5.7113
90	3.3718	3.7139	4.1226
100	2.8549	3.1342	3.4709
150	1.2952	1.4021	1.5371
200	0.7215	0.7724	0.8401

Results show that addition of solvent has a positive effect both on cumulative oil production and WOR. As it can be seen in Figures 6.17 and 6.18 hexane shows a better performance than the two other solvents in this model. Sensitivity analyses were performed to examine the effect of percentage of solvent used. Hexane due to its better function was selected. Figures 6.19 and 6.20 depict cumulative oil production and WOR for hexane co-injection with different hexane volume percentages of 2%, 5% and 10% of total injected fluid. The more solvent is injected, the more cumulative oil is produced due to better mixing and diffusion of solvent in to the bitumen. Therefore 10% by volume of hexane co-injection shows the best recovery response.

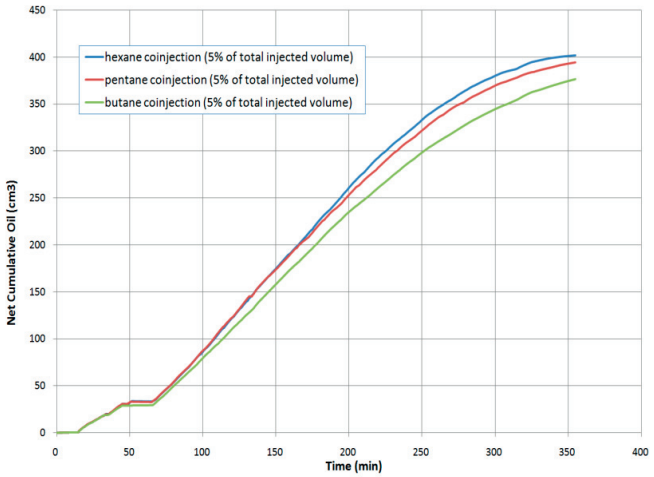

Figure 6.17 Net cumulative oil production – rising steam chamber – different solvent types

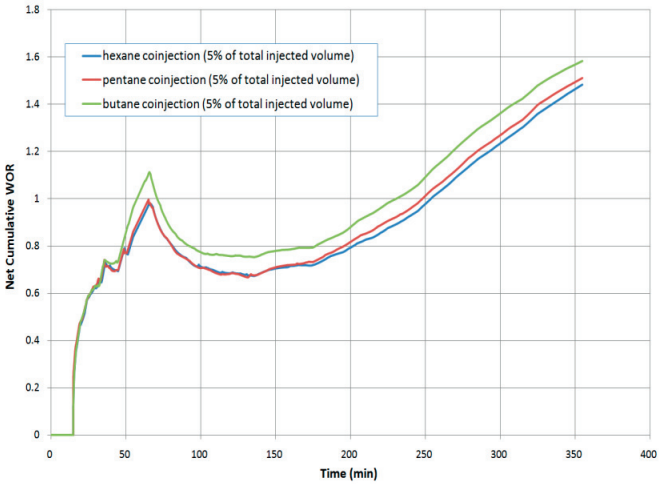

Figure 6.18 Net cumulative water oil ratio – rising steam chamber – different solvent types

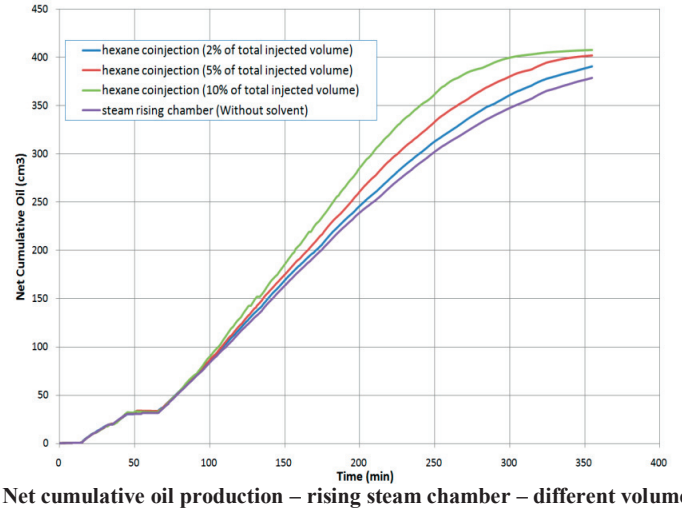

Figure 6.19 Net cumulative oil production – rising steam chamber – different volume percents of hexane co-injection

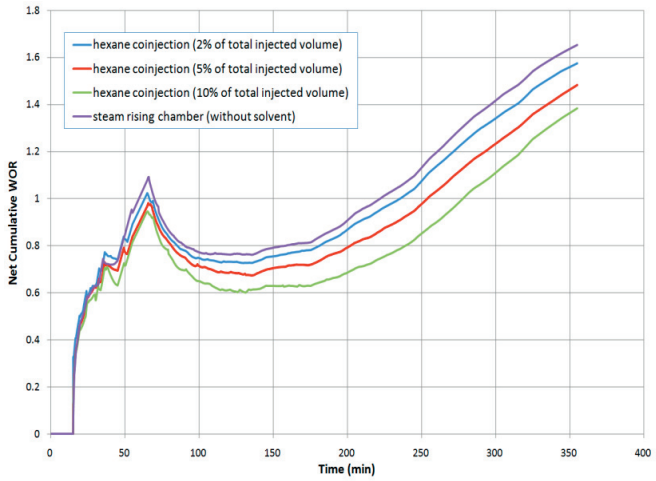

Figure 6.20 Net cumulative water oil ratio – rising steam chamber – different volume percents of hexane co-injection

6.6 Conclusions

This simulation study was based on experimental SAGD model by Chung (1988) and the numerical simulation model of the same experiments by Chow (1993).

The numerical model of the experiments was based on the CMG STARS thermal reservoir simulator and the model was history matched with the experimental results. The history-matched model was used for sensitivity analysis of different reservoir parameters. These parameters affect the final performance of the model and the simulations showed the following results:

- Modelling staggered SAGD showed that placing the injector well diagonally will improve the horizontal sweep in the experimental model.
- Different steam temperatures showed that there is an optimum temperature and above this temperature no significant increased recovery is observed. This temperature was found to be 130 °C in this case.
- Steam quality is another important criteria in the simulation studies. Higher steam quality will increase the production as the injectant will have a higher heat content. However, the economy of the project must be considered as higher steam quality raises the energy requirement. Steam quality of 90 % seemed to be sufficient in our study.
- Increasing the well separation resulted in better recovery response due to earlier rise of steam chamber and better top down sweep in the model.
- Porosity of the formation can affect the performance of SAGD process. Higher porosity resulted in lower values of WOR in this study. Lower WOR is desirable because of reduced costs of water treatment.
- Hindering effect of shale barrier could be dramatic in a SAGD process. The growth of steam chamber can be hindered by shale layers and consequently some parts of the reservoir may remain intact.
- Solvent can assist SAGD process especially when WOR is high and continuing the process is not economic. Solvent can help to reduce the viscosity of bitumen and make it lighter. Besides it can result in using less steam which can be advantageous in lowering the costs of steam generation, reducing green house gas emissions and lowering water consumption. Three normal alkanes were tested in this study as solvents for co-injection with steam. Normal hexane showed reasonable results as a potential candidate for solvent co-injection processes.

Nomenclature

CSS	Cyclic Steam stimulation
ES-SAGD	Expanding Solvent Steam Assisted Gravity Drainage
SAGD	Steam Assisted Gravity Drainage
SW-SAGD	Single Well Steam Assisted Gravity Drainage
WOR	Water Oil Ratio
S_w	Water saturation
k_{rw}	Water relative permeability
k_{row}	Oil relative permeability in the presence of water
S_l	Liquid saturation (S_w+S_o)
k_{rg}	Gas relative permeability
k_{rog}	Oil relative permeability in the presence of gas

Chapter 7

Overall Conclusions

During the course of this study several experimental and numerical investigations were accomplished to study the properties and flow behavior of Athabasca bitumen. Some fluid properties of bitumen were determined experimentally. These properties were further used in numerical simulation studies. Core flooding experiments were also performed during this work. The purpose was to investigate the effect of temperature on the relative permeability curves in heavy oil systems. The conclusions drawn can be summarized as follows:

7.1 Fluid properties

- Viscosity of Athabasca heavy crude was measured using a rotational viscometer from ambient temperature up to 300 °C.
- Athabasca oil was characterized by gas chromatography analysis to C_{39+}. No significant amount of components lighter than C_9 was observed.
- Whole sample molar mass was measured to 534 g/mol by cryoscopy.
- Density at standard conditions of 1 atm and 60 °F was measured to 1.0129 g/cm^3 by a density measuring cell. Density measurements were performed in the temperature range 120-195°C as well where the density was found to vary in the range 0.95-0.90 g/cm^3. A formula was derived based on experimental density data to predict Athabasca bitumen density in the temperature and pressure range studied.

7.2 Relative permeability

- The value of initial water saturation (S_{wi}) was observed to have a tendency to increase as the temperature increased. The same thing happened when the oil viscosity was reduced at the constant temperature.
- The decrease in residual oil saturation (S_{or}) with temperature was spotted in most of the experiments. This decrease was also observed with a lower oil viscosity at the same temperature condition. In some of the experiments, however, this observation was ruled out, which we believed might be due to viscous instabilities.
- It was not possible to predict any increasing or decreasing trend for either oil or water relative permeability values versus temperature at a given water saturation value. The effect of temperature on relative permeabilities is therefore not justified.

- The spread in variations of relative permeability values appeared to be adverse in higher permeable cores, suggesting that viscous instabilities and fingering issues are responsible for these variations.
- The same water saturation range shift that happens by changing the oil viscosity at constant temperature suggests that the decrease in oil/water viscosity ratio can be the cause of relative permeability variations observed at different temperatures.
- The results obtained in this work do not apply in general, as the temperature dependency issue of relative permeabilities is quite case specific.

7.3 Application to SAGD

Numerical modeling was conducted on field scale SAGD and ES-SAGD project to investigate the effect of temperature dependent relative permeability data input in the studies. Below is a summary of this numerical study:

- As the results of experimental work justifies the dependency of endpoint data on temperature, it is therefore suggested to use temperature dependant relative permeability data in numerical reservoir simulations.
- Oil production in both SAGD and ES-SAGD processes was found to be strongly dependant on the end point relative permeability data.
- Comparing the use of fixed relative permeability data with shifting data between the two end points shows different outcomes in terms of oil production curve. This must be considered as a matching criterion, when field data are available.

References

Abasov, M.T., Tairov, N.D., Abdullaeva, A.A., Alieva, Sh.M., Mamedov, A.I. (1976): Influence of Temperature on Relative Phase Permeability at High Pressures., Dokl. Akad. Nauk Azerb. SSR., 8, pp. 31-34. (in English)

Akin S., Bagci S.A. (2001): Laboratory Study of Single-Well Steam Assisted Gravity Drainage Process., J. Petrol. Sci. Eng., 32, pp. 23-33.

Akin, S., Castanier, L.M., Brigham, W.E. (1998): Effect of Temperature on Heavy-Oil/Water Relative Permeabilities., Paper SPE 49021 presented at the SPE Annual Technical Conference and Exhibition, New Orleans, Louisiana, USA. (27-30 Sept. 1998)

Akin, S., Castanier, L.M., Brigham, W.E. (1999): Effect of temperature on heavy oil/water relative permeabilities., Paper SPE 54120 Presented at SPE International Thermal Operations and Heavy Oil Symposium, Bakersfield, California. (March 1999)

Albahlani, A.M., Babadagli, T. (2008): A critical review of the status of SAGD: where are we and what is next?, Paper SPE 113283 presented at the SPE Western Regional and Pacific Section AAPG joint meeting held in Bakersfield, California, USA. (31 March-2 April)

Amyx, J.W., Bass, D.M., Whiting, R.L. (1960): Petroleum reservoir engineering: physical properties., New York: McGraw-Hill.

Ashrafi, M., Soraki, Y., Torsaeter, O. (2012): Effect of Temperature on Athabasca Type Heavy Oil – Water Relative Permeability Curves in Glass Bead Packs., Energy and Environment Research, 2(2), pp. 113-126.

Ashrafi, M., Souraki, Y., Karimaie, H., Torsaeter, O., & Bjorkvik B. J. A. (2011): Experimental PVT Property Analyses for Athabasca Bitumen., Paper CSUG/SPE 147064 presented at the Canadian Unconventional Resources Conference held in Calgary, Alberta, Canada. (15-17 November)

Bagci A.S. (2006): Experimental and Simulation Studies of SAGD Process in Fractured Reservoirs., paper SPE 99920 presented at SPE/DOE Symposium on Improved Oil Recovery, Tulsa, Oklahoma.

Barillas J.L.M., Dutra Jr. T.V., Mata W. (2006): Reservoir and Operational Parameters Influence in SAGD Process., J. Petrol. Sci. Eng., 54, 1-2, pp. 34-42.

Bentsen, R.G. (1985): A New Approach to Instability Theory in Porous Media., SPEJ, pp. 765-779. (Oct)

Buckley, S.E., Leverett, M.C. (1942): Mechanism of fluid displacement in sands., Trans. AIME, 146,107.

Burdine, N. T. (1953): Relative Permeability Calculations from Pore Size Distribution., Trans., AIME, 198, pp. 71-78.

Butler, R. M., McNab, G.S., Lo, N.Y. (1981): Theoretical Studies on the Gravity Drainage of Heavy Oil During In-Situ Steam Heating., The Canadian J. Chem. Engineering, 59, pp. 455-460. (Aug. 1981)

Chen Q., Gerritsen M.G., Kovscek A.R. (2007): Effects of Reservoir Heterogeneities on the Steam-Assisted Gravity Drainage Process., paper SPE 109873 presented at SPE Annual Technical Conference and Exhibition, Anaheim, California.

Chierici, G.L. (1984): Novel Relations for Drainage and Imbibition Relative Permeabilities., SPEJ, pp. 275-276.

Chow, L. (1993): Numerical Simulation of Heavy Oil Recovery by the Steam-Assisted Gravity Drainage Process., M. Eng. Thesis, The University of Calgary, Calgary, Alberta, Canada.

Chung, K.H. (1988): Heavy Oil Recovery by the Steam-Assisted Gravity Drainage Process., Ph.D. Thesis, The University of Calgary, Calgary, Alberta, Canada.

Closmann, P.J.,Waxman,M.H., Deeds,C.T. (1988): Steady-state tar/water relative permeabilities in Peace River cores at elevated temperature., SPE Reservoir Engineering, 3(1), pp. 76-80. (Feb. 1988)

CMG-STARS User's Guide. (2012): Computer Modeling Group Ltd.

Coats, K.H., George, W.D., Marcum, B.E. (1974): Three-Dimensional Simulation of Steamflooding., SPE Journal, Dec. 1974.

Combarnous, M., Pavan, J. (1968): Deplacement par l'eau chaude d'huiles en place dans un milieu poreux., Communication no. 37, III Colloque A.R.T.F.P., pp. 737-757, Pau, Sep. 23-26. (in French)

Corey, A. T. (1954): The Interrelation between Gas and Oil Relative Permeabilities., Prod., 19(1), pp. 38-41.

Davidson, L.B. (1969): The effect of temperature on the relative permeability ratio of different fluid pairs in two-phase systems., JPT, pp. 1037-1046. (August)

Deng, X., Huang, H., Zhao, L., Law, D.H.-S., Nasr, T.N. (2010): Simulating the ES-SAGD process with solvent mixture in Athabasca reservoirs., JCPT, 49(1), pp. 38-46.

Edmondson, T.A. (1965): Effect of temperature on waterflooding., JCPT, pp. 236-242.

Ehrlich, R. (1970): The effect of temperature on water–oil imbibitions relative permeability., Paper SPE 3214 presented at Eastern Regional Meeting of SPE, Pittsburgh, Pennsylvania. (November 1970)

Elliot K.T., Kovscek A.R. (1999): A Numerical Analysis of Single-Well Steam Assisted Gravity Drainage Process (SW-SAGD)., Paper S-10, prepared for the 20th Annual Workshop and Symposium Collaborative Project on Enhanced Oil Recovery International Energy Agency, Enghien-les-Bains, France. (21-24 Sept. 1999)

Esfahani, M.R., Haghighi, M. (2004): Wettability evaluation of Iranian carbonates formations., J. Pet. Sci. Eng. 42, pp. 257–265.

Frizzell, D.F. (1990): Analysis of 15 years of thermal laboratory data: relative permeability and saturation endpoint correlations for heavy oils., Paper SPE 20528 presented at the 65th Annual Technical Conference and Exhibition of the Society of Petroleum Engineers, New Orleans, LA. (September 1990)

Govind P.A., Das S., Srinivasan S., (2008): Expanding Solvent SAGD in Heavy Oil Reservoirs., paper SPE 117571 presented at the SPE/PS /CHOA International Thermal Operations and Heavy Oil Symposium, Calgary, Alberta, Canada.

Hamouda, A.A., Karoussi, O., Chukwudeme, E.A. (2008): Relative permeability as a function of temperature, initial water saturation and flooding fluid compositions for modified oil-wet chalk., J. Pet. Sci. Eng., 63(1-4), December 2008, pp. 61-72.

Honarpour, M., Koederitz, L., Herbert, H.A. (1986): Relative Permeability of Petroleum reservoirs., C.R.C. Press Inc.

Ivory J., Zheng R., Nasr T., Deng X., Beaulieu G., Heck G. (2008): Investigation of Low Pressure ES-SAGD., paper SPE 117759 presented at the SPE/PS /CHOA International Thermal Operations and Heavy Oil Symposium, Calgary, Alberta, Canada.

Jennings Jr., J.W., Pallas, N.R. (1988): An Efficient Method for the Determination of Interfacial Tension from Drop Profiles., Langmuir, 4, pp. 959-967.

Johnson, E. F., Bossler, D. P., Naumann, V. O. (1959): Calculation of Relative Permeability from Displacement Experiments., Trans. AIME, 216, pp. 370-372.

Jones, S. C., Roszelle, W. O. (1978): Graphical Techniques for Determining Relative Permeability from Displacement Experiments., JPT, pp. 807-817.

Kamath V.A., Sinha Sandeep, Hatzignatiou D.G. (1993): Simulation Study of Steam-Assisted Gravity Drainage Process in Ugnu Tar Sand Reservoir., paper SPE 26075 presented at the Western Regional Meeting, Anchorage, Alaska.

Katz, D.L., Firoozabadi, A. (1978): Predicting Phase Behavior of Condensate/Crude-Oil Systems Using Methane Interaction Coefficients., JPT (November 1978), pp. 1649-1655; Trans. AIME, 265.

Khan, M.A.B., Mehrotra, A.K., Svrcek, W.Y. (1984): Viscosity Models for Gas-Free Athabasca Bitumen., J. Can. Pet. Tech., 23(3), pp. 47-53.

Kisman, K.E., Yeung, K.C. (1995): Numerical Study of SAGD Process in the Burnt Lake Oil Sands Lease., paper SPE 30276 presented at the International Heavy oil Symposium, Calgary, Alberta, Canada.

Kumar, Mridul, Inouye, T.A. (1994): Low-temperature analogs of hightemperature water/oil relative permeabilities., Paper SPE 28616 presented at the SPE 69th Annual Technical Conference and Exhibition, New Orleans, LA, U.S.A. (September 1994)

Kumar, S., Torabzadeh, S.J., Handy, L.L. (1985): Relative permeability functions for high and low-tension systems at elevated temperatures., Paper SPE 13670 presented at the SPE 1985 California Regional Meeting, Bakersfield, California. (March 1985)

Law, D.H.S., Nasr, T.N., Good, W.K. (2000): Field-Scale Numerical Simulation of SAGD Process With Top-Water Thief Zone., paper SPE 65522 presented at SPE/Petroleum Society of CIM International Conference on Horizontal Well Technology, Calgary, Alberta, Canada.

Lo, H. Y., Mungan, N. (1973): Temperature Effect on relative Permeabilities and Residual Saturations., Research report RR-19, Petroleum Recovery Institute, Calgary, AB.

Lomeland, F., Ebeltoft, E., Thomas, W.H. (2005): A New Versatile Relative Permeability Correlation., Reviewed paper at the at the 2005 International Symposium of the SCA, Toronto, Canada. (August 21-25)

Maini, B. B., Batycky, J. P. (1985): The Effect of Temperature on Heavy Oil/Water Relative Permeabilities in Horizontally and Vertically Drilled Core Plugs., JPT, 37(8), pp. 1500-1510.

Maini, B.B., Okazawa, T. (1987): Effect of Temperature on Heavy Oil-Water Relative Permeability of Sand., JCPT, 26(3), pp. 33-41.

Mehrotra, A.K., Svrcek, W.Y. (1986): Viscosity of compressed Athabasca bitumen., Can. J. Chem. Eng. 64, 844.

Miller, M.A., Ramey, H.J.Jr. (1985): Effect of Temperature on Oil/Water Relative Permeabilities of Unconsolidated and Consolidated Sands., SPEJ, 25(6), pp. 945-953.

Mollaei A., Maini, B. (2010): Steam Flooding of Naturally Fractured Reservoirs: Basic Concepts and Recovery Mechanisms., JCPT, 49(1), pp. 65-70.

Nakornthap, K., Evans, Ronald D. (1986): Temperature-dependent relative permeability and its effect on oil displacement by thermal methods., SPEJ, pp. 230-242. (May)

Nasr, T.N., Isaac, E.E. (2001): Process for Enhancing Hydrocarbon Mobility Using a Steam Additive., United States Patent No. 6,230,814, 15 May 2001.

Peters, E.J., Flock, D.L. (1981): The Onset of Instability during Two-Phase Immiscible Displacement in Porous Media., SPEJ, 21, pp. 249-258. (April)

Polikar, M. (1987): Relative Permeability Measurements in Oil Sands., PhD Thesis, The university of Alberta, Edmonton, Alberta, Canada.

Polikar, M., Farouq Ali, S.M., Puttagunta, V.R. (1990): High Temperature Relative Permeabilities for Athabasca Oil Sands., SPERE, 5(1), pp. 25-32.

Polikar, M., Puttagunta, V.R., DeCastro, V., Farouq Ali, S.M. (1989): Relative Permeability Curves for Bitumen and Water in Oil Sand Systems., JCPT, 28(1), pp. 93-99.

Poston, S.W., Ysrael, S., Hossain, A.K.M.S., Montgomery III, E.F., Ramey Jr., H.J. (1970): The effect of temperature on irreducible water saturation and relative permeability of unconsolidated sands., SPEJ, pp. 171–180. (June)

Rapoport, L.A., Leas, W.J. (1953): Properties of Linear Waterfloods., Trans. AIME, 198, pp. 139-148.

Salama, D., kantzas, A. (2005): Monitoring of Diffusion of Heavy Oils with Hydrocarbon Solvents in the Presence of Sand., paper SPE 97855 presented at the SPE/PS-CIM/CHOA International Thermal Operations and Heavy Oil Symposium, Calgary, Alberta, Canada.

Schembre, J.M., Tang, G.Q., Kovscek, A.R. (2006): Interrelationship of Temperature and Wettability on the Relative Permeability of Heavy Oil in Diatomaceous Rocks., SPERE, 9(3), pp. 239-250.

Sedaee, S.B., Rashidi, F., Babadagli, T. (2007): Temperature Effects on the Heavy Oil/Water Relative Permeabilities of Carbonate Rocks., J. Pet. Sci. Eng., 59, pp. 27-42.

Sendra User Guide. (2012). http://www.sendra.no

Shilolwd, D. (1965): The effect of moderate temperature change on relative permeability ratios., M.Sc. Thesis, Pennsylvania State U., University Park, YA.

Sigmund, P.M., McCaffery, F.G. (1979): An improved Unsteady-state Procedure for Determining the Relative Permeability Characteristics of Heterogeneous Porous Media., SPEJ, 19(1), pp. 15-28.

Sinnokrot, A.A. (1969): The effect of temperature on capillary pressure curves of limestone and sandstones., PhD dissertation, Stanford U. Stanford, CA.

Sinnokrot, A.A., Ramey Jr., H.J., Marsden Jr., S.S. (1971): Effect of temperature level upon capillary pressure curves., SPEJ, pp. 13–22. (March)

Skjæveland, S.M., Kleppe, J. (1992): SPOR Monograph: Recent Advances in Improved Oil Recovery Methods for North Sea Sandstone Reservoirs., Norwegian Petroleum Directorate, Stavanger, Norway.

Sufi, A.H. (1982): Temperature Effects on Oil-Water Relative Permeabilities for Unconsolidated Sands., PhD Thesis, Stanford University, Stanford, CA.

Sufi, A.H., Ramey Jr., H.J., Brigham,W.E. (1982): Temperature effects on relative permeabilities of oil–water., Paper SPE 11071 presented at 57th Annual Fall Technical Conference and Exhibition of Society of Petroleum Engineers, New Orleans, USA. (September 1982)

Swapan Das (2007): Application of Thermal Recovery Processes in Heavy Oil Carbonate Reservoirs., paper SPE 105392 presented at the 15th SPE Middle East Oil and Gas Show and Conference, Bahrain.

Torabzadeh, S.J., Handy, L.L. (1984): The Effect of Temperature and Interfacial Tension on Water/Oil Relative Permeabilities of Consolidated Sands., SPE/DOE 12689, 4th Symposium on EOR, Tulsa, OK. (April 15-18)

Wagner, W., Pruss, A. (2002): The IAPWS formulation 1995 for the Thermodynamic Properties of Ordinary Water Substance for General and Scientific Use., J. Phys. Chem. Ref. Data, 31, 2, pp. 387-535.

Wang, J., Dong, M., Asghari, K. (2006): Effect of Oil Viscosity on Heavy Oil/Water Relative Permeability Curves., SPE 99763, SPE/DOE Symposium on IOR, Tulsa, OK. (April 22-26)

Watson, R.W., Ertekin, T. (1988): The effect of steep temperature gradient on relative permeability measurements., Paper SPE 17505 presented at the SPE Mountain Regional Meeting, Casper, WY. (May 1988)

Weinbrandt, R.M., Ramey, H.J.Jr., Casse, F.J. (1975): The Effect of Temperature on Relative and Absolute Permeability of Sandstones., SPEJ, 15(5), pp. 376-384.

Welge, H.J. (1952): A simplified method for computing recovery by gas or water drive., Trans .AIME, 195, 91.

Wilson, J.W. (1956): Determination of Relative Permeability under Simulated Reservoir Conditions., AIChE Journal, 2(1), pp. 94-100.

Yang X., Gates I.D. (2009): Combustion Kinetics of Athabasca Bitumen from 1D Combustion Tube Experiments., Nat. Resources Res., 18(3). (Sept. 2009)

Yazdani, A., Alvestad, J., Kjonsvik, D., Gilje, E., Kowaleski, E. (2012): A parametric simulation study for solvent co-injection process in bitumen deposits., JCPT, 51(4), pp. 244-255.

Appendix A

This appendix contains the main papers published as an outcome of this study. These papers were discussed in chapters 2 and 3, and are listed below:

A.1 "Experimental PVT Property Analyses for Athabasca Bitumen", Mohammad Ashrafi, Yaser Souraki, Hassan Karimaie, Ole Torsaeter, Bard J.A. Bjorkvik, paper CSUG/SPE 147064 presented at the Canadian Unconventional Resources Conference, 15–17 November 2011, Calgary, Alberta, Canada.

A.2 "Effect of Temperature on Athabasca Type Heavy Oil – Water Relative Permeability Curves in Glass Bead Packs", Mohammad Ashrafi, Yaser Souraki, Ole Torsaeter, Energy and Environment Research, Vol. 2, No. 2, 2012.

A.3 "Investigating the Temperature Dependency of Oil and Water Relative Permeabilities for Heavy Oil Systems", Mohammad Ashrafi, Yaser Souraki, Ole Torsaeter, Submitted to Transport in Porous Media.

A.1 and A.3

Are not included due to copyright

A.1 Paper CSUG/SPE 147064

CSUG/SPE 147064

Experimental PVT Property Analyses for Athabasca Bitumen

Mohammad Ashrafi, Yaser Souraki, Hassan Karimaie, Ole Torsaeter, SPE, Norwegian University of Science and Technology (NTNU), and Bard J.A. Bjorkvik, SPE, SINTEF Petroleum Research

This paper was prepared for presentation at the Canadian Unconventional Resources Conference held in Calgary, Alberta, Canada, 15–17 November 2011.

Abstract

Extra heavy oil and bitumen reservoirs constitute huge volumes around the world and are attracting attention as alternative energy resources while the light oil reserves diminish. Thermal recovery and steam based methods are the most widely used recovery methods applicable to these highly viscous deposits. Study of steam injection in porous media containing viscous oil requires a good understanding of the physical properties of both reservoir rock and fluid. In particular, there are some bitumen properties that are needed for simulation studies and the most reliable source for these data is laboratory tests.

This paper presents experimental study of some PVT properties of Athabasca crude oil to help provide input data for further numerical studies.

Viscosity of Athabasca heavy crude was measured using a rotational viscometer up to 300 °C. This viscosity data is a more reliable input for simulation purposes. Athabasca oil was characterized by gas chromatography analysis to C_{39+}. No significant amount of components lighter than C_9 was observed. Whole sample molar mass was measured to 534 g/mol by cryoscopy. Density at standard conditions of 1 atm and 60 °F was measured to 1.0129 g/cm^3 by a density measuring cell. Density and molar mass of the C_{39+} fraction were also determined. Density measurements were performed in the temperature range 120-195 °C as well where the density was found to vary in the range 0.95-0.90 g/cm^3. A formula was derived based on experimental density data to predict Athabasca bitumen density in the temperature and pressure range studied. The interfacial tension between oil and steam was measured in the temperature range 120-220 °C by the pendant drop method. The interfacial tension was determined to be between 25 and 18 mN/m with a decreasing trend in the temperature range studied.

The results psented here can be used as reference data for studies related to Athabasca bitumen.

Energy and Environment Research; Vol. 2, No. 2; 2012
ISSN 1927-0569 E-ISSN 1927-0577
Published by Canadian Center of Science and Education

A.2 Paper EER 2(2) 2012

Effect of Temperature on Athabasca Type Heavy Oil – Water Relative Permeability Curves in Glass Bead Packs

Mohammad Ashrafi[1], Yaser Souraki[1] & Ole Torsaeter[1]

[1] Department of Petroleum Engineering and Applied Geophysics, Norwegian University of Science and Technology – NTNU, Trondheim, Norway

Correspondence: Mohammad Ashrafi, Department of Petroleum Engineering and Applied Geophysics, Norwegian University of Science and Technology – NTNU, S.P. Andersens vei 15A, 7491 Trondheim, Norway. Tel: 47-73-591-117. E-mail: mohammad.ashrafi@ntnu.no

Received: August 28, 2012 Accepted: September 14, 2012 Online Published: October 14, 2012

doi:10.5539/eer.v2n2p113 URL: http://dx.doi.org/10.5539/eer.v2n2p113

Abstract

There have been a number of somehow contradictory reports in the literature on the effect of temperature on oil and water relative permeabilities. Although some authors have reported the dependence of relative permeability curves on temperature, others have attributed these dependencies to artifacts inherent in unsteady-state method of relative permeability measurement. In order to further investigate the impact of temperature changes on the relative permeability data, we have conducted laboratory core flooding experiments on heavy oil systems. The porous media used was glass bead packs, and the Athabasca type bitumen with varying viscosities was displaced by hot water. The history matching technique was conducted on production and pressure differential data to get the relative permeability curves.

Results indicated that generally the increase in initial water saturation and the decrease in residual oil saturation are expected by increasing temperature. However, viscous instabilities can rule out the above mentioned trends. No temperature dependency of either oil or water relative permeability can be justified in our tests. The changes in relative permeabilities by temperature are probably related to experimental artifacts, viscous fingering and changes in oil to water viscosity ratio and not fundamental flow properties.

Keywords: relative permeability, unsteady-state method, history matching, end point saturations, heavy oil, viscosity

Nomenclature

Symbols

BPR	Back Pressure Regulator	GB	Glass Beads
HT	High Temperature	JBN	Johnson, Bossler and Naumann technique
k_r	Relative Permeability	LT	Low Temperature
PV	Pore Volume	S_{wi}	Initial Water Saturation
S_{or}	Residual Oil Saturation	SAGD	Steam Assisted Gravity Drainage
SCAL	Special Core Analysis	T	Absolute Temperature, K
μ	Dynamic Viscosity, cP		

Subscripts

o	Oil	w	Water

Superscript

0	End Point Value	*	Normalized Value

1. Introduction

The modeling of heavy oil production by thermal methods requires an in depth understanding of the rock-fluid interaction parameters for these types of reservoirs. The multi phase flow parameters are also crucial for modeling and evaluating the production mechanisms in these types of reservoirs. An important multi phase flow parameter is relative permeability. Relative permeability is the ratio of the effective permeability of a fluid at a given saturation to that at 100% saturation (Amyx, 1960). Wettability changes resulted from temperature increase, have an impact on the relative permeability. Viscosity is also

governed by temperature, and will have important effects on the relative permeability. There are generally two methods of measuring relative permeabilities, namely steady state and unsteady state methods. Both methods have been used in the literature to study the effect of temperature on the relative permeability curves. Looking back in to the literature we can find some contradictory reports on the effect of temperature on the relative permeability (k_r) curves. Some authors have reported an increase in the irreducible water saturation (S_{wi}) and a decrease in residual oil saturation (S_{or}) as the temperature of the system increases. This shift in the saturations results in some changes in the value of k_r as well. There are some reports showing that the value of oil relative permeability (k_{ro}) increases while the value of water relative permeability (k_{rw}) decreases at higher temperatures. The effect of temperature on the end point saturations (S_{wi} and S_{or}) has been reported by several authors (Edmondson, 1965; Combarnous & Pavan, 1968; Poston et al., 1970; Sinnokrot, 1971; Lo & Mungan, 1973; Weinbrandt et al., 1975; Abasov et al., 1976; Maini & Batycky, 1985; Torabzadeh & Handy, 1984; Bennion et al., 1985). All these authors except Combarnous and Pavan (1968) have also reported the change of k_r curves with temperature. Davidson (1969) has indicated the effect of temperature on the relative permeability, while not mentioning anything about the end point saturations. Maini and Okazawa (1987) have considered fixed end point saturations and have confirmed the change in k_r values with temperature. Schembre et al. (2006) have proposed that the rock becomes more water wet at higher temperatures and that affects the relative permeability curves. On the other hand, there are some results published in the literature confirming no effect of temperature neither on the relative permeability nor on the end point saturations (Wilson, 1956; Sufi et al., 1982; Miller & Ramey, 1985). The two latter have concluded that the previously reported temperature dependant behaviors of relative permeability and residual saturations might have been affected by viscous instabilities, capillary end effects and / or difficulties in maintaining material balance (Polikar et al., 1990).

Besides these variations in the reported results, there are very few experimental studies specifically done on bitumen reservoirs of Alberta. Poston et al. (1970) worked on very viscous oils and reported the changes of both residual saturations and relative permeability values. Maini and Batycky (1985) have also conducted their experiments on heavy oil and indicated the variations with temperature except for the k_{rw}. Polikar et al. (1990) worked specifically with Athabasca type bitumen and proposed no dependency on temperature. Sedaee Sola et al. (2007) have performed some experiments using heavy oil and reported dependencies on temperature.

Researchers have used both mineral and crude oil in their studies. Some studies have been done on consolidated core samples while others have used unconsolidated material like sand packs or glass beads. These variations in the experimental conditions have resulted in different and even contradictory results. This implies that the actual effect of temperature on flow behavior of fluids in the rock is case specific.

Due to the contradictory reports and conclusions, which are because of variation in the systems being tested, it seemed necessary to conduct our own core flooding experiments and investigate the dependency of relative permeability curves on temperature. The objective was accomplished by performing core flooding experiments, displacing heavy oil by hot water at different temperatures and using oils with varying viscosities. The production curves and pressure differential data in each experiment were history matched to get the oil and water relative permeabilities.

2. Relative Permeability Calculation Method

There are generally two methods of relative permeability measurement in the oil industry, namely steady-state and unsteady-state. In steady-state technique, a fixed ratio of two immiscible fluids are mixed and injected simultaneously into the porous media until saturation and pressure equilibria are reached. A faster method is unsteady-state technique, which is based on the displacement of one fluid phase by another immiscible fluid phase (Honarpour et al., 1986). In this study we only conduct unsteady-state or displacement method. Relative permeabilities can be calculated from recorded production and pressure differential data of a displacement test. This can be done by either explicit or implicit calculation. The explicit methods mostly used are the JBN (Johnson, Bossler & Naumann) technique (Johnson et al., 1959) and its modified version by Jones and Roszelle (1978). The implicit method or history matching is, however, based on numerical calculation. The relative permeability parameters are adjusted to match the production and pressure differential data from core flooding experiments (Wang et al., 2006). The history matching of data was done using a core flooding simulator called Sendra. This software is a two-phase 1D black-oil simulation model used for analyzing SCAL (special core analysis) experiments. It is tailor made

for revealing relative permeability and capillary pressure from two-phase and multi-phase flow experiments performed in the SCAL laboratory (Sendra user guide, 2012). This software acts as both a core flooding simulator and a history matching tool. Through history matching function, one can match the experimental data by adjusting the relative permeability curves. This is done by choosing the appropriate relative permeability correlation in the simulator. The software is then varying the empirical parameters in the function trying to match the experimental data. For the estimation method used in Sendra, refer to the software manual (Sendra user guide, 2012). There are several relative permeability correlations included in this simulator. Below is a review of these correlations. The normalized water saturation is used in all correlations:

$$S_w^* = \frac{S_w - S_{wi}}{1 - S_{wi} - S_{or}} \tag{1}$$

For simplicity, the formulations are given for oil-water systems; however they behave similar for oil-gas and water-gas systems (Sendra user guide, 2012).

2.1 Burdine Correlation (Burdine, 1953)

$$k_{rw} = k_{rw}^0 \left(S_w^*\right)^{\frac{2+3\lambda}{\lambda}} \tag{2}$$

$$k_{ro} = k_{ro}^0 \left(1 - S_w^*\right)^2 \left(1 - \left(1 - S_w^*\right)^{\frac{2+\lambda}{\lambda}}\right) \tag{3}$$

2.2 Corey Correlation (Corey, 1954)

$$k_{rw} = k_{rw}^0 \left(S_w^*\right)^{N_w} \tag{4}$$

$$k_{ro} = k_{ro}^0 \left(1 - S_w^*\right)^{N_o} \tag{5}$$

2.3 Sigmund & McCaffery Correlation (Sigmund & McCaffery, 1979)

$$k_{rw} = k_{rw}^0 \frac{\left(S_w^*\right)^{N_w} + AS_w^*}{1 + A} \tag{6}$$

$$k_{ro} = k_{ro}^0 \frac{\left(1 - S_w^*\right)^{N_o} + B\left(1 - S_w^*\right)}{1 + B} \tag{7}$$

2.4 Chierici Correlation (Chierici, 1984)

$$k_{rw} = k_{rw}\left(S_{or}\right) e^{-BR_w^{-M}} \tag{8}$$

$$k_{ro} = k_{ro}\left(S_{wi}\right) e^{-AR_w^{L}} \tag{9}$$

$$R_w\left(S_w\right) = \frac{S_w - S_{wi}}{1 - S_{or} - S_w} \tag{10}$$

2.5 LET Correlation (Lomeland et al., 2005)

$$k_{rw} = k_{rw}^0 \frac{\left(S_w^*\right)^{L_w}}{\left(S_w^*\right)^{L_w} + E_w\left(1 - S_w^*\right)^{T_w}} \tag{11}$$

$$k_{ro} = k_{ro}^{0} \frac{\left(1 - S_w^*\right)^{L_o}}{\left(1 - S_w^*\right)^{L_o} + E_o \left(S_w^*\right)^{T_o}} \tag{12}$$

For the analysis of data in this study, all the above mentioned correlations have been tried to get the best possible history matching of the experimental data.

3. Experimental Procedure

3.1 Relative Permeability Measurement Set-up

The flooding set-up used in this study is shown in Figure 1. A core holder is placed in an oven that can be set at any desired temperature up to 300°C. The oven is equipped with window panels and two fans which help to provide a constant temperature by circulating the air inside the oven. End caps of the core holder were designed in such a way that the fluid could be distributed evenly at the injection face. The overburden pressure is provided by viscous paraffin which has a viscosity of around 120 cp at room temperature and is contained in a cylinder with a floating piston. A Quizix positive displacement pump provides the pressure behind the piston using distilled water. This pump can be set to operate at a constant pressure by either displacing or recovering the water. This makes it possible to keep a constant overburden pressure by recovering the extra paraffin due to expansion at higher temperatures inside the oven. A pressure gauge placed on the paraffin line shows the pressure, and is visible through the windows of the oven. Two other pressured vessels are used in order to inject the water or oil alternatively. These two cylinders are also equipped with floating type pistons. The pistons are displaced by distilled water using another Quizix pump that operates at constant rate. The pump's operational range is 0.001 cc/min up to 50 cc/min. A back pressure regulator (BPR) is set inside the oven on the production line. This BPR is used to provide a higher pressure than the atmospheric pressure inside the system to make sure the water is in the liquid phase. A glass tube separator is placed outside the oven. The effluent enters the separator, which is filled with water, at the bottom. The oil phase is gathered on top and the water leaves to another BPR. The produced water is accumulated on a scale. Pressure differential across the core is monitored using a Keller pressure transducer with a 0-3 bar operation range. The transducer is connected to a PC to have a continuous pressure reading.

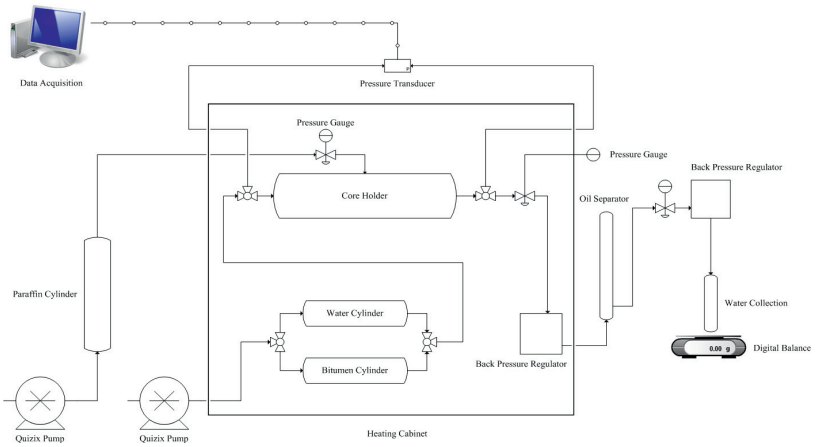

Figure 1. Schematic representation of core flooding setup used in this study

3.2 Porous Media and Packing Procedure

The porous media used was unconsolidated glass beads. Glass beads of different size were packed inside a rubber sleeve. Two metal screens were placed on the top and bottom of the packed media inside the sleeve and in contact with end caps of core holder. These screens were used to obviously prevent the production or any movement of glass beads and at the same time evenly distribute the fluid at the injection port. The rubber sleeve was installed on the inlet end cap, and the metal screen was placed inside and in contact with the end cap face. They were then placed on an electric shaker. While the shaker was

running the glass beads were poured using a funnel until having a pack of desired length. The same packing procedure was always used to make sure we have a homogeneous medium. The diameter of the pack was 3.8 cm and the length was 21 cm.

3.3 Procedure

The packed porous media was installed inside the core holder. After providing the overburden pressure of 25 bars, the packed porous media was saturated with distilled water using a vacuum pump. The porosity of the pack was calculated by doing a material balance on the amount of water left and knowing the exact value of the dead volume of lines connected to the core. The absolute permeability of the packed core was measured vertically using an accurate pressure transducer with an operational range of 0-3 bars. The core holder was then placed inside the oven in horizontal position, and water injection was performed until reaching the desired temperature and pressure inside the core. In the next step, oil was injected at a rate of 0.5 cc/min to initialize the core and calculate the initial water saturation (S_{wi}). Oil injection was continued at S_{wi} to measure effective oil permeability. After initializing the core, the separator was connected and the imbibitions process was initiated by injecting water at a rate of 0.8 cc/min. This rate was even less than 1 PV/h as recommended by Polikar et al. (1990). During the water injection phase, the oil production was recorded versus time, and the pressure differential across the core was monitored as well. The water injection was continued for almost 20 hours. After the experiment, the separator was disconnected and held at a temperature of 40°C for a few days in order for the oil/water meniscus to be separated completely and any possible adjustment to the final oil recovery.

3.4 Oil Preparation and Viscosity Measurement

The type of oil used in this study was a blend of Athabasca bitumen and n-dodecane. The bitumen sample used is obtained from an oil sand reservoir in Athabasca region, produced using SAGD method. The sample has not been exposed to any solvent and the condensed water produced together with the bitumen has been removed at high temperature. The viscosity, density, molecular weight and some other PVT properties of Athabasca bitumen were measured as highlighted in Ashrafi et al. (2011). Bitumen was added to n-dodecane in known amounts, and the mixture was stirred on a magnetic stirrer. Two types of oil were prepared by mixing bitumen with 10% n-C_{12} added and 20% n-C_{12} added on a mass basis. These oils are referred to as OIL10 and OIL20. The properties of bitumen and these two oils are shown in Table 1.

Table 1. Oil properties

Component	Molecular Weight (g/gmole)	Density (g/cc)
Athabasca bitumen	534	1.0129
n-dodecane (n-C_{12})	170.34	0.748
OIL10	440.1	0.9783
OIL20	374.2	0.9459

The viscosities of these two oils are also measured using a digital rotational viscometer as done for Athabasca bitumen (Ashrafi et al., 2011). The viscosity measurements were done in 10 °C intervals, allowing sufficient time at each temperature step to have a reasonable viscosity reading. For pure Athabasca bitumen the measurements were done from room temperature up to 300 °C. While for OIL10 and OIL20, the measurements were done up to 70 °C and extrapolated for higher temperature values. This was due to the possibility of n-dodecane evaporation at higher temperatures. The extrapolation was done using an empirical equation for the viscosity of gas free Athabasca bitumen presented by Khan et al. (1984). This equation is as follows:

$$\ln\ln(\mu) = c_1 \ln T + c_2 \tag{13}$$

In this equation μ is dynamic viscosity of heavy oil sample in "mPa.s" or "cp", at atmospheric pressure and temperature T (K). The constants c_1 and c_2 are empirical and can be found for each sample using experimental data. They can be determined using the least square parameter estimation technique. The applicability of this equation to our bitumen sample was tested and compared with the data provided by Khan et al. (1984) (Ashrafi et al., 2011). The values of empirical constants c_1 and c_2 for the bitumen, OIL10 and OIL20 are presented in Table 2. The viscosity versus temperature curve is also shown in Figure 2.

Table 2. Empirical constants of equation (13) for Athabasca bitumen, OIL10 and OIL20

Component	c_1	c_2
Athabasca bitumen	-3.5912	22.976
OIL10	-3.4563	21.872
OIL20	-3.5094	21.905

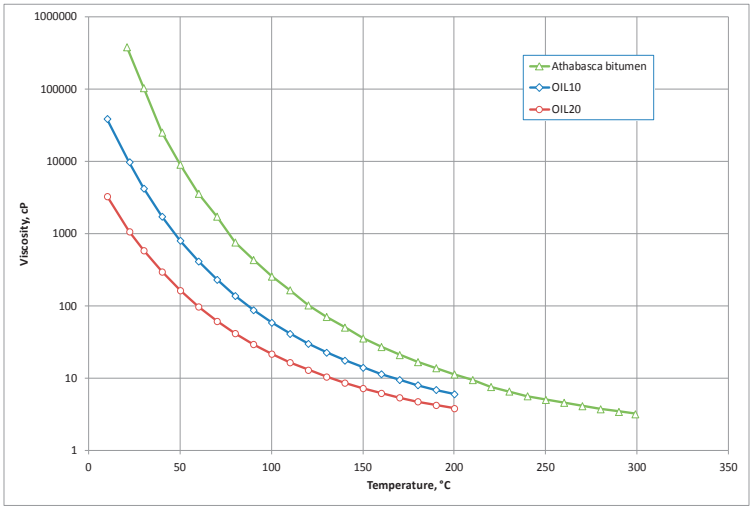

Figure 2. Viscosity of Athabasca bitumen, OIL10 and OIL20 versus temperature

4. Results and Discussion

The porous media used in this study were artificial core plugs made of glass beads (GB) packed inside the rubber sleeve. Two sizes of glass beads were used, 1 millimeter size and 300-425 micron size beads. The absolute permeabilities of cores were measured by injecting water vertically upwards. The absolute permeability was, however, used as an adjusting parameter in simulations by Sendra to match the experimental pressure drop observed. An overview of experimental parameters is listed in Table 3.

Table 3. Experimental conditions

Core properties	
Length	21 cm
Diameter	3.8 cm
Permeability (1mm size GBs packs)	90 to 100 Darcies
Permeability (300-425 micron GBs packs)	40 to 45 Darcies
Flooding Conditions	
System pressure	5 bars
Overburden pressure	25 bars
Oil injection rate	0.5 cc/min

Different sets of experiments were run on glass bead packs. These flooding experiments were designed to examine the effect of various parameters on flow behavior and relative permeability curves. Table 4 summarizes the experiments performed during this study.

Table 4. Experiments performed during this study

Porous Media	Experiment Type	Temperature °C	Oil Type	Injection rate cc/min	Porosity %	Pore volume cc	S_{wi} %
1 mm GBs	LT*	50	OIL20	1	29.01	69.1	20.98
		70	OIL20	1	28.80	68.6	17.49
	HT**	100	OIL20	1	30.06	71.6	19.55
		120	OIL20	1	30.06	71.6	16.76
		120	OIL20	0.8	30.27	72.1	15.95
		140	OIL20	0.8	30.90	73.6	16.30
		100	OIL10	0.8	31.95	76.1	11.83
		120	OIL10	0.8	31.53	75.1	21.30
		140	OIL10	0.8	31.32	74.6	28.15
300-425 micron GBs	HT	100	OIL20	0.8	32.37	77.1	11.02
		120	OIL20	0.8	33.21	79.1	13.91
		140	OIL20	0.8	32.79	78.1	21.13
		100	OIL10	0.8	33.84	80.6	14.02
		120	OIL10	0.8	34.26	81.6	13.48
		140	OIL10	0.8	34.05	81.1	17.88

* Low temperature experiments
** High temperature experiments

As mentioned earlier, the method of relative permeability calculation was history matching the production curve and pressure differential data using Sendra simulator. Different relative permeability correlations were used, and the parameter estimation was done by the software to get the best match. Figure 3 shows the pressure differential match and production curve match for LT experiment at 70°C as an example.

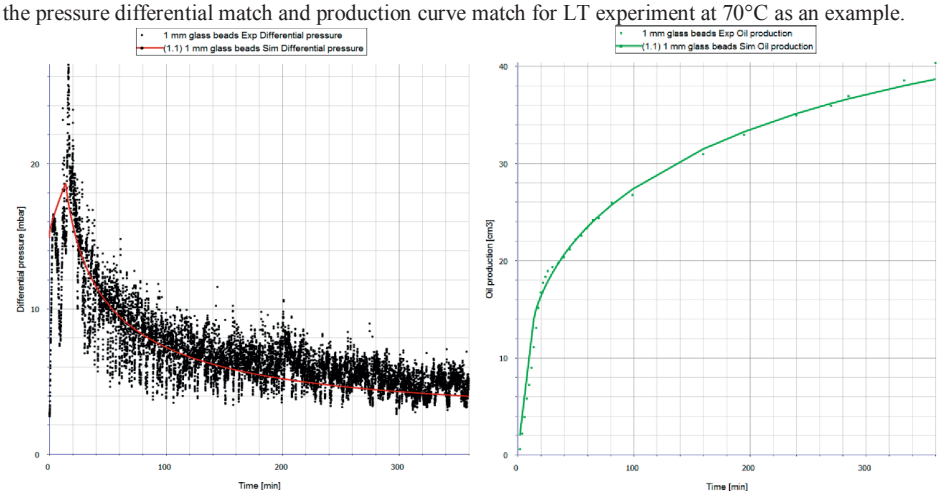

(a) (b)

Figure 3. a) Differential pressure data match for experiment LT at 70°C; b) Production curve match for experiment LT at 70°C. Dots show the experimental data and the continuous lines show the simulation match

The relative permeabilities based on these matches are shown on Figure 4 and compared with 50°C experiment. As shown on this figure the end points are shifted and the permeability curves are also different for the two cases.

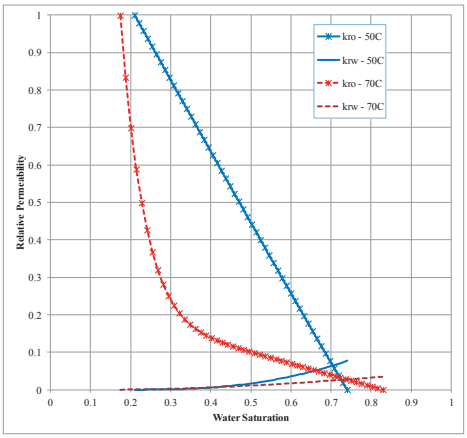

Figure 4. Relative permeability for LT experiments

The relative permeability curves for HT experiments done on 1 mm glass beads (GBs) using OIL20 are shown on Figure 5. These curves are shown on Figure 5b as normalized relative permeability curves. Both water saturation and relative permeabilities are normalized on Figure 5b to only show the difference in curvature of the data. Both high temperature and low temperature relative permeabilities show some variations by temperature. However, no direct conclusion can be drawn at this point.

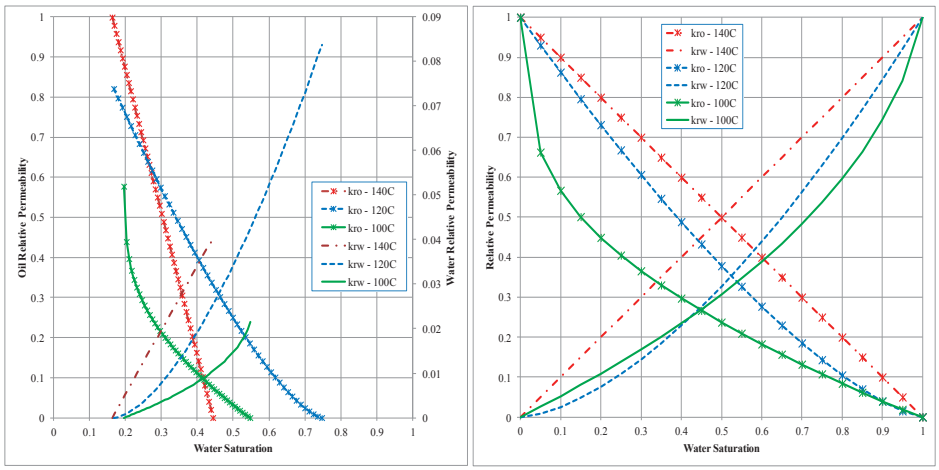

(a) (b)

Figure 5. Relative permeability curves for HT experiments done on 1 mm GBs using OIL20. Normalized values are shown on Figure (b)

The experiment at 120°C was done twice injecting water at different rates. The effect of injection rate on production curves is revealed in Figure 6. As seen in this figure the ultimate recovery is almost the same. However, higher injection rate results in faster recovery. Figure 7 compares the relative permeability data for these two experimental runs. The initial water saturation and residual oil saturation values did not change significantly. The relative permeability curves, however, showed injection rate dependency. The values for oil seemed to be increasing while water relative permeability decreased as the injection rate increased.

The relative permeability curves obtained for the HT experiments on 1 mm GBs media using OIL10 are shown in Figure 8 with the normalized values on the part (b) of the figure. Note that the values of water relative permeability are magnified for better visibility on Figure 8a.

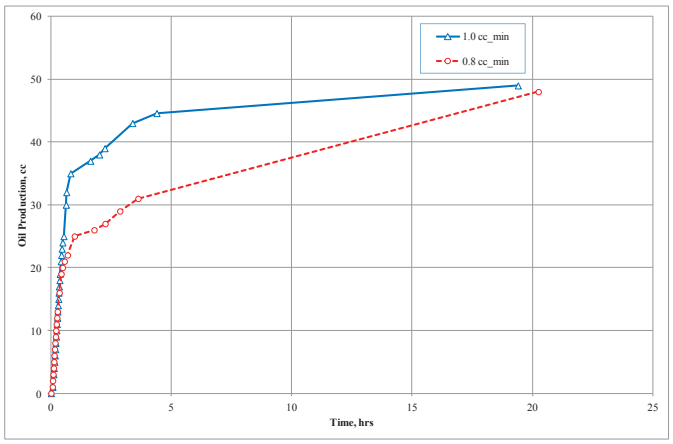

Figure 6. Oil production curves for HT experiments at 120°C (1 mm GBs, OIL20) showing the effect of water injection rate

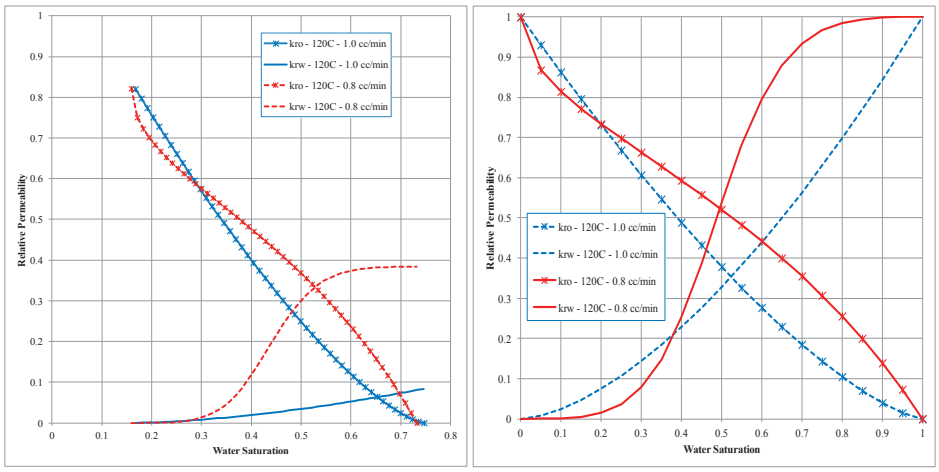

(a) (b)

Figure 7. Relative permeability curves showing the effect of water injection rate. Normalized values on Figure (b)

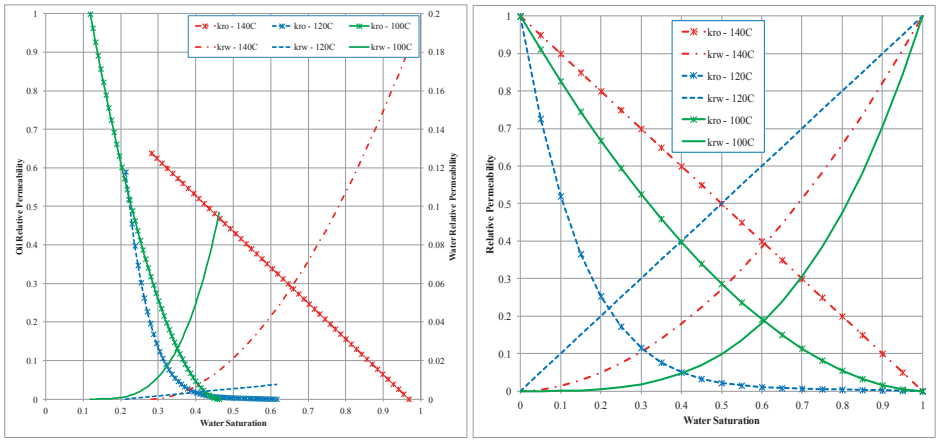

(a) (b)

Figure 8. Relative permeability curves for HT experiments done on 1 mm GBs using OIL10. Normalized values are shown on Figure (b)

The same experiments, done using glass beads of smaller size as the porous media, have resulted in almost the same set of relative permeability curves. There seems not to exist a unique trend and definite dependency on temperature, as the curves have sometimes increased from one temperature to another and then decreased as the temperature has further been increased. The relative permeability curves obtained for HT experiments on 300-425 micron size GBs using OIL10 are shown on Figure 9. Part (a) of the figure shows normal plots of relative permeability versus water saturation. In part (b), however, normalized relative permeability values are plotted against normalized water saturation. Part (c) of the figure shows semi-log plots for two temperatures, namely 120°C and 140°C.

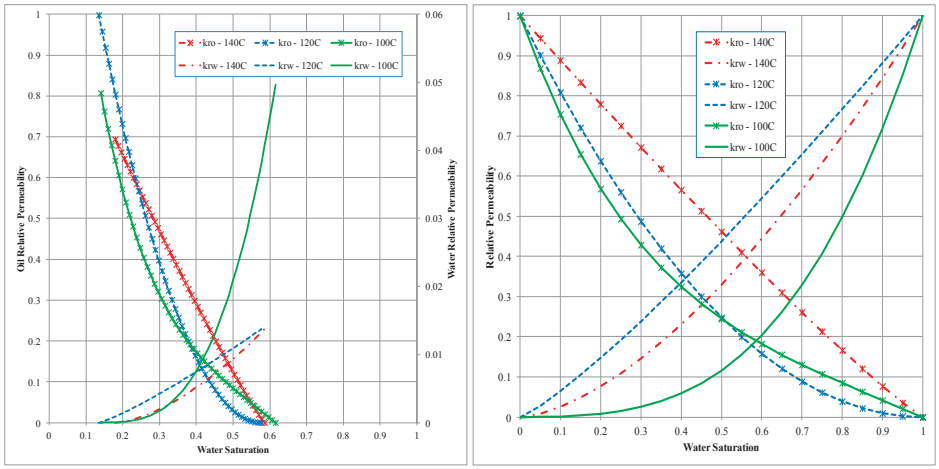

(a) (b)

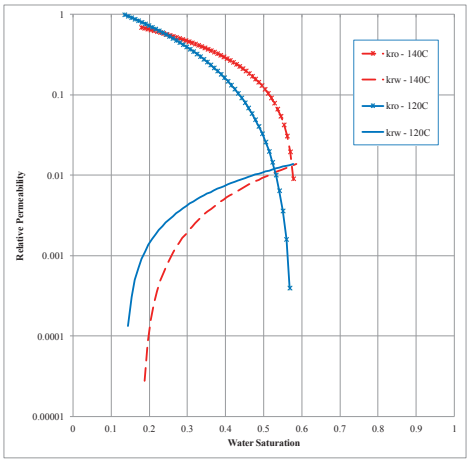

(c)

Figure 9. Relative permeability curves for HT experiments done on 300-425 micron GBs using OIL10. Normalized values are shown on Figure (b) Semi log curve for 120°C and 140°C on Figure (c)

HT experiments performed using OIL20 on the smaller sized GBs, namely 300-425 micron, have been analyzed and the resulting relative permeability curves are revealed in Figure 10.

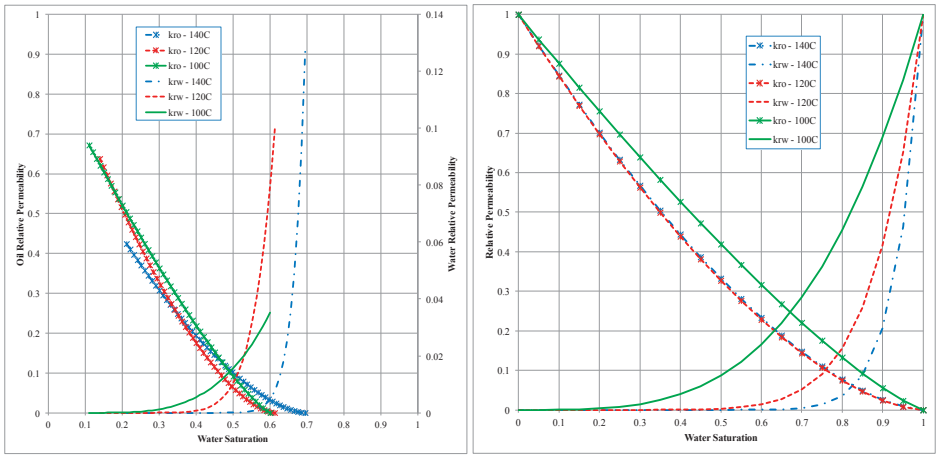

(a) (b)

Figure 10. Relative permeability curves for HT experiments done on 300-425 micron GBs using OIL20. Normalized values are shown on Figure (b)

The increase of initial water saturation (S_{wi}) versus temperature has been spotted generally, although not present in all the experimental results. We believe in those experiments we might have been inside the experimental error margin. But generally the increase in S_{wi} as the temperature increases is expected, as the oil viscosity drops much more than water viscosity. As the result the viscosity ratio of water to oil increases and will result in an unfavorable displacement of water by oil during initialization of core. During the water flooding of oil saturated core, the same interpretation should apply regarding the

residual oil saturation (S_{or}). As the temperature increases the viscosity ratio of oil to water drops, and this results in a more favorable mobility ratio and S_{or} is expected to decrease. However, this was not the case in some of the experiments. We think this could have happened due to viscous instabilities and possible viscous fingering in core flooding experiments. Viscous fingering seems to be inevitable in such an adverse mobility ratio condition, even at low injection rates.

As per the effect of temperature on relative permeability curves, we were not able to determine a unique trend in our experimental results. Dependency of either oil or water relative permeability on temperature is not justified in any of the experiments performed. The spread in relative permeability variation by temperature is even more adverse in the tests with higher permeable GBs (1 mm size). This further suggests that the variations seen can be attributed to viscous instabilities. This has also been reported by several authors. Sufi et al. (1982) and Miller and Ramey (1985) have concluded that the variations in relative permeability with temperature are probably not related to fundamental flow properties and they are rather related to experimental artifacts. Polikar et al. (1990) also stated that it is not possible to predict theoretically what the effect of temperature on relative permeabilities could be, and the results are system specific. Maini and Okazawa (1987) have also concluded that due to several artifacts involved in the experiments no effect of temperature could be justified.

5. Conclusions

In this work, laboratory core flooding experiments were conducted on Athabasca type oil with varying viscosities and using glass bead packs of different size as the porous media. Our aim was to investigate any possible effect of temperature on the oil and water relative permeability curves during imbibitions of water in the cores. For this purpose the oil production curves and the pressure drop across the core were history matched using Sendra core flooding simulator. This simulator acts as an optimization tool to help adjust the relative permeability correlation parameters and come up with the best curves that can match the laboratory measured data. The following conclusions can be drawn from this experimental investigation.

1) The increase of initial water saturation (S_{wi}) versus temperature has been spotted generally, although not present in all the experimental results. We believe in those experiments we might have been inside the experimental error margin.
2) The decrease in residual oil saturation (S_{or}) versus temperature has been observed. However, this was not the case in some of the experiments. We think this could have happened due to viscous instabilities and possible viscous fingering in core flooding experiments.
3) No dependency of either oil or water relative permeability on temperature is justified in any of the experiments performed. Not a unique increasing or decreasing trend could be seen versus the temperature. The spread in relative permeability variation by temperature is even more adverse in the higher permeable tests. This further suggests that the variations seen can be attributed to viscous instabilities.
4) The changes seen in relative permeability curves at different temperatures are probably more related to experimental artifacts and fingering issues than fundamental flow properties. We should, however, mention that the conclusions drawn cannot apply in general, and the temperature dependency issue is quite case specific.

Acknowledgements

We would like to thank Statoil ASA for providing financial support. We also thank Weatherford Petroleum Consultants AS for providing us the license to Sendra.

References

Abasov, M. T., Tairov, N. D., Abdullaeva, A. A., Alieva, Sh. M., & Mamedov, A. I. (1976). Influence of Temperature on Relative Phase Permeability at High Pressures. *Dokl. Akad. Nauk Azerb. SSR., 8*, 31-34.

Amyx, J. W., Bass, D. M., & Whiting, R. L. (1960). *Petroleum reservoir engineering: physical properties*. New York: McGraw-Hill.

Ashrafi, M., Souraki, Y., Karimaie, H., Torsaeter, O., & Bjorkvik B. J. A. (2011). Experimental PVT Property Analyses for Athabasca Bitumen. Paper CSUG/SPE 147064 presented at the Canadian Unconventional Resources Conference held in Calgary, Alberta, Canada, 15-17 November. http://dx.doi.org/10.2118/147064-MS

Bennion, D. W., Moore, R. G., & Thomas, F. B. (1985). Effect of Relative Permeability on the Numerical Simulation of the Steam Stimulation Process. *JCPT, 24*(2), 40-44. http://dx.doi.org/10.2118/85-02-01

Burdine, N. T. (1953). Relative Permeability Calculations from Pore Size Distribution. *Trans., AIME, 198*, 71-78.

Chierici, G. L. (1984). Novel Relations for Drainage and Imbibition Relative Permeabilities. *SPEJ*, 275-276. http://dx.doi.org/10.2118/10165-PA

Combarnous, M., & Pavan, J. (1968). Deplacement par l'eau chaude d'huiles en place dans un milieu poreux. Communication no. 37, III Colloque A.R.T.F.P., pp. 737-757, Pau, Sep. 23-26 (in French).

Corey, A. T. (1954). The Interrelation between Gas and Oil Relative Permeabilities. *Prod., 19*(1), 38-41.

Davidson, L. B. (1969). The Effect of Temperature on the Permeability Ratio of Different Fluid Pairs in Two-Phase Systems. *JPT, 21*(8), 1037-1046. http://dx.doi.org/ 10.2118/2298-PA

Edmondson, T. A. (1965). Effect of Temperature on Waterfloodig. *Journal of Canadian Petroleum Technology, 4*(4), 236-242. http://dx.doi.org/ 10.2118/65-04-09

Honarpour, M., Koederitz, L., & Herbert, H. A. (1986). *Relative Permeability of Petroleum reservoirs*. C.R.C. Press Inc.

Johnson, E. F., Bossler, D. P., & Naumann, V. O. (1959). Calculation of Relative Permeability from Displacement Experiments. *Trans. AIME, 216*, 370-372.

Jones, S. C., & Roszelle, W. O. (1978). Graphical Techniques for Determining Relative Permeability from Displacement Experiments. *JPT*, 807-817. http://dx.doi.org/ 10.2118/6045-PA

Khan, M. A. B., Mehrotra, A. K., & Svrcek, W. Y. (1984). Viscosity Models for Gas-Free Athabasca Bitumen. *J. Can. Pet. Tech., 23*(3), 47-53. http://dx.doi.org/ 10.2118/84-03-05

Lo, H. Y., & Mungan, N. (1973). Temperature Effect on relative Permeabilities and Residual Saturations. Research report RR-19, Petroleum Recovery Institute, Calgary, AB.

Lomeland, F., Ebeltoft, E., & Thomas, W. H. (2005). A New Versatile Relative Permeability Correlation. Reviewed paper at the at the 2005 International Symposium of the SCA, August 21-25, 2005, Toronto, Canada. Retrieved from http://www.scaweb.org/assets/papers/2005_papers/1-SCA2005-32.pdf

Maini, B. B., & Batycky, J. P. (1985). The Effect of Temperature on Heavy Oil/Water Relative Permeabilities in Horizontally and Vertically Drilled Core Plugs. *JPT, 37*(8), 1500-1510. http://dx.doi.org/ 10.2118/12115-PA

Maini, B. B., & Okazawa, T. (1987). Effect of Temperature on Heavy Oil-Water Relative Permeability of Sand. *JCPT, 26*(3), 33-41. http://dx.doi.org/ 10.2118/87-03-03

Miller, M. A., & Ramey, H. J. Jr. (1985). Effect of Temperature on Oil/Water Relative Permeabilities of Unconsolidated and Consolidated Sands. *SPEJ, 25*(6), 945-953. http://dx.doi.org/ 10.2118/12116-PA

Polikar, M., Farouq Ali, S. M., & Puttagunta, V. R. (1990). High Temperature Relative Permeabilities for Athabasca Oil Sands. *SPERE, 5*(1), 25-32. http://dx.doi.org/10.2118/17424-PA

Poston, S. W., Ysrael, S., Hossain, A. K. M. S., Montgomery, E. F. III, & Ramey, H. J. Jr. (1970). The Effect of Temperature on Irreducible Water Saturation and Relative Permeability of Unconsolidated Sand. *SPE Journal, 10*(2), 171-180. http://dx.doi.org/ 10.2118/1897-PA

Schembre, J. M., Tang, G. Q., & Kovscek, A. R. (2006). Interrelationship of Temperature and Wettability on the Relative Permeability of Heavy Oil in Diatomaceous Rocks. *SPERE, 9*(3), 239-250. http://dx.doi.org/10.2118/93831-PA

Sedaee, S. B., Rashidi, F., & Babadagli, T. (2007). Temperature Effects on the Heavy Oil/Water Relative Permeabilities of Carbonate Rocks. *Journal of Petroleum Science and Engineering, 59*, 27-42. http://dx.doi.org/10.1016/j.petrol.2007.02.005

Sendra User Guide. (2012). Retrieved from http://www.sendra.no

Sigmund, P. M., & McCaffery, F. G. (1979). An improved Unsteady-state Procedure for Determining the Relative Permeability Characteristics of Heterogeneous Porous Media. *SPEJ, 19*(1), 15-28. http://dx.doi.org/ 10.2118/6720-PA

Sinnokrot, A. A., Ramey, H. J. Jr., & Marsden, S. S. Jr. (1971). Effect of Temperature Level on Capillary Pressure Curves. *SPE Journal, 11*(1), 13-22. http://dx.doi.org/ 10.2118/2517-PA

Sufi, A. H. (1982). *Temperature Effects on Oil-Water Relative Permeabilities for Unconsolidated Sands*. PhD Thesis, Stanford University, Stanford, CA.

Torabzadeh, S. J., & Handy, L. L. (1984). The Effect of Temperature and Interfacial Tension on Water/Oil Relative Permeabilities of Consolidated Sands. SPE/DOE 12689, 4th Symposium on EOR, Tulsa, OK, April 15-18. http://dx.doi.org/ 10.2118/12689-MS

Wang, J., Dong, M., & Asghari, K. (2006). Effect of Oil Viscosity on Heavy Oil/Water Relative Permeability Curves. SPE 99763, SPE/DOE Symposium on IOR, Tulsa, OK, April 22-26. http://dx.doi.org/10.2118/99763-MS

Weinbrandt, R. M., Ramey, H. J. Jr., & Casse, F. J. (1975). The Effect of Temperature on Relative and Absolute Permeability of Sandstones. *SPE Journal, 15*(5), 376-384. http://dx.doi.org/ 10.2118/4142-PA

Wilson, J. W. (1956). Determination of Relative Permeability under Simulated Reservoir Conditions. *AIChE Journal, 2*(1), 94-100. http://dx.doi.org/ 10.1002/aic.690020120

A.3 Paper TiPM

Investigating the Temperature Dependency of Oil and Water Relative Permeabilities for Heavy Oil Systems

Mohammad Ashrafi . Yaser Souraki . Ole Torsaeter

Is not included due to copyright

Appendix B

Other papers presented in various conferences during the course of my PhD study are listed in this Appendix. Here is a review of these papers. The Appendices B.3 and B.4 only include the abstract of the papers listed, as they were already presented in the main thesis as chapters 6 and 4 respectively.

B.1 "Experimental and Numerical Study of Steam Flooding in Fractured Porous Media", Mohammad Ashrafi, Yaser Souraki, Hassan Karimaie, Ole Torsaeter, paper SPE 144462 presented at the SPE Western North American Regional Meeting, 7-11 May 2011, Anchorage, Alaska, USA.

B.2 "Simulation Study of 2-D SAGD Experiment and Sensitivity Analysis of Laboratory Parameters", Mohammad Ashrafi, Yaser Souraki, Hassan Karimaie, Ole Torsaeter, Jon Kleppe, paper SPE 144582 presented at the SPE Western North American Regional Meeting, 7-11 May 2011, Anchorage, Alaska, USA.

B.3 "Numerical Simulation Study of SAGD Experiment and Investigating Possibility of Solvent Co-Injection", Mohammad Ashrafi, Yaser Souraki, Hassan Karimaie, Ole Torsaeter, Jon Kleppe, paper SPE 145013 presented at the SPE Enhanced Oil Recovery Conference, 19-21 July 2011, Kuala Lumpur, Malaysia.

B.4 "Experimental and Numerical Investigation of Steam Flooding in Heterogeneous Porous Media Containing Heavy Oil", Mohammad Ashrafi, Yaser Souraki, Tor Joergen Veraas, Hassan Karimaie, Ole Torsaeter, paper SPE 144168 presented at the SPE Asia Pacific Oil and Gas Conference and Exhibition, 20-22 September 2011, Jakarta, Indonesia.

The fulltext of Appendix B.1 and B.2
are not included due to copyright

B.1 Paper SPE 144462

SPE 144462

Experimental and Numerical Study of Steam Flooding in Fractured Porous Media

Mohammad Ashrafi, Yaser Souraki, Hassan Karimaie, and Ole Torsaeter, SPE, Norwegian University of Science and Technology (NTNU)

This paper was prepared for presentation at the SPE Western North American Regional Meeting held in Anchorage, Alaska, USA, 7–11 May 2011.

Abstract

Extra heavy oil and bitumen reservoirs constitute a huge proportion of total world oil reserves. Thermal recovery and steam based methods are the most widely used recovery methods in these kinds of reservoirs. Steam injection into fractured heavy oil reservoirs to recover matrix oil has been considered as an efficient EOR method. However, mechanism of steam injection is more complex in fractured reservoirs than in conventional reservoirs. Evaluation of steam injection in fractured porous media requires good understanding of the physical processes between rock and fluids in matrix and fracture. In fact recovery could be a combination of several mechanisms such as viscous forces, capillary imbibition, thermal expansion and gravity drainage.

This paper presents experimental and simulation study of steam flooding in fractured porous media that contains Athabasca heavy oil. Some PVT properties of Athabasca crude oil have been measured experimentally and simulation study was accomplished using a numerical thermal reservoir simulator. A single horizontal fracture and two surrounding matrix blocks have been defined to verify the performance of steam injection in a 20 cm long sandstone core with a permeability of 640 mD saturated with Athabasca heavy crude. Considering a fractured system, sensitivity analyses were focused on the effect of injection rate, fracture permeability and steam quality.

The most important conclusion is that there is an optimum steam temperature and quality for most efficient steam injection. The permeability of the fracture should be low considering both oil production and steam oil ratio (SOR), which is a measure of economy. Matrix permeability of 640 mD in sandstone core provides satisfactory recovery and SOR. Higher matrix permeability can cause very high SOR and affect the economy of the process. Results also clearly show that higher injection rate improve the oil recovery. However, SOR should also be considered at the same time. There is a trade-off between recovery and SOR. It is also clear that lower fracture width shows better recovery while causing high injection pressure at the inlet.

SPE 144582

Simulation Study of 2-D SAGD Experiment and Sensitivity Analysis of Laboratory Parameters

Mohammad Ashrafi, Yaser Souraki, Hassan Karimaie, Ole Torsaeter, Jon Kleppe, SPE, Norwegian University of Science and Technology (NTNU)

This paper was prepared for presentation at the SPE Western North American Regional Meeting held in Anchorage, Alaska, USA, 7–11 May 2011.

Abstract

Bitumen resources constitute a high portion of the total world oil resources. The main recovery mechanism for these high viscous fluids is to reduce their viscosity by the application of heat, mostly by introducing steam.

Among different steam injection schemes, steam assisted gravity drainage (SAGD) has become the method of choice applicable to bitumen and oil sand reservoirs. In these extra heavy oil reservoirs the reservoir has almost no injectivity due to high oil viscosity, and therefore conventional steam flooding is hard to conduct. SAGD, however, reduces the viscosity of bitumen in place and the heated bitumen drains due to gravity forces towards the production well and is then being produced.

Our simulation study is based on the experimental work done by Chung (1988) and the simulation model of this experiment by Chow (1993). Chung′s physical experiment was a 2-D model to simulate SAGD experiment in laboratory.

A reservoir simulation model was built using a numerical thermal reservoir simulator. The model was then tested and validated with Chung′s physical model. Having a valid model, sensitivity analysis was run to examine the effect of different simulation parameters on recovery and steam oil ratio.

The sensitivity parameters tested are steam temperature and quality, the permeability of the model, both horizontal and vertical, different well placement schemes, and the effect of grid refinement. High permeability was found to have a profound effect on recovery.

Different steam temperatures and qualities were examined. The best injection condition was found to be 130 °C and 90% quality, beyond which no increased recovery was achieved.

Different injector and producer placements were tested. Placing injector and producer diagonally in the model showed the best horizontal sweep efficiency in the laboratory model.

The Chung′s experiment was done with Cold Lake crude oil. Our model was tested using bitumen with higher viscosity from Athabasca and results showed that in order to get the same recovery as in the Cold Lake case; the temperature must be increased to 140 °C as compared to 100 °C for the case with lower viscosity oil.

B.3 Paper SPE 145013 abstract

SPE 145013

Numerical Simulation Study of SAGD Experiment and Investigating Possibility of Solvent Co-Injection

Mohammad Ashrafi, Yaser Souraki, Hassan Karimaie, Ole Torsaeter, and Jon Kleppe, SPE, Norwegian University of Science and Technology (NTNU)

This paper was prepared for presentation at the SPE Enhanced Oil Recovery Conference held in Kuala Lumpur, Malaysia, 19–21 July 2011.

Abstract

Bitumen resources constitute a high portion of the total world oil resources. The main recovery mechanism for these high viscous fluids is to reduce their viscosity by the application of heat, mostly by introducing steam.

Among different steam injection schemes, steam assisted gravity drainage (SAGD) has become the method of choice applicable to bitumen and oil sand reservoirs. In these extra heavy oil resources, the reservoir has almost no injectivity due to high oil viscosity, and therefore conventional steam flooding is hard to conduct. SAGD, however, reduces the viscosity of bitumen in place and the heated bitumen drains due to gravity forces towards the production well and is then being produced. Recently hybrid processes are attracting more attentions in the industry. These processes benefit from co-injection of a solvent together with steam. The solvent can diffuse into the bitumen and make it even lighter by reducing the viscosity.

Our simulation study is based on the experimental work done by Chung (1988) and the simulation model of this experiment by Chow (1993). Chung′s physical experiment was a 2-D model to simulate SAGD experiment in laboratory. The Chung′s experiment was done with Cold Lake crude oil. A reservoir simulation model was built using a numerical thermal reservoir simulator. The model was then tested and validated with Chung′s physical model. Having a valid model, sensitivity analysis was run to examine the effect of different simulation parameters on recovery and steam oil ratio.

The sensitivity parameters tested are steam temperature and quality, the porosity of the model, different well placement schemes, and the effect of shale barrier. Different steam temperatures and qualities were examined. The best injection condition was found to be 130 °C and 90% quality, beyond which no increased recovery was achieved. Different injector and producer placements were tested. Placing injector and producer diagonally in the model showed the best horizontal sweep efficiency in the laboratory model. Horizontal shale barrier had a dramatic negative effect on the oil recovery. Vertical shale, however, had a smaller effect. This is because in horizontal case the steam chamber cannot reach to the top layers. Porosity was found to be inversely proportional to the oil recovery and steam oil ratio. Results showed that solvent can help to improve oil recovery and steam-oil ratio. In addition most of the injected solvent could be recovered from production stream. Sensitivity analyses on solvent type and

concentration indicated significant effects on performance of process. Among the solvents used in this study, hexane showed the best recovery performance.

B.4 Paper SPE 144168 abstract

SPE 144168

Experimental and Numerical Investigation of Steam Flooding in Heterogeneous Porous Media Containing Heavy Oil

Mohammad Ashrafi, Yaser Souraki, Tor Joergen Veraas, Hassan Karimaie, and Ole Torsaeter, SPE, Norwegian University of Science and Technology (NTNU)

Abstract

Thermal recovery methods and especially steam flooding have long been considered as the most effective methods to unlock heavy oil reservoirs. These highly viscous hydrocarbon deposits are proven to constitute a huge proportion of total world oil reserves. Large volumes of heavy oil are located in heterogeneous porous media containing high permeable wormholes or non-permeable shale barriers. High permeable zones can be the results of sand migration in loose and unconsolidated sandstones. There is a question of how these non-homogeneities can possibly enhance or hinder the flow of high viscous oil, steam and condensed water under a steam injection process.

This paper addresses experimental and simulation study of steam flooding in heterogeneous porous media that contains Athabasca heavy oil. Some PVT properties of Athabasca crude oil have been measured experimentally and simulation study was accomplished using a numerical thermal reservoir simulator. A horizontal layer of high porosity and permeability was assumed in the middle of a core to verify the performance of steam injection in a 20 cm long sandstone core with a permeability of 640 mD saturated with Athabasca heavy crude. High permeable zone had a permeability of 5 D. Different shale barrier configurations were also considered to examine the effect of these no flow layers. Considering a heterogeneous system, sensitivity analyses were focused on the effect of injection rate, porosity, permeability contrast and thickness of high permeable zone. Different steam temperature and quality cases for core flooding experiment in this system were also investigated.

The most important conclusion is that there is an optimum steam temperature and quality for most efficient steam injection. It was figured out that shale barriers in the model can hinder the flow of oil and cause high residual oil, but their impact is dependent on permeability distribution in the core.

The permeability contrast between the high and low permeable layers should be smaller considering both oil production and steam oil ratio (SOR), which is a measure of economy. Although core permeability of 640 mD provides satisfactory recovery and SOR, higher permeability can cause faster recovery and lower SOR, since the injection can stop earlier. Porosity of the model is found to have an inverse relation with the oil recovery and SOR. Results also clearly show that higher injection rates improve the oil recovery. However, SOR should also be considered at the same time. There is a trade-off between recovery and

SOR. It is also clear that lower thickness for the high permeable zone results in better recovery while causing high injection pressure at the inlet. This corresponds with lower permeability contrast case.